Aeolian dust emission dynamics across spatial scales: landforms, controls and characteristics

Johanna RC von Holdt

January 2018

Thesis presented for the degree of

Doctor of Philosophy

in the

Department of Environmental and Geographical Sciences,

University of Cape Town

Supervisors:

Frank Eckardt

Department of Environmental and Geographical Sciences, University of Cape Town

Giles Wiggs

School of Geography and the Environment, University of Oxford

Martin Hipondoka

Department of Geography, History and Environmental Studies, University of Namibia

Declaration

I, Johanna RC von Holdt, declare that this work is my own and that all contributions from other people's work are properly referenced, cited and acknowledged.

I confirm that I have been granted permission by the University of Cape Town's Doctoral Degrees Board to include the following publication(s) in my PhD thesis, and where co-authorships are involved, my co-authors have agreed that I may include the publication(s):

von Holdt, J.R., Eckardt, F.D. & Wiggs, G.F.S. 2017. Landsat identifies aeolian dust emission dynamics at the landform scale. Remote Sensing of Environment. 198:229–243. DOI: 10.1016/j.rse.2017.06.010

SIGNATURE: Signed by candidate

DATE: 16 January 2018

STUDENT NAME: JRC von Holdt

STUDENT NUMBER: VHLJOH002

Abstract

Variable erodibility (surface characteristics) and erosivity factors (meteorological conditions) result in dust emission dynamics being complex in both space and time. Accounting for local-scale surface variability is critical to our understanding of dust emitting processes. This study identifies mineral dust using remote sensing, establishes emission thresholds through field measurements and identifies particle chemistry for major dust sources in the Central Namib Desert. Examining over 2000 Landsat images over a period from 1972 to 2016, identified 40 days of visually detectable dust, originating from sub-km scale point sources. The observations suggest that dust sources can be identified at the landform scales which particularly include ephemeral river valleys and saline pan surfaces. These persist throughout the 25-year record; however, a gradual shift in source point clusters is noted through time, which can be tentatively attributed to anthropogenic modification of the hydrological systems.

A PI-SWERL (Portable In-Situ Wind ERosion Lab) wind tunnel was used to measure the emission potential of the Landsat derived targets. The most emissive sources were paleo-stockpiles of alluvial silt deposits and associated degraded nebkhas within the Kuiseb River Delta. These had a geometric mean emission flux of 0.076 mg m^{-2} s^{-1}. In comparison, the active channel had a geometric mean emission flux of 0.008 mg m^{-2} s^{-1}, undisturbed desert pavement 0.007 mg m^{-2} s^{-1}, pan surfaces 0.001 mg m^{-2} s^{-1} and wadis within the gravel plains 0.030 mg m^{-2} s^{-1}. The emission thresholds were augmented with site-specific field measurements such gravel cover (%), moisture content (%), particle size (μm), elemental composition (%) and shear and compressive strength (kg cm^{-2}). A Boosted Regression Tree (BRT) machine-learning algorithm identified the most important surface and sediment

characteristics determining dust emission from the measured surfaces. The model explained 70.8% of the deviance in the measured dust flux with the top predictor variables and their relative importance (%) as follows: gravel cover, 16%; moisture content, 14%; kurtosis, 13%; very coarse silt, 13%; very fine sand, 11%; fine sand, 8%; compressive strength, 7%, calcium, 7% and magnesium, 6%. Such an analysis can be used to identify critical thresholds for dust emission and standardise testing protocols. Linking landforms with such emission measurements allow for the assessment of two existing dust emission schemes: the Preferential Dust Scheme (PDS; Bullard et al. 2011) and the Sediment Supply Map (SSM; Parajuli et al. 2017). Although these schemes represent a major advance in our representation of dust emission source areas and erodibility, this study shows that these schemes still need to be improved to accurately depict dust emission potential. For the PDS this would include producing a global rasterised output with quantified dust emission potential and for the SSM, a more accurate classification of the highly emissive geomorphic units.

Landsat source point sediments were subjected to physical and geochemical analyses and compared to samples obtained from passive collectors such as the Big Spring Number Eight (BSNE) and active PI-SWERL exhaust emissions, using an auto-SEM (QEMSCAN). This provided individual particle mineralogy (>2 μm resolution) for a total of approximately 10000 to 60000 particles per sample which enabled a comparison of particle size, shape and mineralogy. The samples consist of a mixture of minerals reflecting the varied metamorphic geology and consists predominantly of feldspar, quartz, mica, other aluminosilicates such as the alteration products epidote and chlorite and low to medium grade metamorphics such as amphibole and pyroxene, iron oxihydroxides, titanium minerals, carbonates and clay minerals. The three sampling approaches resulted in three different representations of dust emitted at source, with differences in size, shape and mineralogy. The BSNE was inefficient at trapping and/or retaining the fine fractions (<20 μm), whereas the surface sediment

sampling resulted in a potential underrepresentation of the <20 μm fraction. The PI-SWERL sample almost exclusively consisted of particles <63 μm. This has consequences for the interpretation of the potential impacts of the dust sampled at the emission source, such as an underrepresentation of the iron concentration in samples obtained with BSNE traps.

There is currently a disconnect between research efforts on dust emission undertaken by remote sensing identifying global transport pathways and inter-annual regional variability ($>10^4$ m) and ground-based testing at grain scale ($<10^{-2}$ m) studies that identify inter-particle interactions controlling surface emission. The high-resolution remote sensing, wind tunnel and auto-SEM data from this study established connections and provide an opportunity to explore dust emission processes across spatial scales. This study demonstrates that correlative empirical machine-learning algorithms can integrate diverse sources of data from different spatial scale analyses. A preliminary predictive BRT model used here identified geological, geomorphological and climate variables as dust emission drivers and predictors. This method enables identification of potential contributing factors to regionally specific dust emission.

Acknowledgements

I would like to start by thanking my supervisors Frank, Giles and Martin. You all played a part in making the last four years unforgettable. To Frank, thank you for taking this long road through Masters and PhD with me. I've enjoyed working with you and appreciate everything you have taught me. You've had to endure my stubbornness, fixation on detail and have allowed me to explore and play. Giles, thank you for the incredible guidance you have provided. You included me in fieldwork and made instrumentation and samples available without which this research would not have happened. You teach, inspire and empower! Martin, thank you for all your support particularly in Namibia. I appreciate your efforts to include me where at all possible including conference presentations, field campaigns and more. I would like to include Matt Baddock here as an unofficial co-supervisor. Thank you, Matt for providing immense support throughout this PhD – in the field, discussions via Skype and teaching me to write. Your encouragement and enthusiasm has kept me going.

To Pippin Anderson and Sharon Adams, thank you for all the support you have given me. Pippin, your empathy and support makes you one of the best Postgrad coordinators. Thank you for always being there to listen and advise. I am grateful to Sharon for all the emotional and administrative support she has provided over the years.

I thank John Compton for teaching me some geology, patiently answering my questions, discussing my work and sharing his lunch.

For helping me navigate the QEMSCAN component of this research, my sincere gratitude to Gaynor Yorath, Lorraine Nkemba and Megan Becker.

Most importantly to my family and friends who have helped me get to where I am now. Chris (partner and unofficial co-supervisor), Catherine and William (off-spring and competent lab and field assistants) – thank you for being part of this PhD with me. You've helped me in the field, in the lab, looked at my pictures, read my work, listened to my stories and enjoyed this research with me. You can even crack an aeolian joke or two by now. More importantly, you've given me the freedom to indulge myself in this research, sometimes being away from home for extended periods of time or being mentally totally consumed. I am deeply indebted to you. It wasn't always easy for you.

The rest of the family, thank you for the support and patience you've shown over the years. To my mom, Suzette, a huge thank you for always being there to help with the kids, keeping

things together, listening when things got tough and for venturing into the field with me deep in the Namib. To Soma, my biggest fan and cheerleader. You make sure I keep leaning in. Rassie and Kate, a special thank you for all your support, even helping with my sample preparation in the kitchen when UCT was shut down.

Michael Cramer – friend, collaborator and unofficial co-supervisor. Over the Malvern we connected and became friends through the explorations into Heuweltjies and Kommetjies. Your enthusiasm to tackle something new and unfamiliar is contagious. You teach and empower willingly. I hope you continue to do so. You have made me a better scientist.

Shakirudeen Lawal and Ruusa Gottlieb – it's been a pleasure to share this journey with you and seeing you complete your own studies. We have enjoyed many conversations, dinners and field trips.

To my friends who have helped with the myriad of school activities and lifts for the kids (Monique, Wendy, Becky and Clair) – thank you for helping us keep it together, looking after my children and being awesome friends.

I am very grateful to the NRF for providing the funding for this PhD and project funds to carry out this research (research project UID89120). Also, for sponsoring me to attend ICAR (International Conference on Aeolian Research) 2016 in Australia.

Gobabeb Research and Training Station, thank you to all the staff that has helped over the years. I love going there! It is one of my favourite places in the world.

Table of contents

List of Appendices

List of Figures

List of Tables

List of Acronyms and Abbreviations

AI: Aerosol Index

AOD: Aerosol Optical Depth

BRT: Boosted Regression Tree

BSNE: Big Spring Number Eight

LEM: Loose erodible material

LSM: Land Surface Map

Masl: Meters above sea level

MODIS: Moderate Resolution Imaging Spectroradiometer

MODIS DB: Moderate Resolution Imaging Spectroradiometer Deep Blue

MSG-SEVIRI: Meteosat Second generation - Spinning Enhanced Visible and Infrared Imager

MWAC: Modified Wilson and Cook

PDS: Preferential Dust Scheme

PM_{10}: particles <10μm in size

PI-SWERL: Portable In-situ Wind Erosion Laboratory

SEM: Scanning Electron Microscope

SSM: Sediment Supply Map

TOMS: Total Ozone Mapping Spectrometer

XRF: X-ray Fluorescence

Chapter 1: General introduction

The aeolian dust cycle occurs over a wide range of spatial and temporal scales that can vary from global to micro spatial scale and temporally from millions of years to a fraction of a second (Kohfeld et al., 2005). The accurate representation of atmospheric dust processes at different scales is important because of the influence dust has at multiple scales from global climate through to regional ecosystems and localised human impacts (e.g. Field et al., 2010; Goudie and Middleton, 2006). The understanding of spatial scale and the linkages between processes at different scales represents an important part of research on aeolian dust emission (Figure 1-1) and the accurate representation of the dust cycle.

The dust cycle involves three main processes: emission, transport, and the deposition of mineral dust (Shao et al., 2011a). The majority of atmospheric mineral dust is mostly emitted from arid preferential source regions and subsequently undergoes transformation during transport due to wet and dry deposition (Lawrence and Neff, 2009). Dry deposition involves the removal of particles from the atmosphere by gravitational settling and turbulent mixing and generally entails coarser sand and silt-sized particles. In contrast, wet deposition predominantly involves the scavenging of very fine clay-sized particles by precipitation (e.g. Baker et al., 2006; Friese et al., 2016; Jung and Shao, 2006; Tegen and Fung, 1994). The quantity and characteristics of the dust are determined at the terrestrial sources of emission and are essential for the downwind characterisation of dust loads which undergo changes during transport and are consequently important considerations when modelling dust emission and ultimately deposition (Mahowald et al., 2014). The accuracy of dust models depends on successfully capturing the complex nature of the interaction between the surface (its erodibility) and meteorological variables (erosivity) but also on accurately identifying dust sources (Parajuli et al., 2014).

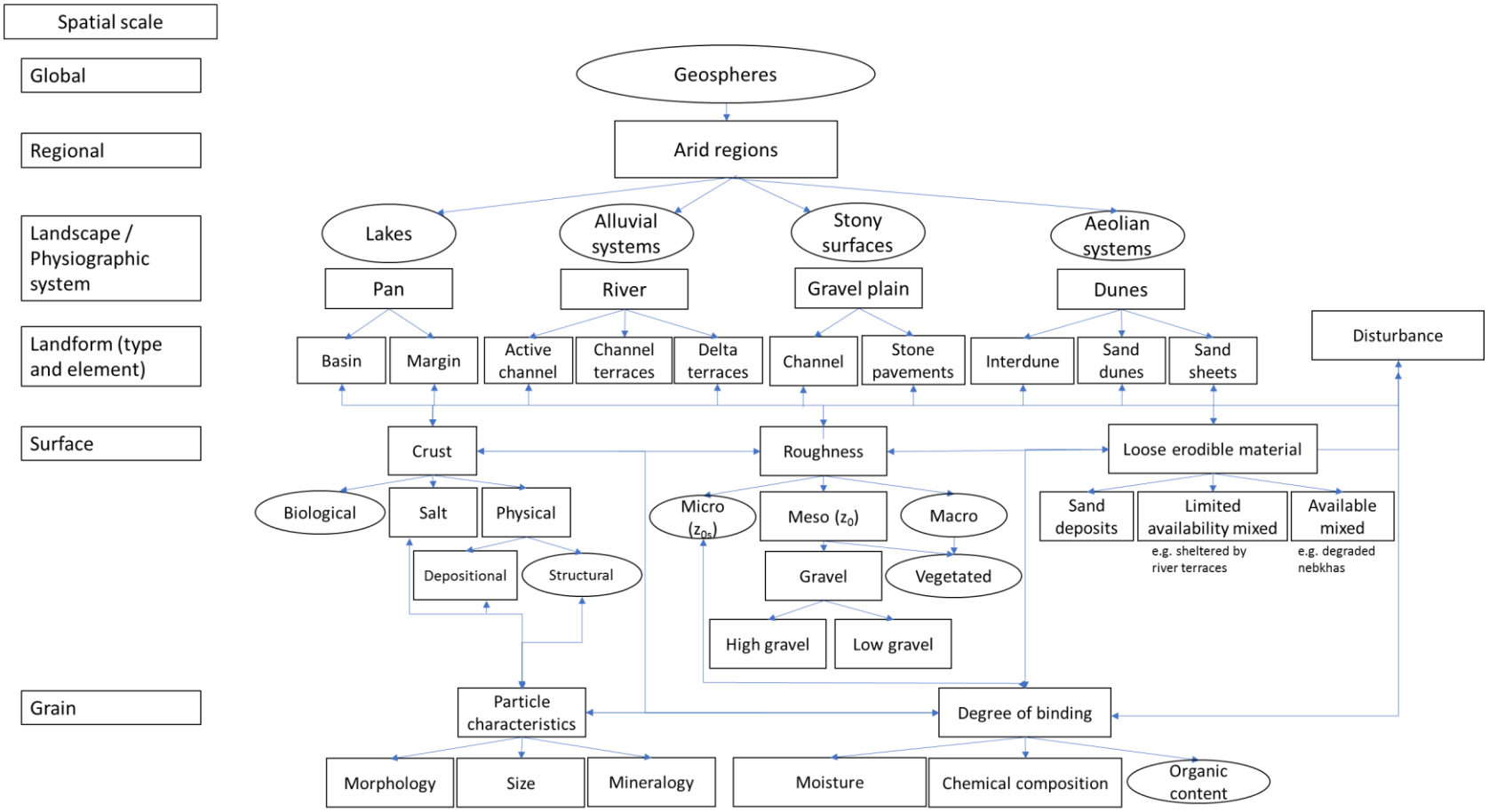

Figure 1-1 Spatial scales and factors that play a role in aeolian dust emission compiled from Bullard et al. (2011); MacMillan et al. (2000); Smith et al. (2011) and Webb and Strong (2011). Rectangles are factors that were given consideration as part of this study and ovals are nomenclature from other studies and factors that are relevant at the spatial scale, but not investigated in this study.

Important themes that have emerged in dust research include the identification of sources, the explanation of emission processes, the characterisation of the dust materials, and the use of this information to inform the modelling of dust transport and impact. Remote sensing data from a global to a landscape scale have been instrumental in identifying dust sources around the world. In contrast, studies involving dust emission processes focus on the opposite end of the scale and encompass a large body of research on the characterisation of dust and the factors that control dust emission. The study of small-scale processes involves a "bottom-up" approach (Kohfeld et al., 2005) and can potentially provide important input and validation to the identification of sources and in dust cycle modelling. The modelling of dust is most relevant at regional to global scale given its influence on regional and global climate and air quality, and conventionally involves a "top-down" approach (Kohfeld et al., 2005). The integration of the outputs of studies from these disparate scales remains a challenge in dust research. This disconnect results in an incomplete understanding of dust emission processes and the dust cycle and therefore results in significant model uncertainties (Shao et al., 2011a). Given the disconnect that results from the different scales, an opportunity exists to improve the linkages in knowledge across the scales to derive more consistent representations and interpretation of dust emission processes.

1.1 Dust emission source identification

Considerable progress has been made in terms of the identification of dust sources and "hot spots" (Prospero et al., 2002). Remote sensing data have made a significant contribution to the study of source areas with reasonable certainty at the landscape scale (Figure 1-1) with various sensors, including TOMS (Prospero et al., 2002; Washington et al., 2003), MSG-SEVIRI (Schepanski et al., 2007, 2012) and MODIS (e.g. Baddock et al., 2009; Bullard et al., 2008; Miller, 2003; O'Loingsigh et al., 2015; Vickery et al., 2013). TOMS has been

instrumental in highlighting the importance of large inland draining basins as important sources of dust with the Bodélé Depression regarded as the world's foremost dust source (Prospero et al., 2002; Washington et al., 2003). Subsequently, attention has been drawn to the importance of small-scale sources, such as floodplains, alluvial fans, rivers and wadis (Ginoux et al., 2012; Schepanski et al., 2007, 2012; Vickery et al., 2013). With a maximum resolution of 250 m MODIS has provided the most accurate spatial evaluation of the sources of dust emission but is still not high enough to identify the actual landforms that act as dust sources. As a consequence, the interpretation of MODIS imagery to identify dust point sources often involves a subjective assessment of where the exact origin of the plume is (Lee et al., 2009). Furthermore, the identification of plume origins necessitates an interpretation of the emission potential of the geomorphic units within the landscape and often requires additional information such as topographic, soil and geological maps, aerial photography and field observations (Baddock et al., 2016; Bullard et al., 2011).

Field-based efforts to monitor and measure dust emission, guided in many instances by identification with remote sensing data, have provided important information regarding the influence of surface properties, process drivers, quantification of fluxes and the characterisation of emitted dust (e.g. Gillette et al., 2004; Goossens and Buck, 2011; Haustein et al., 2015). These studies have used a combination of various instruments, including wind towers, dust samplers, such as BSNEs and MWACs, meteorological stations and saltation flux instruments (e.g., Sensit Probes) (e.g. Bullard et al., 2011; Chappell et al., 2008; Goossens, 2004; Zobeck et al., 2003). Bryant (2013) highlights the fact that placement of the measuring equipment is often situated at some distance from the actual source of dust emission and it is therefore difficult to determine which surfaces are responsible for dust production. This disconnect thereby introduces uncertainty in determining the processes governing dust emission, the quantity of dust emitted and the characteristics of the dust. The

accurate identification of dust sources, potentially at a landform and higher resolution (Figure 1-1) will enable field observation to be directed at the surfaces that are highly emissive. The opportunity to test the actual surfaces that emit dust will provide the ability to study the processes involved and factors that control the erodibility of the surface, as well as an accurate characterisation of the emitted dust.

1.2 Surface characterisation at the source

Several factors have been identified as controlling the erodibility of a surface, such as particle size, moisture content and binding energy (crusting) (Gillies, 2013). These factors act at a micro (particle) level, but exert an influence across several scales to result in dust emission being highly variable in time and space. Particle size and moisture content have an influence on the binding energy that holds the particles together to resist the removal of the particles from the surface (Bagnold, 1941; McKenna Neuman and Nickling, 1989). Further factors that have been highlighted as potentially influencing the binding energy and hence erodibility of a surface includes mineralogy such as salts and carbonates (Buck et al., 2011; Chepil and Woodruff, 1963; Sweeney et al., 2016) and organic content (McKenna Neuman and Maxwell, 2002). Surface roughness is another factor that influences the emission potential of surfaces by determining the aerodynamic roughness length (z_o) and shear velocity (Nield et al., 2013). These factors combined have the potential to influence the threshold at which erosion processes start by either lowering or raising the threshold friction velocity of the wind (Gillies, 2013).

Field and laboratory wind tunnels have made important contributions in our understanding of the surface controls of dust emission. These field studies have traditionally consisted of large, portable wind tunnels that attempt to replicate the atmospheric boundary layer conditions to simulate aeolian dust emission processes (e.g. Baddock et al., 2011; Gillette et al., 1980;

Maurer et al., 2010; Zobeck et al., 2013). The last 10-years have seen numerous field studies using a PI-SWERL (Portable In-Situ Wind Erosion Lab) wind tunnel (Etyemezian et al., 2007) to measure the dust emission potential of the surfaces from a variety of landforms found in desert regions (e.g. Bacon et al., 2011; King et al., 2011; Sweeney et al., 2011, 2016). The portable nature and size of this instrument allows for the testing of many surfaces in locations that would not have been accessible by conventional wind tunnels. The spatial scale of testing with the PI-SWERL is at the level of a specific surface type, potentially down to controls occurring at the particle scale (~ 10^{1} to 10^{-2} m), given the size of the PI-SWERL (0.57 m diameter). The PI-SWERL dust flux measurements also allow the opportunity to characterise the surfaces based on criteria that potentially influence their erodibility at the particle scale. Munkhtsetseg et al. (2016) looked at the effect of moisture content, whereas King et al. (2011) used a multivariate analysis to determine significant correlation between dust emission and factors such as particle size, calcium carbonate, organic content, pH and selected cations. In addition, the PI-SWERL measurements can be used to establish an erodibility index at the surface, landform and potentially the landscape spatial scale. This will provide a measure of quantification of dust emission potential which would be comparable between geomorphologies and different source regions of the world.

1.3 Dust characterisation at source of emission

Dust emitted from different regions of the world will have different influences due to the different sediments at the source, the transport pathways, interactions and modes of deposition. The characteristics of the emitted dust are set at source and have important consequences for what happens downwind in terms of the magnitude of the impact and the distance travelled, climatic impacts on the atmosphere and nutrient supply to terrestrial and marine ecosystems. An accurate representation of the physicochemical properties of the dust

at the source of emission is important for modelling of the dust cycle and for assessing potential effects of the dust (Kok et al., 2012; Mahowald et al., 2014). The methods we use to measure and sample dust emission at source, or as close as possible to the source, becomes a critical consideration for obtaining an accurate representation of the composition and quantification of the entrained sediments at the start of the dust cycle. A variety of methods have been employed to sample dust including wind tunnels (e.g. Bacon et al., 2011; Lafon et al., 2006; Sweeney et al., 2016; Wang et al., 2015; Wang et al., 2017), passive samplers such as Big Spring Number Eight (BSNE) and Modified Wilson and Cook (MWAC) traps (e.g. Fryrear, 1986; Gillette et al., 1997; Warren et al., 2007; Hahnenberger et al., 2015; Dansie et al., 2017a) or using surface sediments as an indication of the potential supply of erodible material (e.g. Wang et al., 2005; Reynolds et al., 2007; Battachan et al., 2015; Dansie et al., 2017b; von Holdt and Eckardt, 2017).

The techniques employed to analyse the physico-chemical properties of the physically sampled particles also determine the level of detail we can acquire from the sampled sediments. The determination of size, mineralogy and shape of the dust particles are important parameters to assess the reach and impact of the emitted dust (Formenti et al., 2011; Mahowald et al., 2011, 2014). However, these characteristics are mostly determined separately with different techniques and for mineralogical analysis on specific size fractions obtained by physical separation such as sieving. Particle size analysis is complicated not only by the different measures of particle diameters, but also by the different ways to represent the size distributions. Particle size can be characterised by aerodynamic, geometric and optical diameters and represented on the basis of mass, volume, surface area or number of particles (Formenti et al., 2011; Mahowald et al., 2014). The different representations will have relevance for different influences. For example, a number size distribution will be dominated by smaller particles and be most relevant to radiation and cloud processes (Sokolik et al.,

2001; Dusek et al., 2006). In contrast, the mass size distribution will be dominated by larger particles and control deposition and hence biogeochemical impacts. The large size ranges that are present in mineral dust present a real challenge to the representation of the size distributions (Formenti et al., 2011). Inefficiencies and inaccuracies in sampling and analytical techniques will have important consequences for our assessment of potential impacts. One important field of study where sampling accuracy is crucial is the assessment of the nutrient and fertilisation capability of aeolian dust, with sampling bias potentially resulting in significant over or underestimation of nutrients delivered to downwind ecosystems.

Aeolian dust delivers important nutrients to ecosystems, with the fertilisation potential of dust to the ocean well known. Nutrients such as nitrogen, phosphorous and iron in dust are important drivers of primary productivity in the ocean by influencing phytoplankton growth and consequently the carbon cycle (Jickells et al., 2005; Jickells et al., 2015; Mahowald et al., 2005; Martin et al., 1994). The importance of the provision of Fe to the ocean has resulted in a significant research effort, partly due to the limited understanding we still have regarding the bioavailability of the Fe (Mahowald et al., 2009). Although fluvial inputs into the ocean are regarded as the largest source of sediments and Fe to the oceans (Poulton and Raiswell, 2002), the potentially limited reach due to containment and settling of the sediments in water means aeolian processes provide an important pathway for Fe to reach the deeper parts of the ocean (Baker and Croot, 2010; Jickells & Moore, 2015; Mahowald et al., 2009; Okin et al., 2011). This is even more pronounced in arid regions where ephemeral rivers rarely reach the sea, such as the westward flowing rivers of the Namib Desert (Jacobson et al., 1995). Although the analysis technique used to determine the bioavailability of the Fe is an important consideration, it is equally important to ensure that the sediments that are sampled are representative of the dust load from a source region and as such careful consideration

should be given to the method used and associated spatial accuracy in obtaining a physical sample.

1.4 Modelling of dust emission

Improvement in the modelling of dust emission remains an important goal of current research since a limitation of existing models is their limited capacity to accurately account for the spatiotemporal variability of dust sources (Parajuli et al., 2014, Shao et al., 2011a). The spatiotemporal variability of emissions is represented by a combination of wind velocity and surface features and the interaction between the two. This interaction accounts for the location of dust sources in space, as well as the distribution and magnitude of emissions in time (Callot et al., 2000). The surface features are central to emission as they are not only able to affect the wind velocity, but also determine the threshold wind velocity at which erosion starts to take place and soil particles are released (Gillies, 2013). A number of factors have been identified as controlling the erodibility of a surface. Parameterising these factors, their interactions and the resultant erodibility of a surface in a simplified manner for use in modelling remains a significant research challenge. The spatial disparity that exists between field-based measurements and regional and global modelling results in a disconnect between the different research efforts. Resolving the small-scale variability of dust emission at landform and sub-landform scale and the ability to connect these results across different scales could result in significant improvements in the measurement and modelling of dust emission. The accurate identification of sources at the landform scale and using these source areas to carry out ground-based fieldwork to determine the dust emission potential and characteristics of these sources could be used as inputs and validation of proposed dust emission schemes.

1.5 Anthropogenic influences on dust emission

One of the greatest uncertainties that remain is the impact of human activities on dust emission, with various estimates of the contribution of anthropogenic sources to the global dust load (Ginoux et al., 2010). Ginoux et al. (2012) suggest that anthropogenic sources account for 25% of dust emission, but that there are large regional differences, for example, the contribution of anthropogenic sources in Australia accounts for 75%, but only 8% in North Africa. Tegen and Fung (1995) give an estimate of 30-50% and Sokolik and Toon (1996) suggest that 20-30% of dust sources are anthropogenic predominantly due to land use change and disturbance as a result of agricultural activities. In contrast, Tegen et al. (2004) approximate that less than 10% of dust emission emanates from agricultural areas.

Anthropogenic sources can be either due to direct disturbance or indirect modification. Direct disturbance due to land use change such as from agricultural activities has been easier to account for than indirect modification of systems. Ginoux et al. (2012) used a global dataset providing the fraction of agriculture within a 0.1° grid cell to identify anthropogenic dust sources (Goldewijk, 2001). The modification of systems, for example, water diversion and extraction, is sometimes difficult to account for. An example of an anthropogenic dust source due to water extraction that is easily identifiable is the desiccation of the Aral Sea. The extremely large dried up lake area is the source of exposed saline sediment as a result of the diversion of water for large-scale agricultural activities from the 1960s and 1970s and is now regarded as a major saline dust source in the world (Abudawaili et al., 2010). Not all indirect modifications are as easily identifiable as those related to the Aral Sea and accounting for the contribution and changes to dust emission adds further complexity to the representation of this type of anthropogenic source, especially given the potentially dynamic nature of these modifications.

1.6 Research question and aims

1.6.1 Problem statement

Aeolian dust plays an important role in many of the earth's systems. Preferential source areas of dust around the world have been identified with the aid of satellite imagery. Despite many advances in our understanding of the emission of dust, significant uncertainty remains regarding the dynamics of the dust source areas, the controls that govern the emission processes, how we identify and measure these at a given resolution, and how to incorporate them into the modelling of dust emission. The spatial and temporal scale at which these sources, their dynamics and controls are studied is a vital consideration for any research effort. Dust emission processes are potentially highly variable, both in terms of time and space. Accounting for this local-scale variability remains a critical issue in our understanding and representation of the processes involved. There is currently a disconnect between research efforts undertaken at different spatial scales, from low spatial resolution remote sensing datasets more suited to identifying global transport pathways and inter-annual regional variability ($>10^4$ m) to particle scale ($<10^{-2}$ m) studies identifying inter-particle interactions influencing emission from surfaces. Establishing connectivity between research undertaken and data generated at different spatial scales is important to develop an accurate understanding of the potential of aeolian dust emission.

Within southern Africa, the Namib Desert has proven to be one of the most active dust-producing areas in the region. The dust source areas within the Namib Desert appear to potentially consist of various geomorphic units which are representative of desert areas around the world, including alluvial systems consisting of river channels and terraces, lakes comprising playas and sabkhas, aeolian systems which incorporate various sand deposits and gravel plains composed of stony surfaces and ephemeral drainage channels or wadis. The

contribution of each of these geomorphic units to dust emission has not been established due to the limitation of adequate spatial resolution satellite imagery to determine the origin of the plumes with certainty. Using a combination of satellite imagery with a spatial resolution to identify dust sources at the landform scale and fieldwork would enable the controls and processes that play a role in dust emission from these surfaces to be determined and the dust emitted to be investigated.

1.6.2 Aim

The aim of this study was to use a multiscaled approach to accurately identify and characterise the small-scale dust sources within the Namib Desert by using a combination of remote sensing, field-based measurements and laboratory testing. In addition, to investigate whether the connection between the various spatial scales can be used to improve our understanding of dust emission processes, the characterisation of dust and provide input and validation for the modelling of dust emission.

This dissertation is structured with three objectives in support of this aim. Each objective is represented as an independent, but interrelated chapter. The manner in which the chapters traverse scale is shown in Figure 1-2 below (adopted from Figure 1-1 at the start of this section).

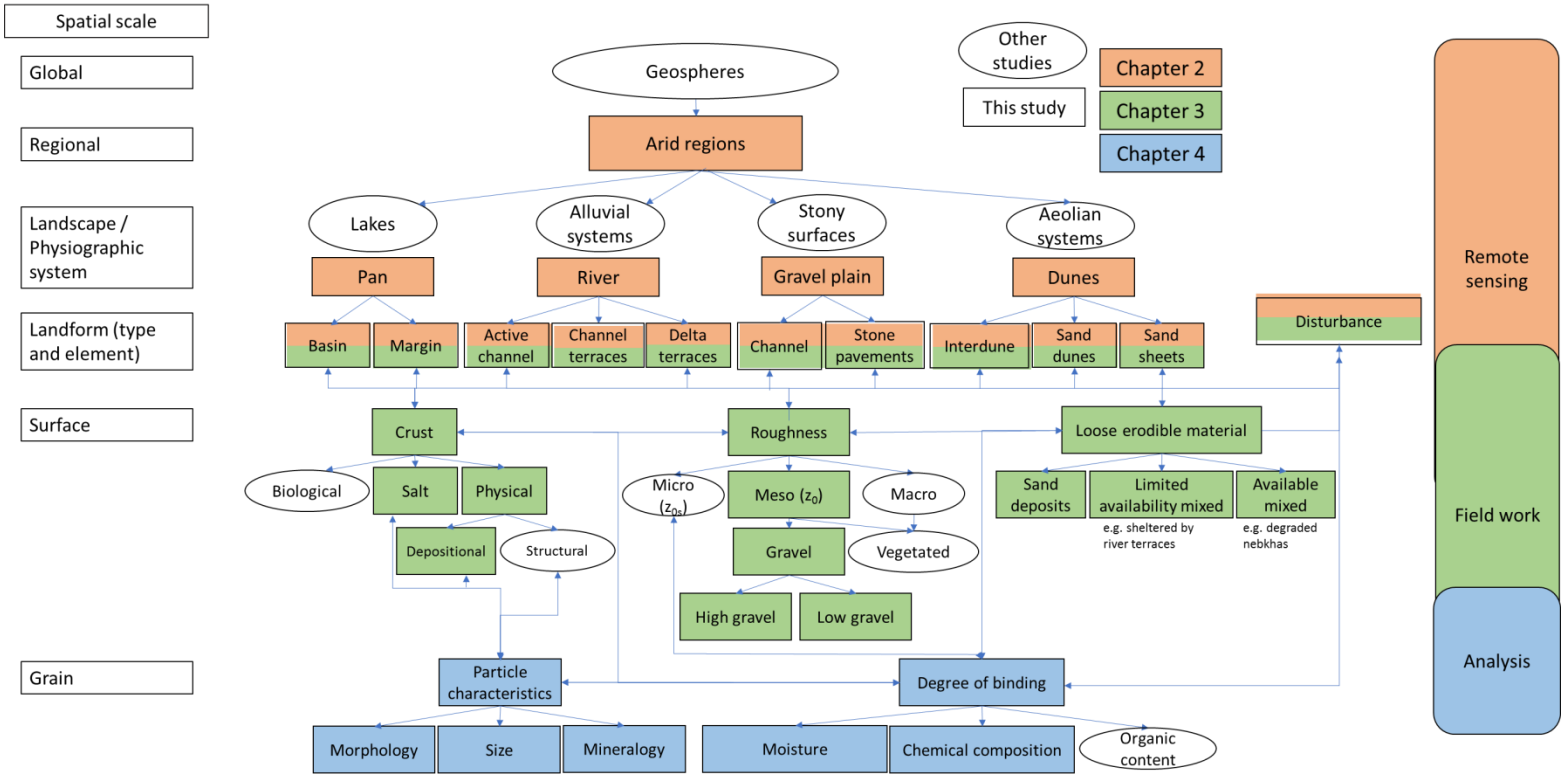

Figure 1-2 Spatial scales and factors that play a role in aeolian dust emission with colour coding relating the spatial scale at which each content chapter (paper) relates to.

1.6.3 Objectives

1.6.3.1 Objective 1: Identification of dust sources at high-resolution

Various satellite sensors with differing temporal, radiometric and spatial resolutions have been used to study dust. TOMS with 100 km and UV, MSG with 3 km and IR, MODIS 250 m and RGB. These sensors have been used to identify the major dust emission sources in various parts of the world. However, the resolution of these sensors does not allow for the accurate identification of source points or surfaces that emit dust at a local-scale. To date, satellite sensors that have higher spatial resolution, but poor temporal resolution, such as Landsat, have not been used to study dust due to the limitations presented by the lack of image frequency (16-day repeat overpass). However, the use of this higher spatial resolution satellite imagery (at the expense of temporal resolution) will enable the identification of dust source points at a local-scale with an accuracy that has not been achieved previously. These data can be used to guide fieldwork and direct optimal placement of monitoring equipment and locations for testing. The objective of this chapter is to identify the sources of dust emission in the Namib Desert with remote sensing to the landform scale, which is at a higher resolution than previously achieved.

1.6.3.2 Objective 2: Emission potential and surface characteristics at source

Dust cycle processes are studied at different scales, with modelling predominantly taking place at the regional to global scale and field-based process studies at a sub-landform scale ($<10^1$ m). Connecting results from studies done at such disparate scales remain problematic. Local-scale dust sources identified with higher resolution satellite imagery and fieldwork can provide important inputs to geomorphic mapping efforts to represent dust emission for use in global models. Portable wind tunnel measurements offer the opportunity to measure the dust emission potential of source surfaces, which provides the opportunity to investigate the

geomorphic units responsible for dust generation in detail. Process data generated at the sub-landform scale can be used to validate the dust emission potential mapping output produced. The objective of this paper is to use the high-resolution dust source identification from objective 1 to guide fieldwork to determine the emission potential and characteristics of the surfaces that emit dust at a sub-landform scale and use these data to assess proposed dust emission schemes for modelling purposes. In addition, this fieldwork will be used to determine the significant factors that control dust emission from these surfaces to improve testing protocols and as input to dust emission schemes that represent erodibility.

1.6.3.3 Objective 3: Dust sampling and characterisation

The mineralogy and size of the emitted dust determine the environmental impact and distance travelled. Different minerals have been shown to have different effects. For example, the deposition of iron-rich dust has been linked to an increase in ocean photosynthetic production (i.e. primary production). In addition, the size of the particles could play a role in the availability of the iron, as finer particles will have a larger surface area and potentially be larger contributors of iron to the ocean. The accurate characterisation of dust at the source of emission is important for investigating the type and magnitude of the impacts from emitted dust on the climate and ecosystems. An important consideration is the method used to obtain a sample of the emitted dust for analysis. The high-resolution dust source identification from objective one and the sampling and measurement carried out as part of the fieldwork in objective two will be used to compare different measurement and sampling methods to characterise the dust emitted from the Namib Desert source landforms and how this affects the determination of nutrient and fertilisation potential.

1.7 Thesis structure

The three objectives set out in the introduction will be covered in the following three content chapters. The first content chapter (2) deals with the identification of dust emission sources in the Namib Desert at high-resolution using Landsat data for a time period of 27-years. This work also highlights how dust sources evolve through time as a result of significant human modification. Chapter 3 uses the identification of these sources to identify areas that formed part of an extensive field campaign to investigate the surfaces that are highly emissive. Chapter 4 further explores the dust emitted from these surfaces and the methods used to sample and measure these sediments and the consequences of these approaches to the characterisation of the dust. The concluding chapter provides an overview of what I have done and what contribution this research has made to the study of aeolian dust. It also details what I have not done as part of this research and makes suggestions for future research endeavours.

All data used in this study will be made available in Figshare once the papers have been published. This data can be accessed with the following link:

https://doi.org/10.25375/uct.c.4081484

Chapter 1 Introduction	**Chapter overview** Chapter 1 provides the theoretical context for this study and sets out the purpose, aims and objectives.
Chapter 2 *Landsat identifies aeolian dust emission dynamics at the landform scale*	**Chapter overview** This chapter focuses on the identification of dust emission sources and provides a high-resolution dust source map of the Namib Desert study area. In addition, it highlights the significant contribution that anthropogenic modification has made to the emission patterns in this region. **Submission details** von Holdt, J.R., Eckardt, F.D. and Wiggs, G., 2017. Landsat identifies aeolian dust emission dynamics at the landform scale, Remote Sensing of Environment, 198, 229-243.
Chapter 3 *Assessing landscape dust emission schemes using combined ground-based process and remote sensing data*	**Chapter overview** Chapter 3 uses the high-resolution dust source identification and ground-based dust emission measurements and surface testing to assess three proposed dust emission schemes for use in modelling as well as the determination of significant factors that control the erodibility of the surfaces that emit dust. **Submission details** Final stages of review by co-authors and submission intended in February 2018
Chapter 4 *Influence of sampling approaches on physical and geochemical analysis of aeolian dust in source regions*	**Chapter overview** This chapter assesses three different sampling approaches for the characterisation of dust guided by the high-resolution source identification. This analysis confirms that careful consideration should be given to the method used to sample entrained dust for determination of the nutrient and fertilisation potential of the sediments. **Submission details** Review in progress by co-authors and submission date not set.
Chapter 5 Conclusion	**Chapter overview** This chapter considers the findings of the study and recommendations are made for future research studies.

1.8 Regional setting

The study area is situated in the Namib Desert in Namibia, which has been identified as one of the major sources of aeolian dust emission in southern Africa (Figure 1-3) (Vickery et al., 2013). Twelve ephemeral rivers traverse the escarpment with a maximum elevation of approximately 2000 masl and flow westward through the Namib Desert towards the Atlantic Ocean (Figure 1-4). The rivers in the larger catchments originate on the escarpment where rainfall in the headwaters averages 350-400 mm/year and generate the flow that reaches the lower river in the low relief Namib Desert. The rainfall becomes insignificant towards the coast dropping to < 25 mm/year, where fog precipitation becomes a significant source of moisture (Eckardt et al., 2013; Gottlieb, 2018). The floods in the rivers seldom reach the ocean resulting in the deposition of silty sediments within the channels and floodplains towards the terminal stages of the rivers and result in convex shaped river profiles (Jacobson et al., 1999). The geology of the river catchments encompasses a variety of rock types (Figure 1-5). The Kuiseb and Omaruru rivers are situated predominantly within Damara sequence rocks dominated by schists and dolomites and granite intrusions. The upper Huab River prominently consists of the granites and gneisses of the Epupa, Huab and Ababis Metamorphic complexes and the Fransfontein Granite Suite. Further downstream the Huab River catchment also encompasses lavas, sandstones and shales of the Etendeka group and the Karoo Supergroup.

The alluvial deposits of the rivers in the central Namib hold important supplies of groundwater and supports urban and industrial development within the region (Jacobson et al., 1995). The towns of Walvis Bay, Swakopmund and Henties Bay all rely on the aquifers of the Kuiseb and Omaruru Rivers for water supply (GCS, 2011). Mining, tourism and fishing are the main industries within the region (MME, 2010), with large amounts of water

abstracted from the aquifers for mining activities (Wassenaar et al., 2013). Tourism within the Namib Desert relies heavily on nature and adventure based tourism (Heinze, 2009) and as a consequence large parts of the area consist of protected areas, such as the Skeleton Coast Park, the Namib Naukluft and Dorob National Park.

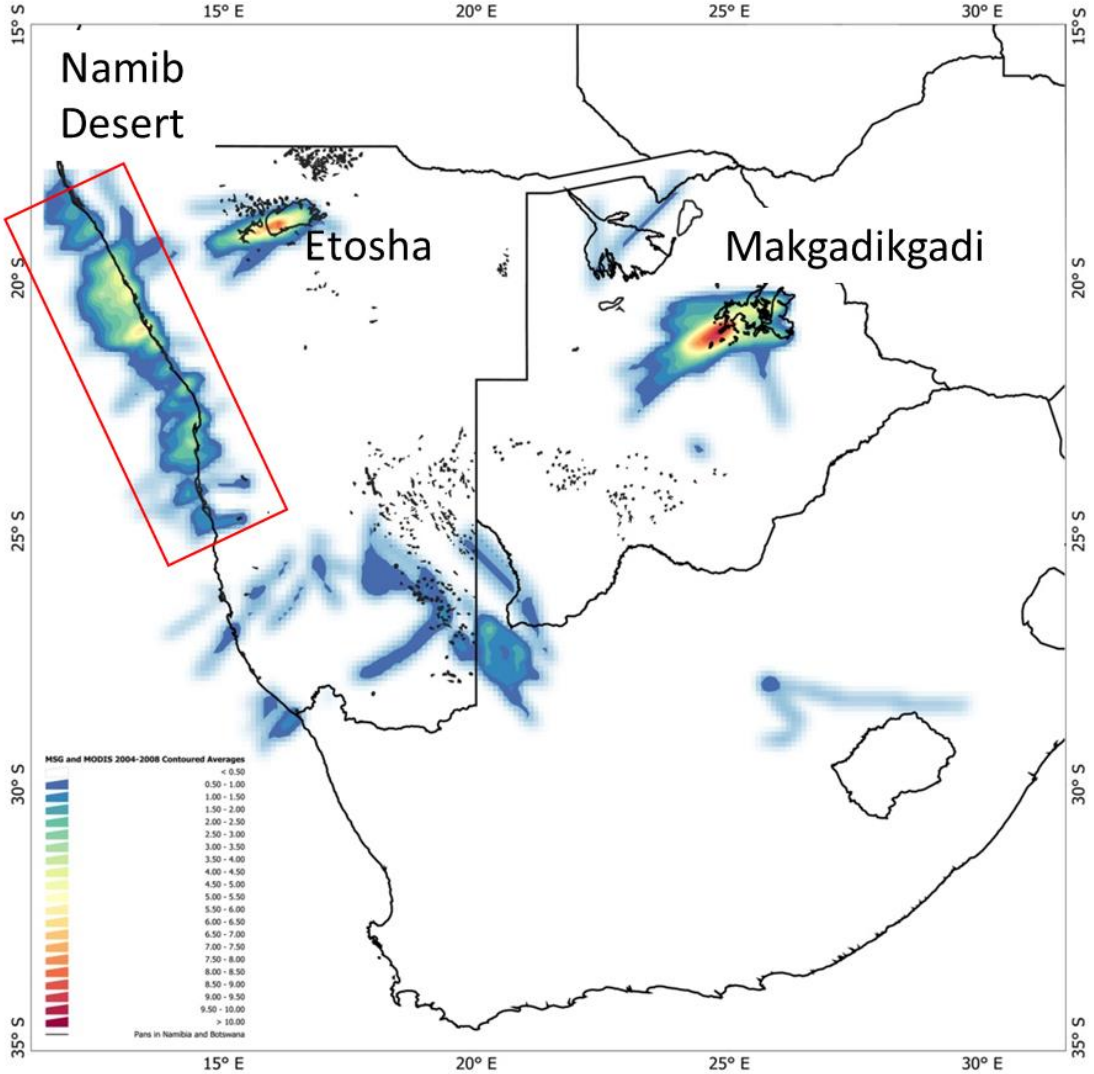

Figure 1-3 Dust plume activity over Southern Africa between 2005 and 2008 as identified by MODIS and MSG satellite imagery from Vickery (2010).

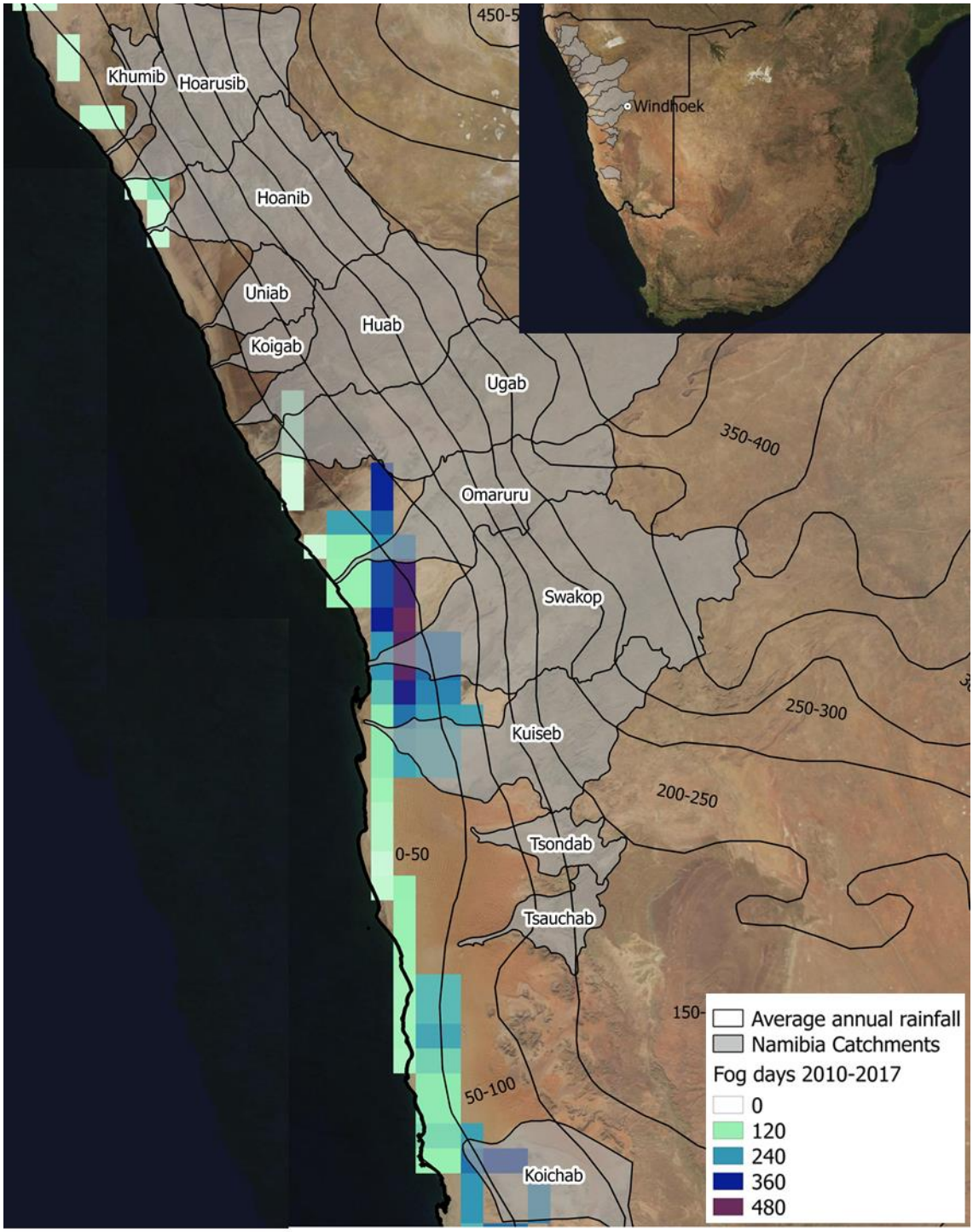

Figure 1-4 Major ephemeral catchments (Mendelsohn et al., 2002), mean rainfall isohyets (mm) (Namibia Resource Consultants, 1999) and number of fog days (Gottlieb, 2018). Background image from MODIS Blue Marble composite.

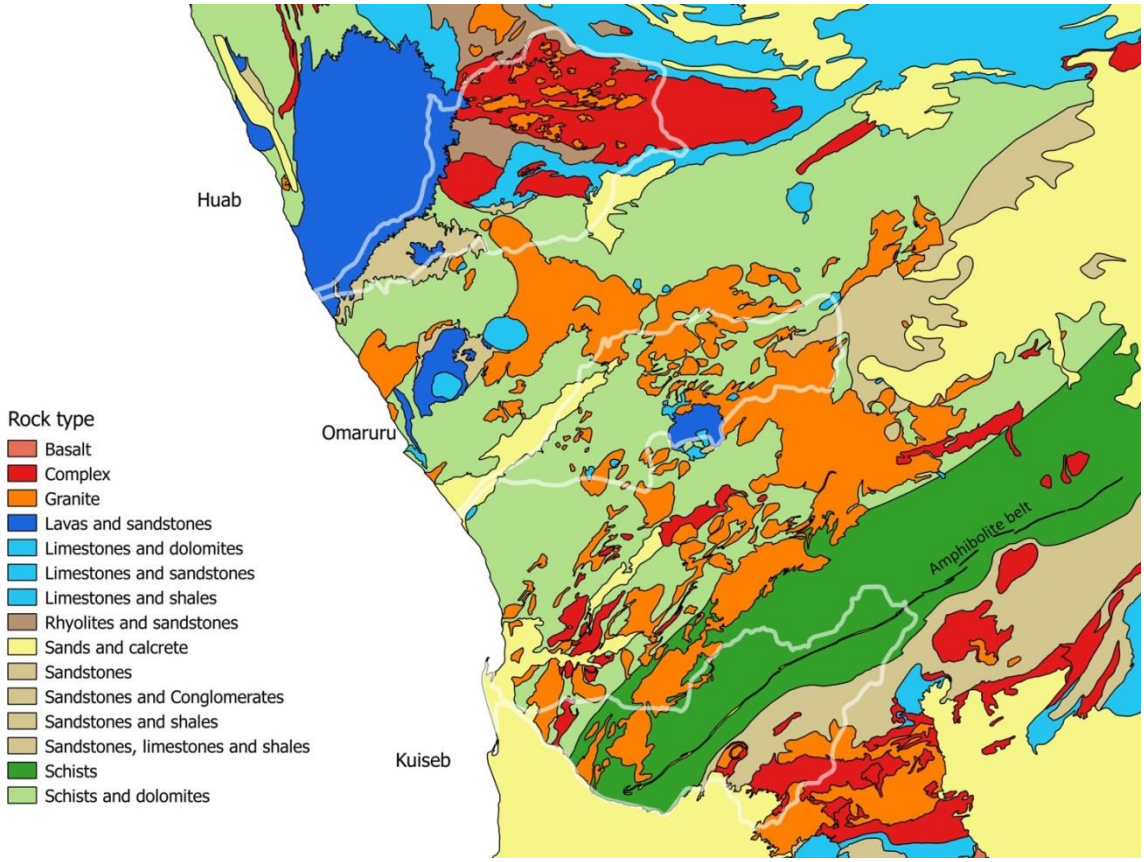

Figure 1-5 Geology of the Namib in terms of main rock types with three river catchments; Huab, Omaruru and Kuiseb(Shapefiles available from http://www.uni-koeln.de/sfb389/e/e1/download/atlas_namibia/e1_download_physical_geography_e.htm).

Chapter 2: Landsat identifies aeolian dust emission dynamics at the landform scale

J R von Holdt[a]

F D Eckardt[a]

G F S Wiggs[b]

[a] Department of Environmental and Geographical Science, University of Cape Town, Private Bag X3, Rondebosch, Cape Town, 7701, South Africa; jrvonholdt@gmail.com; frank.eckardt@uct.ac.za

[b] School of Geography and the Environment, Oxford University Centre for the Environment, University of Oxford, Oxford, OX1 3QY, UK; giles.wiggs@ouce.ox.ac.uk

Status: Published in Remote Sensing of the Environment on 1 September 2017

Citation: von Holdt, J.R., Eckardt, F.D. and Wiggs, G., 2017. Landsat identifies aeolian dust emission dynamics at the landform scale, Remote Sensing of Environment, 198, 229-243.

2.1 Abstract

The modelling of windblown mineral dust emissions remains a challenge. This is in part due to the coarse spatial and temporal resolution of the data on which these models are based, but also because the processes and mechanisms of aeolian dust emission are not well understood. Satellite imagery has been used extensively in the study of dust from the late 1990s with important contributions being made in terms of sources, transport pathways and deposition areas. Using MODIS imagery, the Namib Desert has been identified as one of the largest sources of dust in southern Africa. The opening of the Landsat archive presents the opportunity to investigate these events at a higher spatial resolution (up to 15 × 15 m) than previously possible. Despite the low temporal resolution, we used Landsat imagery to identify 40 major dust episodes over the last 25 years that originated primarily from the ephemeral river valleys and pan complexes, providing new insight into the spatial and temporal evolution of the dust sources from dryland surfaces. Examination of the imagery enabled the identification of local-scale landform source points to direct ground-based testing of the surfaces responsible for dust emission. Emissivity tests were undertaken using a PI-SWERL portable wind tunnel in three of the major dust-producing river systems along the Namib coast, namely the Kuiseb, Omaruru and Huab Rivers. Preliminary observations suggest that human impact on the hydrological systems in two of the river basins, to cater for the increasing demand of water, have dramatically altered the emission patterns of dust. The source areas of greatest dust emission are found to be located on recently deposited fluvial surfaces which are not active in the contemporary environment.

2.2 Introduction

Windblown dust has significant impacts on the earth's climate (IPCC 2013) and biogeochemistry, including the atmosphere, ocean and terrestrial systems (e.g. Knippertz & Stuut, 2014; Maher et al., 2010; McTainsh & Strong, 2007; Soderberg & Compton, 2007; Xuan & Sokolik, 2002). The aeolian dust cycle can be divided into three general stages, namely, the emission of dust from source areas, transport in the atmosphere and deposition of dust both on land and in the ocean (Mahowald et al., 2005). The influence of the emitted dust on other Earth systems depends largely on its physical characteristics including size, mineralogy and morphology of the particles (Formenti et al., 2011). These particle characteristics are in turn determined by the physical attributes of the emissive dust sources. Improving our understanding of the characteristics of dust sources will improve our understanding of how, when and where dust emission takes place. Remote sensing has been used extensively in identifying dust sources (Table 2-1), initially at a global scale and currently at landscape scale resolution.

The major global atmospheric dust sources were first identified with the use of the Total Ozone Mapping Spectrometer (TOMS) Aerosol Index (AI) (Herman et al., 1997; Prospero et al., 2002; Washington et al., 2003). This index is best suited to identifying large and consistent regional dust sources, such as the Bodélé Depression and Etosha Pan. This data set has certain spatial and temporal constraints when applied to atmospheric dust, with the result that it has been most useful in highlighting longrange transport and dispersion, and inter-annual and seasonal variations of higher altitude dust loadings, with a clear bias towards the world's large inland basins. Some of these constraints include the inability to detect dust at low altitudes (< 1–2 km) or non-UV absorbing aerosols, such as sea-salt particles and sulphates (Mahowald, 2004). Consequently, several areas known to emit dust, for example,

the Gobi Desert of Mongolia, Kuwait and the Namib Desert, are not represented in the TOMS AI (Washington et al., 2003) (Figure 2-1 e). The importance of many of these dust sources have been highlighted with the advent of remote sensing data of higher spatial and temporal resolution and utilising different wavelengths. Two of the sensors that have been widely used include the Moderate Resolution Imaging Spectroradiometer (MODIS) and Meteosat Second Generation (MSG) Spinning Enhanced Visible and Infrared Imager (SEVIRI).

Table 2-1 Dust source scale and nomenclature from large-scale regions to surface types and grain size analysis.

Spatial classification (adapted from MacMillan et al. 2000 and Smith et al. 2011)	Map scale:	Dimension	Webb and Strong, 2011		DEM resolution (MacMillan et al. 2000)	Dust data (remote sensing, field observation and laboratory analysis)		Source areas	Global		Southern African	
		m	m			Spatial resolution	Temporal resolution					
Physiographic region	1 000 000	10 000	$>10^4$	Regional	9x9km, 1x1km	13x24km TOMS, 4x4km MSG, 1x1km Seawifs	Daily, 15 minutes, Daily	Large-inland draining basins, agricultural areas	Bodele Depression, Lake Eyre basin	Prospero et al., 2002; Washington et al., 2003	MAK (Botswana), Etosha (Namibia), Kuiseb River (Namibia), Free State (RSA)	Eckardt and Kuring, 2005; Wiggs and Holmes, 2011; Vickery et al., 2013
Physiographic system	100 000	1 000	10^3	Landscape	100x100m	250x250m MODIS	Twice daily	Lakes, alluvial systems, stony surfaces, aeolian systems (PDS as per Bullard et al. 2011)	Strzelecki dunefields (Australia), alluvial deposits and floodplains of the Channel Country (Australia)	Bullard et al, 2011; Lee et al., 2012	Kuiseb river delta (Namibia)	Vickery and Eckardt, 2013
Landform type	10 000	100	10^2	Plot	10x10m	15x15m Landsat	16 days	Lake margins, active river channel, delta terraces			**Current study**	
Landform element	1 000	10	10^1		5x5m	Fieldwork		Landforms and surface characteristics	Playa salt crust, aeolian ripples, silt crust, biological crust, stone pavements	Bacon et al., 2011; King et al., 2011; Sweeney et al., 2016; Wang et al., 2012		
Surface type	100	<1	$<10^{-2}$	Grain		Fieldwork, Laboratory						

MSG-SEVIRI data has a better spatial and temporal resolution than TOMS (Table 2-1) with the infrared wavelength channels being suited to detect dust as a result of the temperature difference between the dust and the land/ocean surface (Schepanski et al., 2007; Schepanski et al., 2012). Although the spatial resolution still limits the identification of dust sources at a regional scale, the 15-minute data acquisition is one of the main advantages of this sensor. This allows the dust plumes to be tracked from the source region and for each event to be linked to meteorological conditions as the dust event progresses. The MSG infra-red data performs better over land than over the ocean or adjacent to coastal regions due to the decreased temperature differential between the dust and water; and the large influence of columnar water vapour (Brindley et al., 2012).

MODIS is suitable for studying aeolian dust activity, either by using true colour imagery, taking advantage of the colour difference between the land/ocean surface and the dust (O'Loingsigh et al., 2015; Vickery et al., 2013) (Figure 2-1b), or using spectral techniques based on brightness temperature differences between different wavelength bands to enhance the dust signal (Baddock et al., 2009; Bullard et al., 2008; Miller, 2003). The higher spatial resolution of the VIS bands means that sources of individual events can be identified at a landscape scale and inventories of commonly emitting source areas can be determined. In addition, the twice-daily overpass (Terra and Aqua) provides enough coverage to create a time series of dust events from specific landscapes, allowing comparisons of dust emission frequency to be made between different sources. However, this method of dust source detection also has limitations, particularly when using simple true colour composites. Lee et al. (2009) point to the fact that many dust sources are in fact small areas and not discrete points. Furthermore, a certain amount of subjectivity is involved in selecting these areas, especially when the plumes are faint or the images not clear. Despite the moderate spatial resolution of c. 250 m, the effective resolution of plume detection is in the order of ≈ 10 km

(Bullard et al., 2008). Another limitation is that the identification, or pinpointing, of an emitting part of the land surface, does not provide any measure of the intensity of the emission at each eroding point. Lastly, O'Loingsigh et al. (2015) in a study from Australia found that dust event frequency, according to true colour MODIS images, was significantly underestimated when compared to data from a near-surface integrating nephelometer, due to its temporal resolution and cloud cover.

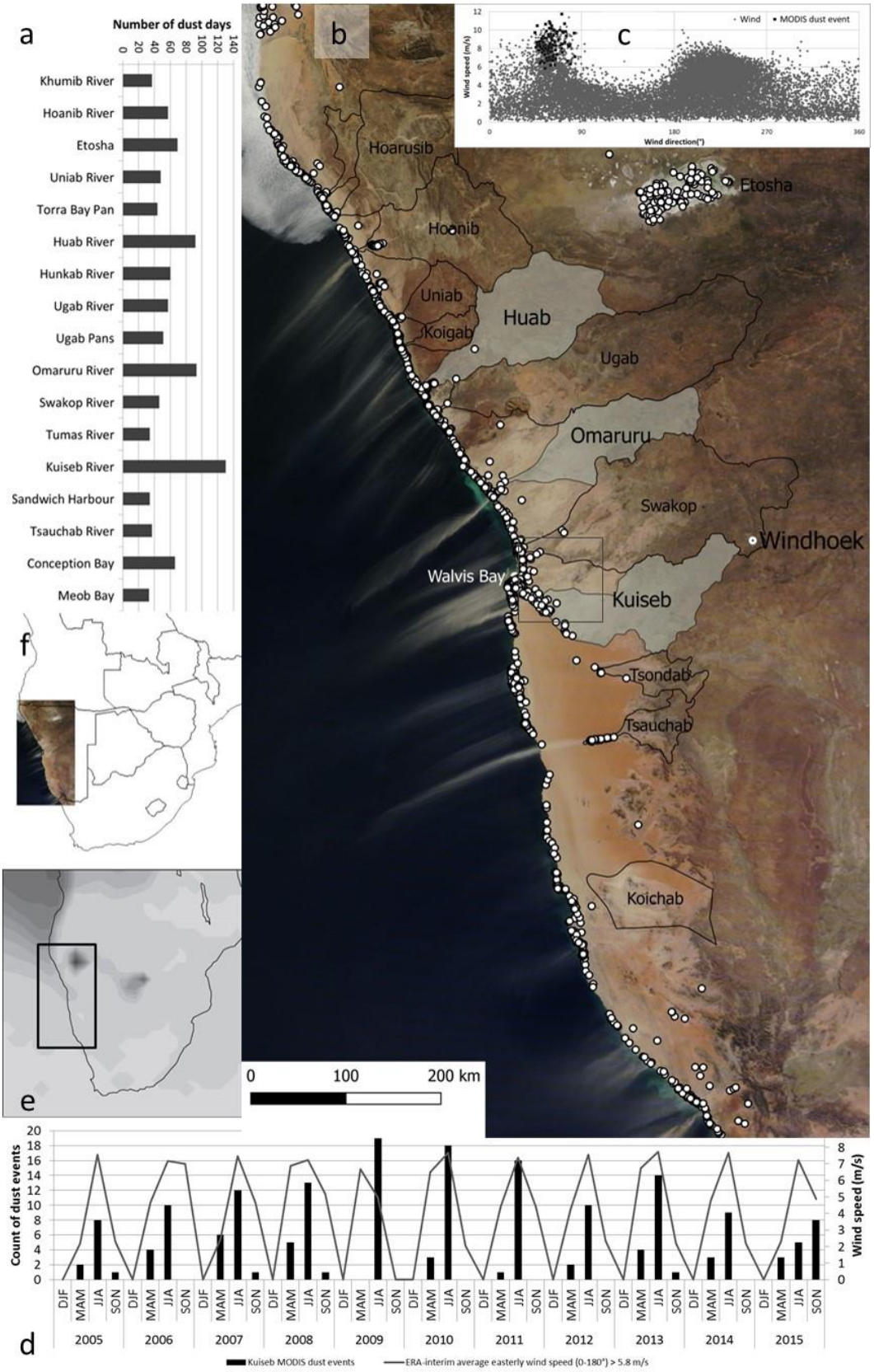
a
Number of dust days
0
20
40
60
80
100
120
140
Khumib River
Hoanib River
Etosha
Uniab River
Torra Bay Pan
Huab River
Hunkab River
Ugab River
Ugab Pans
Omaruru River
Swakop River
Tumas River
Kuiseb River
Sandwich Harbour
Tsauchab River
Conception Bay
Meob Bay
b
c
Wind
MODIS dust event
Wind speed (m/s)
Wind direction(°)
Hoarusib
Etosha
Hoanib
Uniab
Huab
Koigab
Ugab
Omaruru
Swakop
Windhoek
Walvis Bay
Kuiseb
Tsondab
Tsauchab
Koichab
0
100
200 km
f
e
d
Count of dust events
Wind speed (m/s)
DJF
MAM
JJA
SON
2005
2006
2007
2008
2009
2010
2011
2012
2013
2014
2015
Kuiseb MODIS dust events
ERA-interim average easterly wind speed (0-180°) > 5.8 m/s

Figure 2-1 Dust emission from Namibia. (a) Dominant Namibian dust sources according to MODIS from 2005-2015 with dust days greater than 30 (b) MODIS Terra true colour composite for 17 June 2010 (c) Wind speed versus wind direction. Dust events identified with MODIS are only associated with winds from the north-east quadrant. Grey dots are wind events from Era-Interim and black dots are MODIS events for corresponding time step (d) Time series for the dust events identified with MODIS and average seasonal easterly wind events > 6 m s^{-1} for the Kuiseb River (Era-interim data extracted for Kuiseb area as indicated with box) (e) TOMS identified Etosha and MAK as main sources, but not the Namib coast (figure from Washington et al., 2003) (f) Placement of larger study area within southern Africa. River catchment shapefile from Mendelsohn et al. (2002).

Notwithstanding these limitations, several studies have attempted to link MODIS identified dust sources (as geographical coordinate points) with geomorphology and land use/cover for various regions (Baddock et al. 2011, Hahnenberger et al. 2014, Lee et al. 2012, Vickery et al. 2013). In these studies, the geomorphological classification and land use/cover categories used to determine the land surface that each emission point was associated with were identified with a combination of topographic, soil and geological maps, high-resolution satellite imagery, aerial photography and field verification where possible. An example of such a classification is the preferential dust source (PDS) scheme (Baddock et al., 2016) developed by Bullard et al. (2011). Although an important step forward, the dust sources identified with the medium resolution satellite imagery of MODIS and the geomorphological units associated with them are still not at a high enough spatial resolution to identify the specific landforms responsible for emission.

Only a very few of the geomorphological units that have been identified as dust sources have been the subject of intensive field observation and measurement attempts to better understand and quantify the processes of dust emission (Bryant, 2013; Haustein et al., 2015). This is because the resolution of dust source mapping from remote sensing data to date, still only provides a landscape scale assessment (≈ 10 km) of where the dust-producing surfaces are located. Using these data to guide the location of field observation and measurement involves a substantial jump in scale, as measuring equipment for data collection is often situated within or downwind of a particular landform element deemed to act as a dust source (considering scales from ~ 10 m to ~ 100 m). Selecting sites for field observation therefore involves interpreting the landscape on the basis of the available knowledge of the landforms present and making a judgement regarding their emission potential based on factors that affect dust production, such as sediment supply and availability; and the fluvial-aeolian interactions of these within a system (Field et al., 2009; Bullard and McTainsh, 2003).

The dust source regions and landscapes of southern Africa have been studied by Eckardt et al. (2001) by means of hand-held Space Shuttle photography, by Eckardt and Kuring, (2005) with the aid of SeaWiFS and by Vickery et al. (2013) using MODIS and MSG (Table 2-1). The TOMS Aerosol Index identified the dry lake beds of the Makgadikgadi pan complex and Etosha Pan as southern Africa's major sources (Prospero et al., 2002; Washington et al., 2003). The MODIS imagery used for the study by Vickery et al. (2013) consisted of true colour composites. These images were particularly useful in identifying the Namib Desert coast as an important regional dust source for the period from 2005 to 2008 due to the easily recognisable light dust over the dark ocean. The Namib Desert, on the other hand, was not identified as an important regional dust source using TOMS AI (Figure 2-1e) or MSG. The failure of TOMS AI to detect the Namib Desert as a dust source region is potentially a result of the dust being at low altitude and the likely presence of non-UV absorbing aerosols. Using MODIS, Vickery et al. (2013) concluded that 62% of all detectable plumes from southern Africa for the period from 2005 to 2008 originated from the Namib Desert coastal sources, with dust emission predominantly associated with the strong north-easterly Berg winds from April to August.

The Namib Desert embraces a variety of physiographic systems, including the ephemeral westward flowing river catchments, pan complexes, dune fields and low relief gravel plains. Similar systems have been identified as potential dust sources in many arid regions of the world (Table 2-1). Each of these systems encompasses several landforms, such as the floodplain terraces and active channels of rivers; basins and margins of playas and sabkhas; and stone pavements and wadis of the gravel plains. These landforms are also present in the Namib Desert and some have been shown to have an ample supply of appropriate sized sediments that can be entrained by the wind (von Holdt and Eckardt, 2017; Dansie et al.,

2017c). However, the erodibility and actual contribution of these landforms to the dust load has not been determined.

Landsat, which offers a much higher spatial resolution, has been used to study dust to a lesser extent than other sensors primarily due to its poor temporal resolution (Kaufman et al., 2001; Chavez et al., 2002), such that no studies have systematically used Landsat to identify dust source areas. A dust event captured by Landsat, however, offers the opportunity to investigate the source points in greater detail than has been done in the past. The archive of Landsat imagery made publicly available by the USGS provides an easily accessible platform to search and download these data. Although the temporal resolution is poor (one overpass every 16-days), the 30 × 30 m resolution (15 × 15 m with the panchromatic band for Landsat 8) offers a level of spatial detail not possible with other continually collected satellite data used to date. These images provide the ability to identify with greater accuracy and detail specific landform types and elements responsible for dust emission for wind erosion events captured by Landsat. The ability to identify these dust emitting small-scale source terrains and surfaces means they can be subjected to surface characterisation and dust emission tests using field experiments. One such instrument that has become widely used in dust research is the PI-SWERL portable mini wind tunnel to test the erodibility and emission potential of surfaces in dust source areas (Bacon et al., 2011; Etyemezian et al., 2007; King et al., 2011; Sweeney et al., 2011). The placement of dust measurement and sampling equipment, such as the PI-SWERL, can be optimised based on accurate local-scale dust source identification using Landsat.

The study presented here utilised the higher spatial resolution of Landsat to identify the small-scale geomorphology and landform types that act as dust sources in the Namib Desert. The study area was chosen based on the analysis of MODIS true colour images for an 11-year

period (2005–2008 carried out by Vickery et al., 2013 and 2009–2015 carried out as part of the present study), which identified persistent dust sources from Namibia. Finally, field visits were undertaken to determine the local-scale source points identified with the Landsat imagery and the aeolian dust emission potential of the sites was determined using a PI-SWERL portable wind tunnel.

2.3 Methods

2.3.1 Identifying dust source systems

MODIS true colour composites from the Terra and Aqua sensors were used to identify source areas of plumes from Namibia using the same method as Vickery et al., 2013 for the study period from 2005 to 2008. In addition, processed MODIS true colour images (bands 1,2,3) were obtained from the MODIS Rapidfire online facility for the period from January 2009 to May 2012, followed by NASA Worldview up to 2015. The images analysed as part of the study by Vickery et al. (2013) were reanalysed as part of this study to ensure consistency. The source points for visible dust on images were identified by placing a point where the plume origin was judged to be and attributing these points to a physiographic system, such as specific catchment areas or pan complexes. These source areas highlighted the most active dust source systems within the Namib Desert which then provided the focus areas for the higher spatial resolution Landsat analysis.

2.3.2 Identifying landform types responsible for aeolian dust emission

The available Landsat archive accessible with LandsatLook Viewer (http://landsatlook.usgs.gov/) was studied to identify images in which windblown dust was visible. Over 2,000 images were examined as part of this study available on the online archive, consisting of a subset of Landsat 1-8 images. Cloud cover was restricted to a maximum of 20 %. Full resolution Level-1 product individual band files were downloaded for images with visible dust and stacked using Erdas Imagine 2015-16 (Leica Geosystems, Atlanta, Georgia, USA). The same software was used for Landsat 7 ETM+ and 8 OLI images to merge the high-resolution panchromatic band with the medium-resolution multispectral data to improve the resolution of the multispectral images from 30 m to 15 m. Dust was

detected on selected Landsat 7 images with SLC-off, but these were excluded from the analysis for areas where the imagery did not provide complete coverage. Various band combinations were tested for optimal identification of plume origin, of which two combinations were selected and used for all source point identification: the true colour (3,2,1 for Landsat 5 and 7 and 4,3,2 for Landsat 8) and false colour image comprising bands 7,4,2 for Landsat 5 and 7; and bands 7,5,3 for Landsat 8. In addition to identifying dust plume origins, the false colour image was particularly useful in distinguishing different landforms within the landscape. Four of the Landsat 5 scenes used (listed in the supplementary section), lacked the geometric accuracy to be perfectly aligned and had to be geo-rectified. The maximum error encountered amounted to approximately 500 m. This problem occurs for some of the older scenes as a result of the use of predictive instead of definitive ephemeris data to record the position and velocity of the satellite at the time the data is collected (USGS EROS User Services, pers com, https://landsat.usgs.gov/what_is_definitive_ephemeris.php). This information is available in the scene metadata.

The Landsat images were interrogated using various local contrast enhancements by applying linear minimum and maximum histogram stretches with Erdas Imagine, both over land and over the ocean. Performing local area histogram stretches to specific areas and around specific features provided maximum clarity for plume source point identification. A min-max stretch over the ocean resulted in images which showed the full extent of the dust plumes. Source points were identified manually and classified according to two categories. Firstly, as "certain" for source points that could be clearly identified and for which the plume origin could be associated with a specific landform type or element. Secondly, as "uncertain" if a plume was visible, but the plume origin could only be linked to a physiographic system and not linked to specific landform types or elements.

A list of all the Landsat imagery used as part of this study is provided in section 7.1. All data are available in the supplementary section of the online version of this article.

2.3.3 Dust emission frequency: reanalysis wind data

ERA-Interim 10-metre wind speed data corresponding to the 11-year MODIS record was used to compare the frequency of MODIS dust events to the frequency of wind events with sufficient friction velocity to entrain dust for the Kuiseb River catchment (Dee et al., 2011). This reanalysis data set was chosen as it has a better correlation with MODIS deep blue aerosol optical depth (AOD) as a measure of dust loading in the atmosphere than NCEP/NCAR reanalysis 1 data (Kjeldsen et al., 2014). For the purposes of this comparison, the threshold friction velocity was taken as the minimum wind speed at 10 m for which dust was detected with MODIS (6 m s^{-1}). Six-hourly horizontal (u10) and vertical (v10) wind components were downloaded from the ECMWF Public Datasets web interface at 0.125° resolution for the study site from 2005 to 2015. Data for specific areas were extracted and mean values across latitude and longitude computed for every 6-hour time interval (12am, 6am, 12pm and 6pm) using Climate Data Operators (CDO) software v1.7.2 (http://www.mpimet.mpg.de/cdo). Calculated u10 and v10 vector components were corrected with the relevant off-set and scaling factors, from which wind speed and wind direction were computed. This data set was also used to determine the wind speed on an event basis where indicated.

2.3.4 Characterising dust potential of surfaces

Fieldwork was carried out in selected areas based on the MODIS and Landsat dust source point analysis. The Portable *In-Situ* Wind ERosion Lab (PI-SWERL) (Etyemezian et al., 2007; Sweeney et al., 2011, 2016) was used to test the dust emission potential of landform elements guided by the most certain Landsat source points. The PI-SWERL consists of a

cylindrical chamber which is placed over the test surface with a shear stress applied to the surface by means of a rotating annular ring set at a fixed height of 0.07 m from the surface. Once the applied shear stress exceeds the entrainment threshold any emitted dust is monitored by a DustTrak monitor, mounted on top of the chamber, using a light scattering technique to measure the concentration of PM_{10} (particles with optical diameter $\leq$ 10 μm). The PM_{10} size range has traditionally been regarded as the most important fraction due to its long-range suspension and transport potential and recognition of its influence on air quality and potential health impacts (Goudie, 2014; Prospero, 1999; US EPA, 1995). Estimates of dust flux from the PI-SWERL have been shown to correlate well with large field wind tunnels (Sweeney et al., 2008). The small size, portability and ease of use of the PI-SWERL enables the testing of many more surfaces than previously possible and in locations that are difficult to access.

Experiments with the PI-SWERL consisted of between 3 and 7 replicates with all runs conducted as a ramp test up to 3300 rpm, at a constant flow rate and a run time at maximum rpm of 180 seconds. A rotation speed of 3300 rpm provides a friction velocity, u* of between 0.55 and 0.58 m s^{-1} for the majority of the surfaces tested as part of this study, where the effective friction velocity depends on the surface roughness of the test surface (Etyemezian et al., 2014; PI-SWERL manual v1.3, 2011). A constant rotation speed was chosen to compare emissions from all the surfaces at different sites tested. This friction velocity is in agreement with previous studies that used the PI-SWERL (King et al., 2011; Sweeney et al., 2011) and exceeds the threshold at which saltation is initiated (Fryberger, 1979; Stout, 2007). Saltation in an aeolian context is the movement of sand-sized particles by wind in short hops or leaps. This mechanism has been regarded as essential for dust emission as the saltating sand grains bombard the surface, and consequently results in the release of dust-sized particles for suspension. Direct aerodynamic entrainment of small dust-sized particles has thus far been

regarded as insignificant in comparison due to the binding strength of interparticle cohesive forces (Shao et al., 1993).

PI-SWERL measurements were conducted at the end of the dry winter dust season in September 2015. Rainfall in the Namib Desert averages less than 25 mm/year towards the coast and occurs predominantly in conjunction with sporadic convective summer thunderstorms (Eckardt et al., 2013). Fog occurs more regularly than rain in the Namib Desert, but the quantity of fog-water precipitation on a daily basis is very low (Lancaster et al., 1984). The average annual precipitation (rain and fog) for 2015 at the Kuiseb delta was 12 mm

(http://www.sasscalweathernet.org/weatherstat_infosheet_we.php?loggerid_crit=E7631). With the highest amount of precipitation recorded in January (4.9 mm, 40 % of the annual precipitation) and September recording no precipitation events. Further north at the Omaruru River, the average annual precipitation for 2015 was even less at 9.1 mm, with September recording only 0.8 mm (http://www.sasscalweathernet.org/weatherstat_infosheet_we.php?loggerid_crit=31200). Unfortunately, there are no monitoring stations close to the Huab River to obtain accurate amounts, but conditions will be similar to that reported for the Kuiseb and Omaruru regions. This is in stark contrast to the headwaters of these rivers situated on the escarpment, where rainfall increases to approximately 350 mm/year and flow in the rivers only occur when sufficient rain has fallen in the highlands predominantly in summer (Jacobson et al., 1995). The quantity and extent of the floods vary, but they rarely reach the Atlantic Ocean. The Kuiseb River has only reached the ocean 18 times in the last 180 years, with the last flood to reach that far occurring in 2011 (data from Gobabeb Research Station, Morin et al., 2009). Testing was only conducted during the hottest part of the day when all dew present from the previous night had evaporated.

2.4 Results

The extended 11-year record from 2005 to 2015 identified the Kuiseb, Omaruru and Huab River catchments as the three dustiest systems within the Namib Desert (Figure 2-1 a and b). The events identified with MODIS true colour images take place only in conjunction with high magnitude north-easterly winds (Figure 2-1 c), which occurred predominantly during winter (JJA) as noted by Vickery et al. (2013). Figure 2-1 d shows the number of dust events compared to the 10 m easterly winds according to Era-Interim greater than 6 m s^{-1} for the same period and highlights the seasonality associated with dust events identified with MODIS. Winds of this magnitude occurred for 16 % of the 11-year period, with 11.2 % from the south-west and 4.1 % from the north-east (Table 2-2).

The higher frequency of dust emission events from the Kuiseb, Omaruru and Huab catchments increased the likelihood of dust events being captured by Landsat's repeat coverage of every 16 days. Consequently, Landsat images used from the available archive focused on these areas and included images taken along three paths (179, 180 and 181) and five rows (73-77) from 1972 onwards (Figure 2-2 b). A total of 40 images with visible dust events were found, starting from 1989 up until 2016 and include images from Landsat 5, 7 and 8 (listed in the supplementary section). The image from 21 July 1989 (Figure 2-3) was excluded from this analysis as it was deemed to be an extreme event and the source points associated with this image were therefore regarded as potential anomalies.

The Landsat source points identified from 39 event days for the most prolific systems are depicted in Figure 2-2 (a). At this regional scale, the dust source map does not appear very different from the MODIS source map (Figure 2-1 b). Using the superior spatial resolution of Landsat and zooming into the local-scale is where the advantage of using this sensor becomes apparent. Figure 2-2 insets 1 – 6 shows Landsat images for selected events, with the clearly

visible individual dust plumes and the source points that were identified for that specific event. Drawing conclusions regarding the frequency of emission from various landform types and elements between various systems using the Landsat source point classification should be done with caution due to the poor temporal resolution of these data. Notwithstanding, the Kuiseb, Omaruru and Huab Rivers provided the largest number of dust events identifiable in Landsat and, more importantly, consistently emitted dust from the same landforms. These data are in agreement with MODIS due to the closeness of the Landsat and MODIS Terra overpass (equatorial crossing time of 10:00 AM for Landsat and 10:30 AM for Terra).

The following sections identify the dust sources within each river valley. However, it should be noted that although this study uses the river catchments as the basis for classifying the dust source points, the specific emission surfaces are not exclusively of fluvial nature. Some of the identified points of emission do not strictly fall within the hydrological catchment of the rivers, but they do receive significant local aeolian input from the fluvially deposited sediments of the rivers and for the sake of this analysis are classified as falling within the specific river's sphere of influence.

Table 2-2 Wind events according to Era-interim capable of producing dust for all directions. Note that dust events recorded by MODIS were only detected with the north-east wind. Wind events exceeding 6 m s^{-1} occurred for 16 % of the time in the 11-year period. Era-interim data can be used to determine potential dust days, which can then be linked to any satellite sensor's record by the corresponding overpass for a specific area.

Wind speed ($m\ s^{-1}$)	Number of wind events				NE only		
	NW	SW	SE	NE	Wind events at night > 6 $m\ s^{-1}$	Number of MODIS dust events	Wind events for which dust detected (%)
All	1555	8059	2894	3560			
6-8	50	1765	17	457	108	74	16 %
8-10	2	40	1	184	58	91	49 %
+10	0	0	0	14	3	11	79 %
Total > 6	52	1805	18	655	169	176	27 %
					26 %		
Total % > 6 of total	0.3 %	11.2 %	0.1 %	4.1 %			

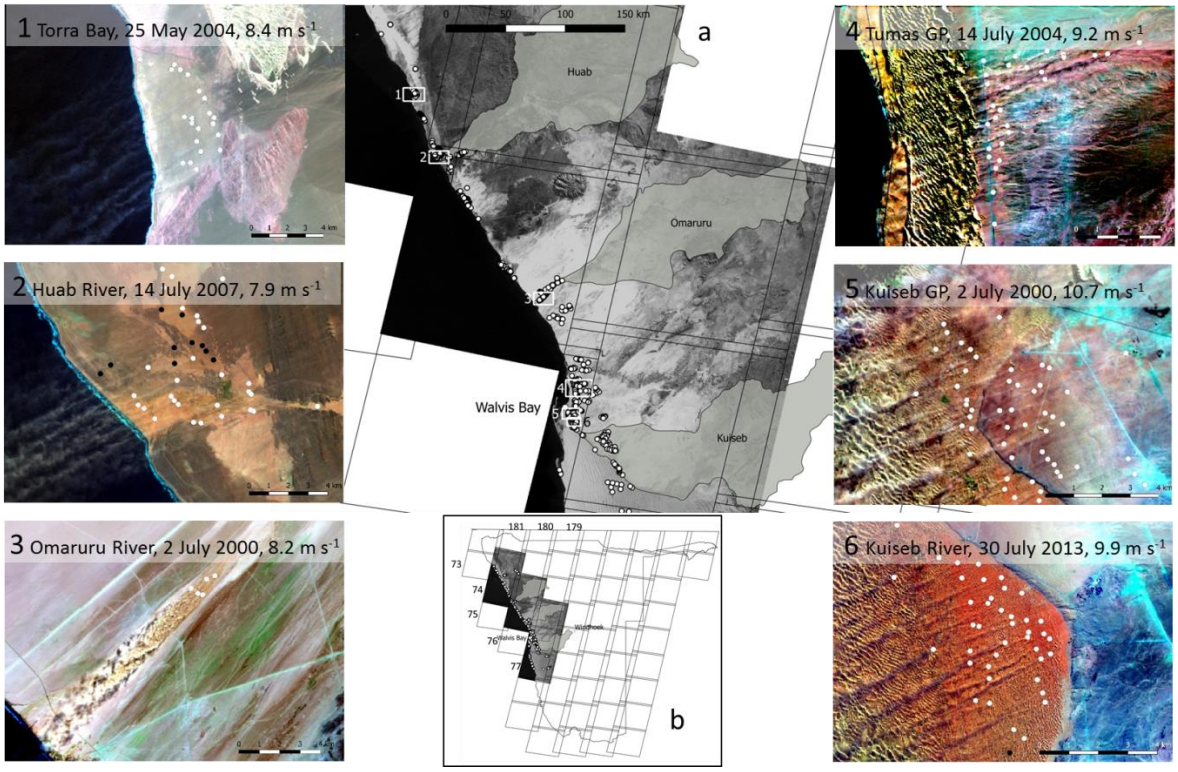

Figure 2-2 Dust emission sources identified using Landsat from 1990 to 2016. Insets 1-6 are examples of false colour dust images (bands 742 and 753) and source points identified, with corresponding Era-interim maximum wind speed on the day of the event. White dots are "certain" source points and black dots "uncertain". All source points are provided in the supplementary section.

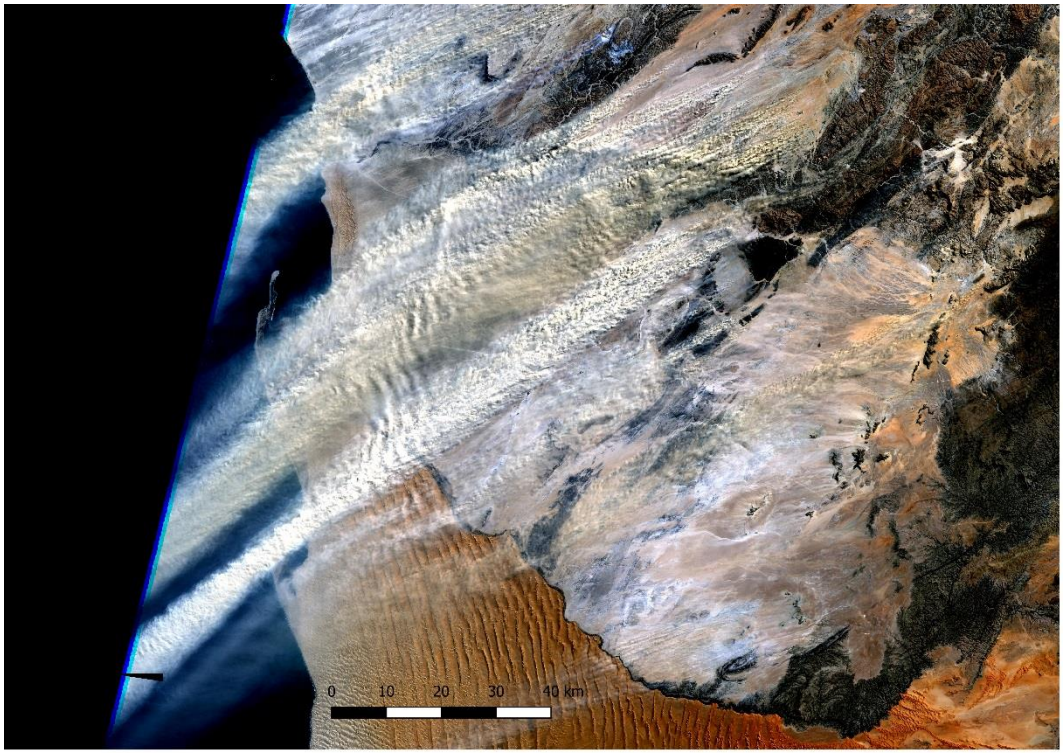

Figure 2-3 An extreme dust event captured by Landsat 5 on 21 July 1989. This event is known as the Superstorm of 1989 and Era-interim wind data for this day shows 10-metre wind speeds of up to 40 m s^{-1}, compared to a maximum of 12 m s^{-1} from 2005 to 2015.

2.4.1.1 Kuiseb river dust sources

The Kuiseb River is the most active catchment with the highest percentage of the MODIS dust images for Namibia showing dust originating from this area (on 58 % of all images showing dust). Figure 2-4 shows a shift of dust source points, with most of the Landsat points originating from a northern arm of the delta, whereas the MODIS source points from the period of 2005-2008 (Vickery et al., 2013) were all placed in the southern arm. The gravel plain further inland produced 20 % of the dust source points identified with Landsat for the Kuiseb landscape, compared to 67 % of the dust source points from the Kuiseb delta northern arm. Only 3 % of the plumes could be placed in the river channel, whereas the precise landform origin of 10 % of the plumes could not be determined and were therefore classified as "uncertain". The gravel plain consists of both stone pavements and ephemeral dry washes or wadis intersected by playas. The northern arm of the delta has remained a consistent source of dust with dust plumes visible from 1989 to the present. Another persistent landform identified within this region is the Tumas River terraces (Figure 2-4) situated just east of the dune corridor between Walvis Bay and Swakopmund.

The PI-SWERL analysis conducted at a selection of source points identified with Landsat not only provides confirmation of these landforms as significant dust sources, but also the potential mechanism of dust emission from these surfaces. The depositional silt crusts of the terraces both in the Kuiseb and the Tumas are the predominant sources of fluvially deposited fine material that are eroded and suspended during high magnitude wind events. The highest emissions recorded by the PI-SWERL were from between the silt terraces in the Kuiseb northern arm (Figure 2-5 line a). The consolidated silt crusts of the terraces are also able to emit significant quantities of dust, but primarily with the presence of sand for sandblasting. Figure 2-5 lines (b) and (c) show the PM_{10} concentrations respectively from the Kuiseb and Tumas terraces with abundant quantities of sand present, compared to reduced emissions with

negligible amounts of sand present (line d). The gravel plain stone pavements provided some of the lowest emissions tested during this study (an average of 5 mg/m^3) when armoured with a dense gravel cover (> 30 %), but had much higher emission with low-density gravel covers (< 30 %) (an average of 28 mg/m^3). Disturbed stone pavements were shown to potentially emit substantial quantities of dust (75 mg/m^3). The dust emission potential of the stone pavements of the gravel plain will be discussed as part of a separate study.

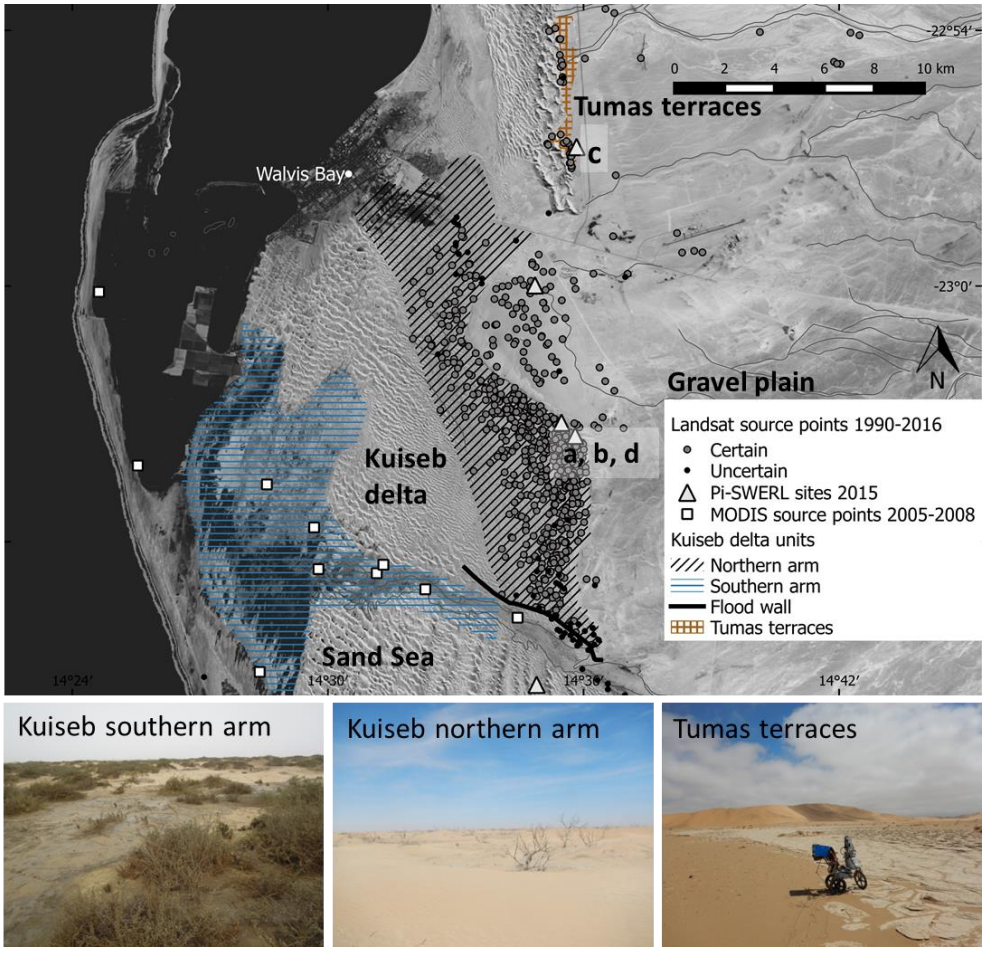

Figure 2-4 Dust emission sources identified using Landsat imagery in the Kuiseb River delta. The emission points are situated predominantly in the abandoned northern arm of the delta, whereas the MODIS source points from 2005 – 2008 (Vickery et al., 2013) were placed in the fluvially active southern arm. The northern arm was blocked off in 1961 to prevent flooding in Walvis Bay and resulted in an extensive area of abandoned terraces with an available supply of depositional sediments. The PI-SWERL sites from field observations conducted in September 2015 are indicated with triangles a, b, c and d correspond with PI-SWERL results and inset photo presented in Figure 2-5.

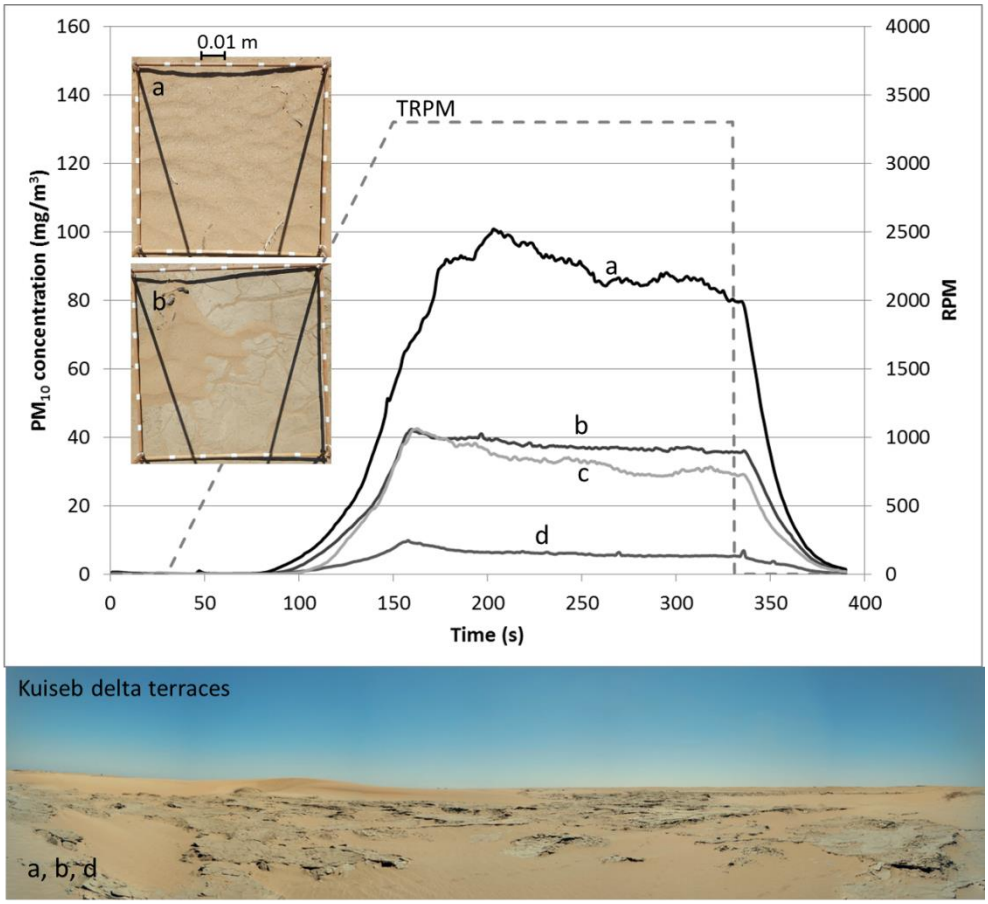

Figure 2-5 Dust emission potential of the Kuiseb River. The PI-SWERL results show the most emissive surfaces are the unconsolidated material between silt terraces (a), followed by the silt crusts when there is an abundant supply of sand present (b: Kuiseb northern arm and c: Tumas). In contrast, significantly reduced emissions are produced from silt crusts with negligible sand present (d). Photo insets show the surfaces from the Kuiseb before a PI-SWERL run. Panorama shows the silts and sands of the Kuiseb northern arm terraces. Photo of the Tumas terraces corresponding to (c) is included in Figure 2-4. TRPM denotes the targeted RPM produced by the PI-SWERL.

2.4.1.2 Omaruru River dust sources

84% of the identified emission points in the Omaruru River catchment were located within the floodplain channel in the downstream section of the river (Figure 2-6). The position of the source points remains within the river channel, initially originating from the most downstream position in the river where it is still aligned with the direction of the predominant high magnitude north-east winds. However, the source points undergo a shift, first moving upstream and gradually downstream to its present position over a period of 20 years. This change of source areas through time is shown in Figure 2-6. The field visit to the present Omaruru Landsat source points in the river channel revealed that the river channel and floodplain consists almost entirely of two surfaces, namely nebkhas and gravel-covered, degraded silt crusts. The PM_{10} concentrations emitted in the PI-SWERL tests from the gravel-covered silt crusts proved to be negligible (Figure 2-7 line b), compared to significant emissions from the nebkha fields (line a). Many of the nebkhas had sparse and dying vegetation cover, providing very little protection from the wind. In certain areas, what appeared to once be nebkhas only show the remnants of dead vegetation, including large trees (Figure 2-6, photo inset).

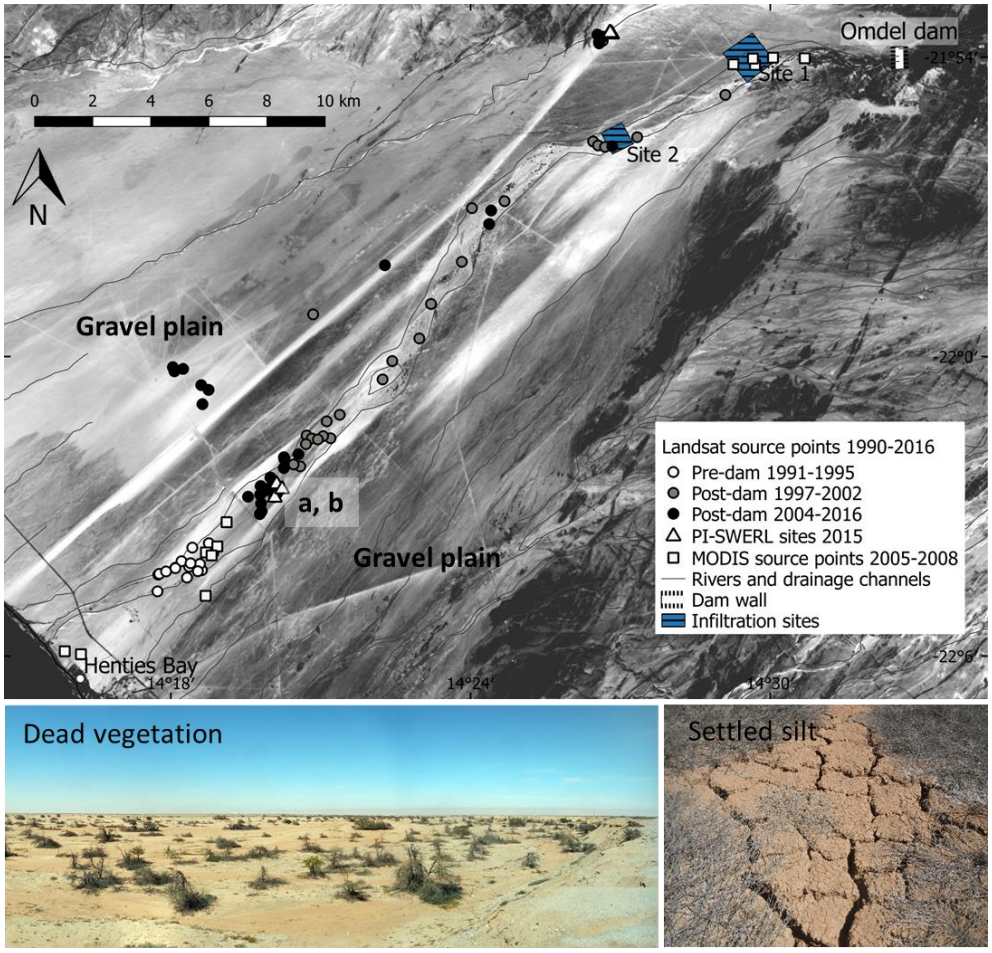

Figure 2-6 Dust emission sources identified using Landsat imagery for the Omaruru River. This shows a longitudinal evolution of emission sites with time, consequent upon building of the Omdel dam in 1995. The surfaces responsible for dust have moved from downstream before the modification, to upstream afterwards and then appear to be gradually moving downstream as the sediment supply is depleted. Photos show the dead vegetation after being starved of water and sediments, and the settled silt collected at the dam wall. The PI-SWERL sites a and b correspond with PI-SWERL results and inset photo (for a) in Figure 2-7.

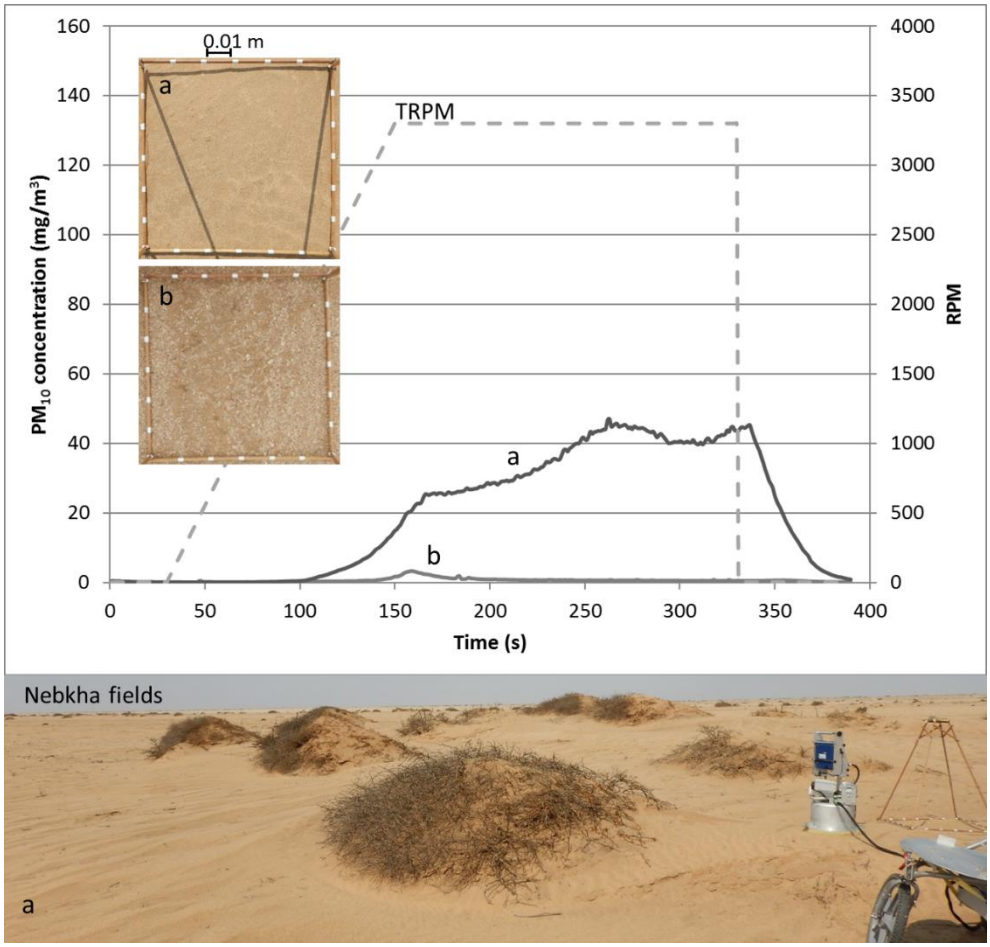

Figure 2-7 Dust emission potential of the Omaruru River. Graph and inset (a) shows PM_{10} concentrations from the nebkha fields in the present source area compared to that from the surrounding gravel-covered silt crusts (b). The nebkhas have vegetation that ranges from dead to fairly intact. The surfaces of river channel further upstream consist of the remnants of nebkhas with dead trees, surrounded by gravel lag deposits as shown in photo inset (b). Photo insets of surfaces before PI-SWERL run.

2.4.1.3 Huab River dust sources

The Huab River persistent source points are more widely spread than the previous two river systems and are mainly concentrated around the Huab playa situated to the north of the river (34 %), the delta (16 %), an upstream river channel site (21 %) and the gravel plain within this landscape (29 %). Most of the gravel plain sources are situated just north of the delta and surrounding the playas (Figure 2-8). The PI-SWERL tests from this landscape reveal that the nebkhas and silt crust terraces (with sand present) are the most emissive surfaces in the area (Figure 2-9). The upstream site (at a, b and d) consists of silt crusts on the river terraces that become significant sources of dust in the presence of saltating sand. In addition, the river terraces are covered to a great degree by nebkhas varying in vegetation condition from healthy to completely dead. Much less dust is produced from the active channel, with significantly less dust coming from the occasional and sporadic silt deposits found within the active channel (an average of 29 mg/m^3) and virtually no dust coming from the active channel sands (an average < 1 mg/m^3). The terraces in the delta identified as a persistent dust source area consisted of large areas with no vegetation cover. PI-SWERL tests confirm the possibility of significant emissions from this landform (Figure 2-9 c). Testing done on the Huab playa proved difficult due to the persistent foggy conditions on the coast. Moisture is a significant control on dust emission (Gillies, 2013) and the presence of hygroscopic salts on the pan surface attracts moisture from the atmosphere with high humidity conditions. The diurnal cycle of condensation wetting and drying and fog precipitation along the coast could have a significant influence on dust production from the playas and sabkhas (Reynolds et al., 2007). Further research is needed to investigate the role of fog conditions on dust emission processes.

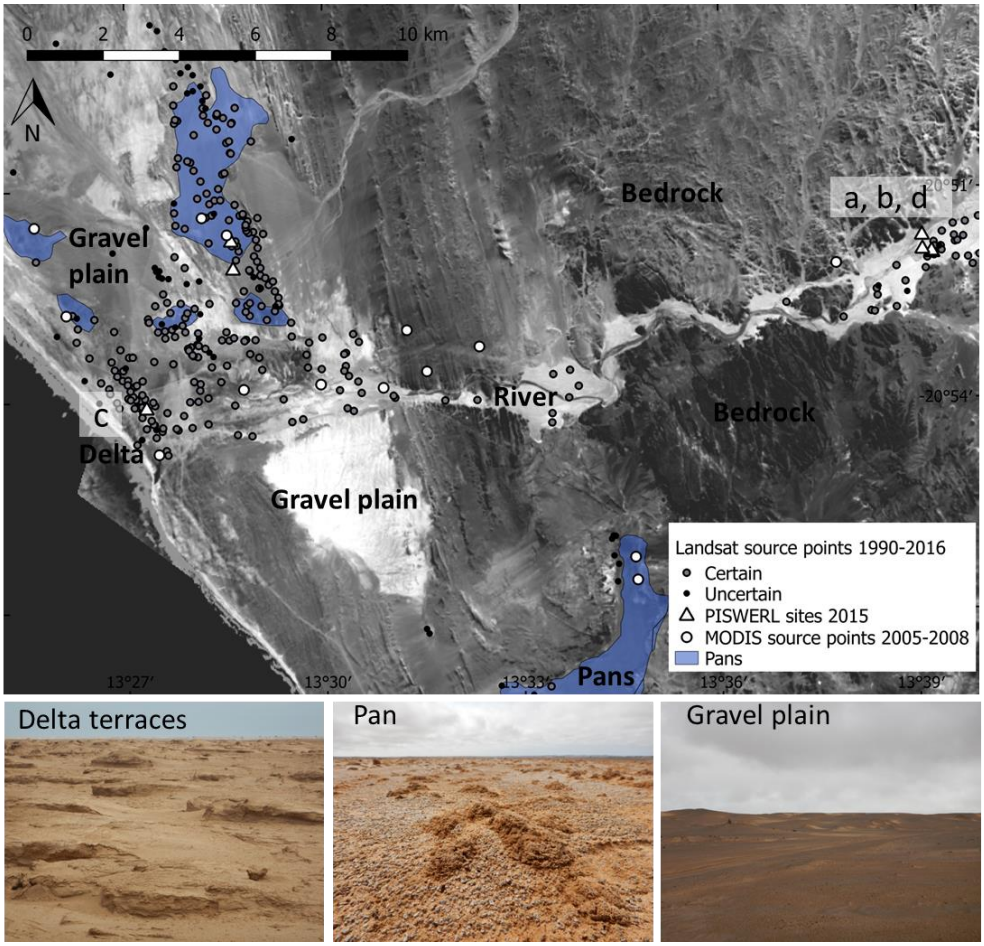

Figure 2-8 Dust emission sources identified using Landsat imagery in the Huab River. The source points are distributed over a greater area, with the upstream section (a, b and d), delta (c) and playas (pan) proving to be consistent sources of dust. The delta terraces that are most emissive are devoid of vegetation. The incised channel's alignment with the high magnitude north-easterly wind potentially plays a role in the emissivity of the terraces in the upstream section of river acting as a consistent source of dust. The PI-SWERL sites a, b, c and d correspond with PI-SWERL results and inset photo (for a, b and d) in Figure 2-9.

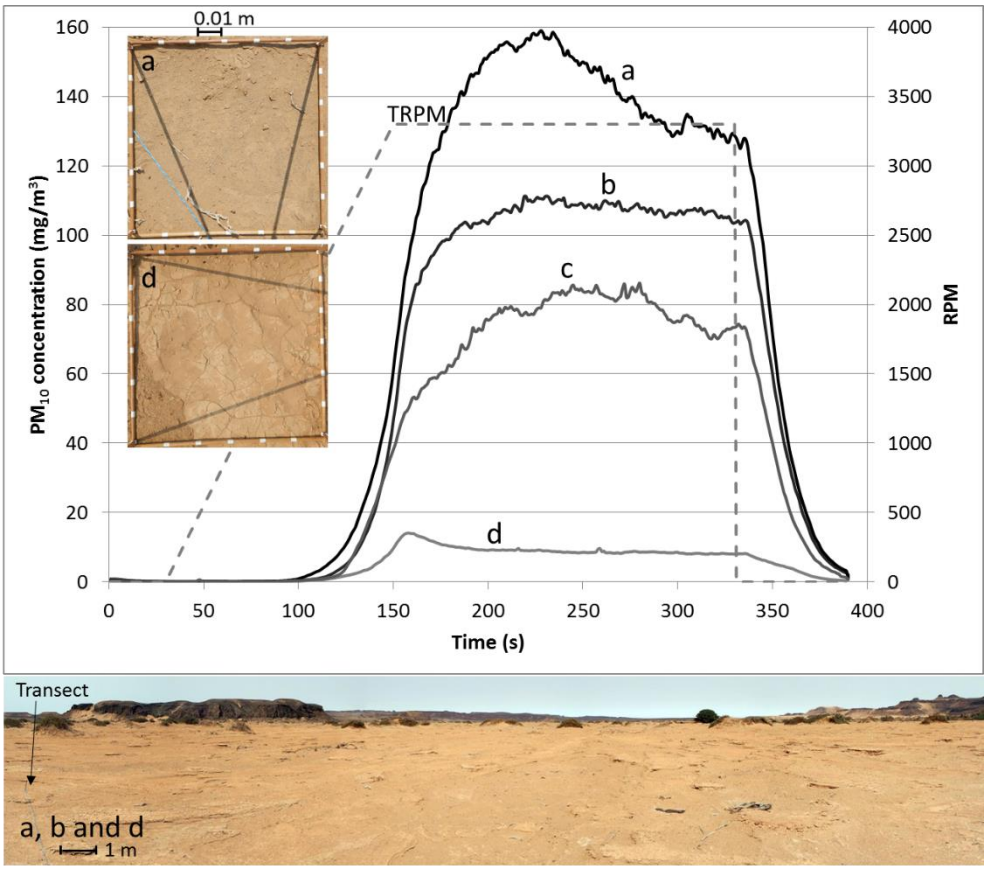

Figure 2-9 Dust emission potential of the Huab River. The graph shows the PM_{10} concentrations from the nebkhas in upstream section of river (a), which cover the river silt crusts of the terraces. These silt crusts are significant sources of dust in the presence of sand (b), compared to much reduced emission potential where negligible sand available for saltation (d). The nebkhas in the delta (c) were also highly emissive. Photo insets taken before PI-SWERL testing. Panorama shows silt terraces identified as predominant dust source in the upstream section of river (facing upstream).

2.5 Discussion

Landsat imagery has enabled us to identify the landform elements that act as source points for aeolian dust emission in three ephemeral river catchments at a local spatial scale. In the Kuiseb and Omaruru Rivers the source points for dust emission appear to centre around sites of significant direct anthropogenic modification, whereas the Huab River has not undergone the same degree of modification. All 12 major ephemeral rivers (Figure 2-1) flowing through the Namib Desert originate in the wetter highlands and drain westward towards the Atlantic Ocean. These rivers rarely reach the sea and aeolian transport is often the only way the fluvially deposited sediments reach the ocean (Dansie et al., 2017c). Groundwater within the alluvial deposits of the river systems is the major source of water for this region. The Kuiseb and Omaruru Rivers produce significant volumes of water for the mining industry and urban use from their aquifers.

The identification of the dust emission source points using MODIS in the southern arm of the Kuiseb delta is subjective given the effective resolution of MODIS as suggested by Lee et al. (2009) and is dependent on the information about the area available when performing the classification. It is intuitive to place the source points in the southern arm based on the fact that the river has only flowed in the southern arm since 1961 and the existence of an abandoned northern arm is not widely known. Given the fluvial-aeolian interaction that occurs in many ephemeral river systems in drylands, it would be reasonable to assume that the sediments deposited after the floodwater dissipates (Jacobson et al., 2000) would act as a supply source for dust emission (Bullard and Livingstone, 2002). Historical records state that the northern arm used to be the main flood channel and the river, when in flood, would flow directly through Walvis Bay towards the sea (DWAF, 1991; Huntley, 1985). This channel was abandoned when a flood wall was built in 1961 to direct the water into the southern arm

to prevent any further flooding of Walvis Bay. This desiccated northern arm of the delta has been a consistent source of dust for the duration of the Landsat record, with this hydrological modification taking place long before the Landsat program started in 1972. As the floodwall predates the start of the Landsat record, it is unclear what the dust emission pattern was prior to the blocking off of the northern arm. The silt terraces, situated at the terminal stages of the Tumas River, have been cut off by a railway line and road and our data show that they have acted as consistent dust emission sources. Water flow and sediment recharge are severely restricted to the silt terraces due to the funnelling effect caused by the limited number of culverts underneath the built structures.

The abandoned section of the Kuiseb River delta consists of extensive, exposed depositional silt sediments surrounded by sand supplied from the Namib Sand Sea to the south where the sand crosses the river (Figure 2-4). Both the silt sediments and sand are important components of the dust emission process involved at this site. Tests conducted with the PI-SWERL confirm the dust emission potential from these surfaces of the northern arm of the Kuiseb delta (Figure 2-5). The emission potential of the silt terraces in the Tumas River (Figure 2-4 marked as c) is very similar to those found in the Kuiseb River delta when sand is present. The mechanism of entrainment in this system is dominated by saltation as the silt crusts are sandblasted during wind events of sufficient magnitude. The resulting unconsolidated sediment is easily entrained and potentially builds up as the terraces erode due to the repeated bombardment by sand and other loose erodible material (LEM) from a variety of wind directions, predominantly the lower magnitude, higher frequency south-west winds (Table 2-2). The conditions determining the availability of these unconsolidated sediments for entrainment remains uncertain and could be dependent on the direction of the wind and protection afforded by silt crusts acting as roughness elements whilst they are still intact.

The modification to the Omaruru River hydrological system is more recent, but more severe than in the Kuiseb River. The Omdel dam (Figure 2-6) was completed in 1995 approximately 38 km upstream from the coast with the aim of increasing the infiltration of water to the aquifer by removing suspended silts and clays from the flood water (DWA, 1995; WBG, 2013). This is achieved by collecting all the water flowing down the river in the dam during the rainy season (Oct-Feb), after which the suspended sediments are allowed to settle out and collect at the bottom for 6-8 weeks. Once the sediments have settled out, the clear water is released from the top by a pump tower into settling areas where it infiltrates the aquifer. There is no water recharge downstream of the settling areas situated at approximately 27 and 32 km from the coast (Figure 2-6 site 1 and 2) and the dam therefore starves the downstream river of sediment. Our data show that this modification has changed the dust emission pattern of the Omaruru River significantly.

The imagery available prior to construction of the dam wall, show the dust originating from the lower sections of the river channel aligned with the high-magnitude north-easterly winds (Figure 2-6). This is similar to what is found for river systems elsewhere in the world, where dust originates from the low-slope, low-fluvial energy terminal stages of a river (Koven and Fung, 2008). The sources of dust emission appear to initially move upstream after dam construction (1997-2002) and then gradually migrate downstream towards the latter part of the study period (2004-2013). At the start of the Landsat record, prior to dam construction, dust emission from this river appears to be much reduced compared to plumes identified later in the time series. Here the Landsat time-series provides a good low-resolution temporal record of the evolution of the dust emission source points following the change in river hydrology.

The absence of downstream water flow and sediment recharge following the construction of the dam wall resulted in the dust emission source points shifting 8 km upstream to nebkha

fields surrounded by fluvially deposited river silts, now starved of surface moisture. The lack of water and flood sediments has had severe consequences for the vegetation in the river, especially in the nebkha fields found along the entire river section downstream of the dam wall. Since the hydrological modification the sediments were increasingly exposed due to the die-back of the vegetative roughness, resulting in erosion by the wind and eventually depletion of entrainable sediments. This has resulted in the dust emission source points gradually moving downstream to where they are situated at present. The lack of fluvial recharge and constant deflation has turned the silt crusts into lag deposits. In addition, the river silt crusts under the gravel has become increasingly hardened and degraded without the replenishment and reorganisation of physical crusts that the surface water flow provides. The settling silt accumulating at the dam wall has not been shown to produce dust, most likely because of its position within the protective incised canyon and the absence of sand to sandblast the deposits of silt crusts. The wind streaks emanating from the vicinity of the infiltration sites are composed of light coloured sands in nebkha fields, which originate from the active channel in the river (Figure 2-6). The alignment of the river with the north-east wind is potentially significant for exit points of sand for the wind streaks.

From the field investigation and PI-SWERL testing it appears that the present source area is made up mainly of small degraded nebkhas (Figure 2-7 photo) surrounded by gravel-covered river silt crusts. The PI-SWERL results show that the most likely source of dust is the sparsely vegetated nebkha fields (Figure 2-7 a), being significantly more emissive than the silt crusts (Figure 2-7 b). These gravel-covered river silt crusts can be considered as a human-induced gravel plain following the alteration of the river hydrology. The question remains to what extent the modification of the river has potentially changed the dust emission from this system. From the Landsat imagery, it would seem that the quantity of dust emitted has increased substantially as none of the images prior to the construction of the dam wall

shows the dramatic plumes witnessed post-construction (Figure 2-2 photo 3). In addition, the post-construction longitudinal progression of the source points downstream and the completely degraded nebkhas would appear to suggest that this river system will have a finite lifespan as a dust source. Once the nebkha vegetation are all dead and the sediments depleted, all that will remain is a hardened river silt crust covered with gravel with very little emission potential.

The Huab River in comparison has undergone much less direct hydrological modification compared to the previous two river systems, with the coastal road running through the delta the only barrier to flow in the downstream dusty sections of the river. The identified dust emission source points in the Huab River are shown to be consistently located in three distinct areas. These are an upstream section of the river valley itself, and around both a delta and a playa situated north of the river (Figure 2-8). The emission sites located in the upstream river valley are within the floodplain and consist of extensive silt crust terraces covered to a large degree with nebkhas. Testing with the PI-SWERL has shown these nebkhas to be the most emissive features within this system (Figure 2-9 a). As was the case for the Kuiseb River, the silt crust terraces only emit dust in the presence of sand or other loose erodible material (LEM), such as broken pieces of crust, to initiate saltation (Figure 2-9 line b). In contrast, crusts without sand or other LEM for saltation emit very little dust (Figure 2-9 line d).

The degraded nebkhas of the Huab delta also emitted significant amounts of dust when tested with the PI-SWERL (Figure 2-9 c). Large areas of the delta appear to consist of degraded nebkhas with very little to no vegetative cover remaining, the area downstream (west of the coastal road) being completely bare (Figure 2-8). These areas are a source of sediment for entrainment not only by the high magnitude wind events from the north-east, but also during the predominant southerly winds. This can be seen on the Landsat image in Figure 2-8 as

"fingers" of deposited dust extending to the north of the delta onto the gravel plain. The sediment deposited on this low-density gravel plain area to the north become available for entrainment when the north-east Berg wind blows as is evident from the Landsat imagery (Figure 2-2 photo 2). PI-SWERL testing of this gravel plain yielded very little dust flux possibly due to high atmospheric humidity on the day of testing.

The ERA-Interim 10 m wind data for the Kuiseb River suggests that winds with the potential to emit dust from all directions occur only 16% of the time. As the MODIS and Landsat dust events identified in this study were only associated with winds from the north-east, the question remains as to what the dust potential of the predominant south-west winds is. MODIS and Landsat true colour images are not ideal for detecting dust emitted by the south-west wind, due to the lack of colour contrast between the transported dust and the surface. In addition, there are north-east winds of sufficient magnitude to emit dust for which none is detected with MODIS (Table 2-2). It is evident that friction velocity alone does not determine emission potential: only 27 % of the potential dust-producing north-east winds was captured by MODIS as emitting dust, with this percentage increasing as the wind strength increased. Table 2-2 shows a breakdown of the ERA-Interim wind events from the north-east capable of producing dust, compared to the dust events captured by MODIS. The three wind events exceeding 10 m s^{-1} for which no dust was detected by the MODIS true colour composites occurred during the night.

The significance of the dust associated with the high magnitude wind events needs further investigation, both in terms of the quantity of dust and the impact of this dust. Field observation and measurement is vital to determine the dust signature and footprint across all seasons, wind directions and speeds. Furthermore, ground-based techniques to account for dust emission and transport is also important to determine what the factors are that control dust emission, both in terms of environmental conditions and surface characteristics. To

guide fieldwork and determine the optimal location of measurement and testing equipment requires improved knowledge at higher spatial resolutions regarding dust emission processes and sources. The spatial resolution of Landsat imagery provides the opportunity to investigate dust emission at a local, landform scale. A more detailed analysis of the surfaces and landforms that produce dust will be considered in a separate chapter to follow. This will include a more in-depth look at surface characterisation, location of landforms within the landscape and erodibility controls and will provide the basis for integrating this research into schemes like the PDS proposed by Bullard et al. (2011)

2.6 Conclusion

This study analysed a dataset covering a period of 27 years from 1989 to 2016. Unlike any other sensor, Landsat constitutes the longest continuous record with over 40 years of available imagery. Given its high spatial resolution, it is not surprising that Landsat offers one of the most detailed examinations of dust emission sources, especially when compared to TOMS, MSG and MODIS. We have demonstrated that the limited temporal resolution of the data is compensated for to a good degree by the length of the archive, which can yield sufficient dust events to advance our understanding of dust emitting landforms and their temporal dynamics including river catchments, coastal sabkhas and inland playas. This study also hints upon the dust emission potential of the vast Namib gravel plain, which has been overlooked as a potential dust source to date.

The attribution of source points for aeolian dust emissions achieved with Landsat can guide field observations. Our observations for Namibia's three dustiest west coast catchments stresses the regional importance of elevated, fluvial, paleo silts and terraces as significant sources of dust, which is accentuated by the decay of nebkha fields in response to recent and ongoing hydrological changes. Landforms that were not identified as emitters of detectable

dust plumes in Landsat imagery were the sandy ephemeral river channels as well as sand dunes and sand seas. Although the sand seas themselves appear not to be significant dust sources, the presence of sand for saltation is vital for dust production from soft silty surfaces. According to various image records, coastal pans are known to be significant dust sources, but prevailing foggy and moist conditions during the study period prevented meaningful PI-SWERL measurements. Results of this nature may provide a comparison of erodibility between different landforms and the different physiographic systems. Such results can make an important contribution to the development of preferential dust schemes (PDS) such as those developed by Bullard et al. (2011). Given the importance of anthropogenic modification to dust production from the Namib river catchments, we suggest that a category for modified and disturbed landscapes would be a suitable addition to such schemes.

The Landsat record for the Central Namib provides some evidence for dust emission changes in response to water management strategies especially for the Kuiseb and Omaruru River which are home to a series of extraction and diversion schemes. However, distinguishing natural from anthropogenically emitted dust remains difficult. A fluvial-aeolian connection for dust production has been highlighted by others, including Koven and Fung (2008) who suggests that dust emission is potentially greatest in systems where there has been a disruption in normal fluvial processes. It would appear that this may apply to our observations here.

This study has demonstrated that the global, long-term Landsat record can identify temporal and spatial dust emission patterns at a landform scale. Automatic screening, dust detection and flagging of the entire Landsat archive could potentially further global dust source research by identifying the most emissive landforms and increased emission potential associated with anthropogenic modification.

2.7 Acknowledgements

This research was funded by the National Research Foundation in South Africa as part of a bilateral South African/Namibian research project, number: UID 89120. The authors would like to thank Matt Baddock for assistance in the field and valuable comments on the manuscript. Also, we thank Jo Nield, Ruusa Gottlieb and Peter Bridgeford for field assistance. Thank you to Martin Hipondoka for guidance and assistance in obtaining the necessary permits to conduct this research. We thank the Namibian Ministry of Environment and Tourism for their support and assistance for the duration of this research. This research was conducted under MET permit number 2076/2015. Lastly, we thank the reviewers for their valuable contributions to this manuscript.

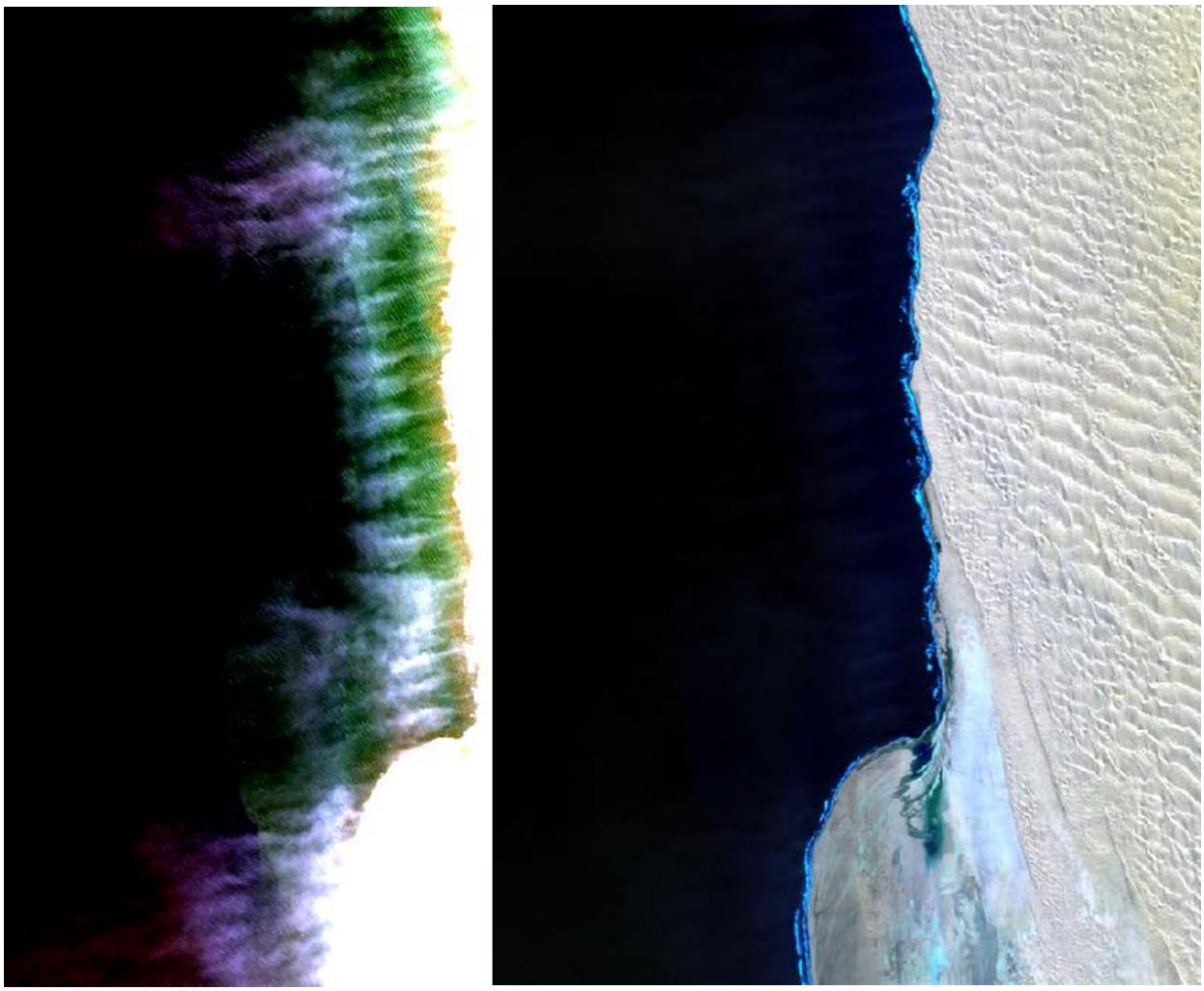

Figure 2-10 EXTRA IMAGE: Dust channelling by Namib Sand Sea dunes at Conception Bay. Image on left created from Landsat false colour (bands 753) image with histogram stretch over dust and water and on right histogram stretched over land and water.

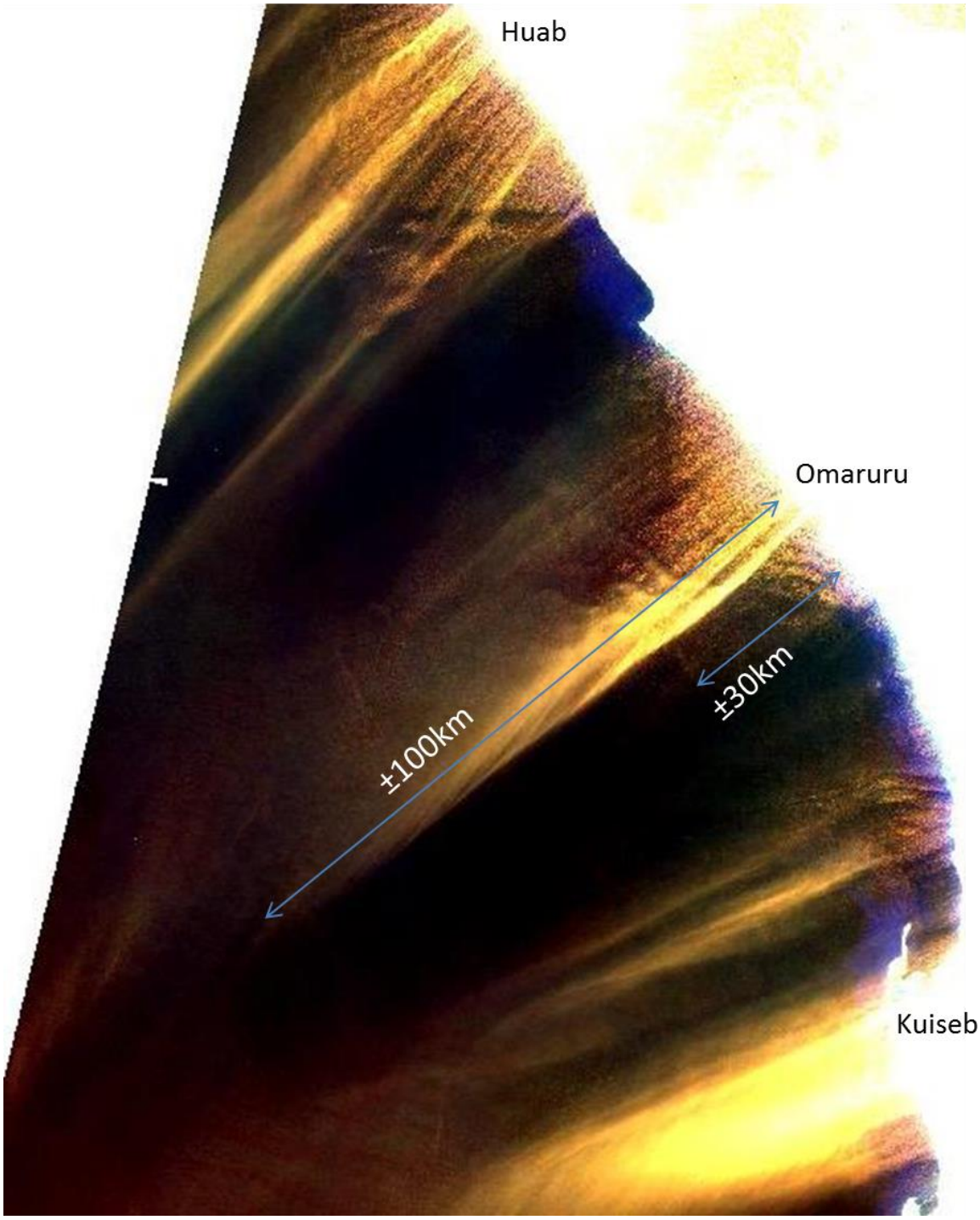

Figure 2-11 EXTRA IMAGE: Dust plumes versus sand plumes. Image created from Landsat false colour image (bands 753) using histogram stretch over dust and water.

Figure 2-12 EXTRA IMAGE: Dust from the paleo-silt terraces in the Hoanib River. Photo courtesy of Rassie van Niekerk

Chapter 3: Assessing landscape dust emission schemes using combined ground-based process and remote sensing data

J R von Holdt[a]

F D Eckardt[a]

M.C. Baddock[b]

G F S Wiggs[c]

[a] Department of Environmental and Geographical Science, University of Cape Town, Private Bag X3, Rondebosch, Cape Town, 7701, South Africa; jrvonholdt@gmail.com; frank.eckardt@uct.ac.za

[b]Department of Geography, Loughborough University, Loughborough, LE11 3TU, UK, email: m.c.baddock@lboro.ac.uk

[c] School of Geography and the Environment, Oxford University Centre for the Environment, University of Oxford, Oxford, OX1 3QY, UK; giles.wiggs@ouce.ox.ac.uk

Key points:

- High-resolution Landsat analysis and ground-based testing provides landform-scale data to assess proposed dust emission schemes for modelling
- Recent dust emission scheme assessed present a novel approach to represent erodibility but still need to be improved
- Boosted Regression Tree model potentially useful method to identify variables controlling surface erodibility for inclusion in schemes

3.1 Abstract

Different modelled simulations of aeolian dust emission vary by an order of magnitude due to the spatiotemporal heterogeneous nature of such emissions. An erodibility factor is often incorporated in models in an effort to constrain the location and magnitude of dust emissions. Several landscape-scale dust emission schemes representing erodibility have been proposed, but validation of such schemes has mainly been attempted indirectly with medium-resolution remote sensing data of mineral aerosol loadings and high-resolution land surface mapping. In this study, we used dust source points identified with Landsat and field-based dust emission measurements to assess the accuracy of dust emission schemes that aim to represent erodibility for use in dust-cycle modelling. The sub-landform scale dust emission measurements were carried out with a Portable In-situ Wind Erosion Laboratory (PI-SWERL) wind tunnel guided by landform scale source points identified with the aid of Landsat imagery. A Boosted Regression Tree (BRT) analysis identified the significant factors for erodibility using the PI-SWERL dust flux measurements and various surface characterisation tests, such as moisture, particle size, degree of crusting and mineralogy. Despite substantial recent improvements in dust emission schemes, our assessment finds that they still do not accurately reflect the dust emission potential. The accurate identification of dust sources combined with ground-based testing to measure emissivity provide valuable input and validation for assessment of dust emission schemes. The determination of factors that control emission can provide further inputs for the improvement of dust-cycle modelling.

Plain Language Summary

Atmospheric mineral dust plays an important role in many earth system processes, including influencing the climate, providing nutrients to marine and terrestrial ecosystems and affecting human health. To determine the effect atmospheric dust has on the climate and environment requires accurate modelling of its emission at source, its transport through the atmosphere, and its deposition. To enable regional to global modelling of the dust cycle, therefore, requires the realistic representation of where and when dust emission takes place. However, the highly variable nature of dust emission has resulted in modelling attempts producing

disparate results. This research study uses Landsat remote sensing data to accurately identify emission sources and ground-based testing using a portable wind tunnel to assess two dust emission schemes used in climate models. Despite substantial recent improvements in the proposed schemes, our data show that the global representation of dust emission does not yet offer a true reflection of the source areas on the ground. The heterogeneous nature of dust emission is predominantly as a result of the highly variable nature of the surfaces. Our analysis identified several factors which control the potential for surfaces to emit dust that can be used as inputs to improve dust modelling.

3.2 Introduction

Wind-driven processes of sediment transport play an important role in the Earth system and as a result have been the focus of many modelling attempts (Ravi et al., 2011, Shao et al., 2011). The dynamics of mineral dust emission are fundamentally controlled by a combination of the power of the wind to erode (erosivity) and the resistance of an emitting surface to erosion (erodibility) (Webb & Strong, 2011). Interactions between erosive and resisting forces are complex and result in dust emission being highly heterogeneous through space and time (e.g. Bryant et al., 2007; Gillette, 1999; Gillies, 2013; Mahowald et al., 2003; Taramelli et al., 2013). Improvement in the modelling of dust emission remains an important contemporary research goal since existing models have a limited capacity to accurately account for the spatiotemporal variability of dust emission within dust sources (Haustein et al., 2015; Parajuli et al., 2014; Shao et al., 2011).

Modelled simulations of dust emission must account for factors that affect the threshold friction velocity (u^*_t), and as a result, the erodibility of the surface, which is highly variable through space and time (Marticorena & Bergametti, 1995). Some of the major drivers influencing the variability of the erosion threshold for dust-producing surfaces include moisture content, particle size, degree of crusting (including physical, saline and biological soil crusts), and mineralogy of surface sediments (e.g. Belnap & Gillette, 1998; Gillette et al., 1982; McKenna Neuman & Nickling, 1989; Munkhtsetseg et al., 2016), as well as surface roughness (characterized by the aerodynamic roughness length, z_o) (Raupach et al. 1993). Incorporating the influence of these surface characteristics into soil erodibility and dust emission predictions is one of the biggest challenges for model simulations, especially given that global data sets of these input variables are not always available, or at a sufficient spatial scale for model ingestion.

In recognition of its importance, a representation of source erodibility is often included to improve the ability of dust models to constrain the observed spatial heterogeneity of emissions (Zender et al., 2003). Several dust emission mapping schemes at the landscape scale have attempted to account for erodibility as a mask of potential dust sources for use in dust models (e.g. Ashpole & Washington, 2013; Baddock et al., 2016; Bullard et al., 2011; Parajuli et al., 2014, 2017). The erodibility factor has typically been based on various physical assumptions of the influence of geomorphology, topography and hydrology on dust emission (Ginoux et al., 2001; Zender et al., 2003). Alternatively, empirical approaches based on satellite-derived data, such as surface reflectance (e.g. Grini et al., 2005) have also been formulated. Bullard et al. (2011) and Parajuli et al. (2014) present high-resolution land-surface classifications based on the potential of specific geomorphic types and land covers to generate emission. A recent global dust emission scheme by Parajuli et al., (2017), the Sediment Supply Map (SSM), combines the physical characteristics of hydrology based on upstream drainage area derived from a digital elevation model combined with empirically derived surface reflectance from the MODIS blue channel. The combination of these two data sets encapsulates two important aspects of sediment supply, namely the accumulation of fine sediments in basins to account for the provision of dust-sized material, and the reflectance of different land surface types based on their surface sediment supply potential (Parajuli et al., 2017). The SSM is a landscape scale (~500 m) erodibility map that provides a global numerical estimate of dust emission potential designed to easily be incorporated within dust-cycle models. The scale at which dust emission processes are investigated has a marked influence on the representation of emission variability in space. Scales vary from grain to surface ($<10^{-1}$ m), through landform ($\sim10^{1}$ - 10^{2} m), landscape ($\sim10^{3}$ m) to regional and global scale ($>10^{4}$ m) (Webb & Strong, 2011). To date, recent dust emission mapping schemes have not been assessed rigorously by ground-truthing and it remains uncertain how well they account for the potential variability in emission known to exist at both the landform and sub-landform scale (Sweeney et al., 2011).

Validation of dust emission schemes such as the SSM with ground-based data is a challenge because of the disconnect between process studies performed at the landform to sub-landform scale and regional and global modelling studies attempting to represent the surface at a landscape scale. Variability of emission from dust-producing surfaces has been difficult to investigate at a sub-landform scale due partly to the limitation posed by a coarse spatial resolution in remote sensing together with a lack of dedicated field studies evaluating this

sub-landform variability (Haustein et al., 2015). The understanding of dust emission processes has been greatly enhanced by studies that have identified dust sources on global, regional and landscape scales through various remote sensing approaches primarily using the Total Ozone Mapping (TOMS) and more recently Moderate Resolution Imaging Spectroradiometer (MODIS) sensor (e.g. Baddock et al., 2016; Bullard et al., 2008, Ginoux et al., 2012; Huang et al., 2007, Lee et al, 2012, O'Loingsigh et al., 2015; Prospero et al., 2002; Schepanski et al., 2007, 2012; Vickery et al., 2013; Washington et al., 2003). However, a fuller appreciation of the smaller-scale controls contributing to the variability in dust emission must also depend on the characterisation of dust sources at a sub-landform scale. Such a focus provides the opportunity to identify and quantify the contribution of dust from specific landforms, and the combination of surfaces they are made of. The utility and methodological considerations of a high-resolution approach have recently been demonstrated by von Holdt et al., (2017) who used Landsat imagery covering a 25-year period to identify the landform-scale dust sources in the Namib Desert.

The increased spatial resolution of Landsat (15-30 m) compared to other remote sensing data used to date (e.g. MODIS 250-1000 m) has improved accuracy for dust source-point identification at a landform level and directed the targeted collection of field data down to the sub-landform scale (von Holdt et al., 2017). The spatial variability of dust emission at sub-landform scale has been investigated by several studies using a PI-SWERL (Portable In-Situ Wind Erosion Lab) wind tunnel (Etyemezian et al., 2007) to measure the dust emission potential of surfaces from a variety of landforms found in desert regions (e.g. Bacon et al., 2011; King et al., 2011; Sweeney et al., 2011, 2016). The size and portable nature of this instrument allows for the multiple-replicate testing of many surfaces in locations that would not be accessible by conventional, larger footprint wind tunnels. Furthermore, given the size of the PI-SWERL (0.57 m diameter), the spatial scale of testing with the PI-SWERL is at the level of those controls occurring at the grain to surface scale ($<10^{-1}$ m). The guidance for surface sampling using PI-SWERL based on dust source observations from high-resolution satellite imagery provided an advance for the spatial sampling of surface emissivity by von Holdt et al. (2017). Their detailed Landsat analysis identified areas where targeted measurements can provide the opportunity for a surface- to landscape-scale assessment of dust emission variability.

Resolving the small-scale variability of emission provides data to help validate dust emission schemes and provide further inputs to improve how erodibility is characterized in dust

modelling. The aim of this study was to use a portable wind tunnel to estimate relative emissivity from different surface types, in the specific context of land classification schemes recently proposed to represent the surface in dust modelling efforts. Assessment of measured dust fluxes from classified surfaces contributes a novel test of these new schemes. For known dust-producing areas in Namibia, the location of field-based emission sampling using PI-SWERL was informed by knowledge active source points identified by Landsat imagery.

The use of dust source identification at a landform scale from detailed remote sensing to facilitate emission measurements at a sub-landform scale enables the assessment of emission variability across a range of spatial scales. In order to consolidate the surface characteristics at testing sites, the secondary aim was to use the emission measurements and various surface characterisation tests in a boosted regression tree (BRT) analysis to determine the erodibility factors for the dust source points. This technique has the potential to enable the most significant variables be incorporated into dust emission schemes, with potential for input into modelling efforts and the standard testing protocols of dust emitting surfaces.

3.3 Regional setting and field sites

The Namib Desert has been identified as one of the major southern Africa dust sources (Vickery et al., 2013; von Holdt et al., 2017), identifiable at the hemispheric scale (Ginoux et al., 2012). This region comprises several desert landforms, including 12 westwards flowing ephemeral rivers, numerous small inland playas and large sabkhas, sand sheets and dunes and extensive areas of stony surfaces comprising gravel pavements dissected by channels (Jacobsen et al., 1995; Goudie & Viles, 2015). Dust emission from the Namib Desert has been mostly associated with the terminal stages of the dry river valleys and coastal sabkhas (Vickery & Eckardt, 2013; von Holdt et al., 2017). The Kuiseb, Huab and Omaruru rivers were identified as the most emissive rivers based on MODIS true colour imagery analysis from 2005 to 2015, whereas Conception Bay and the Ugab Pans where the most emissive sabkhas (von Holdt et al., 2017) (Figure 3-1 a). Von Holdt et al. (2017) tested different landform types present in the three most emissive rivers with a PI-SWERL wind tunnel. The

present study analyzed the emission potential on sites identified by von Holdt et al. (2017), as well as the Ugab sabkha (marked U in Figure 3-1 a).

3.4 Methods

3.4.1 Geomorphology and dust emission scheme mapping

Geomorphological units were mapped following the landscape categories used by Bullard et al. (2011) in their Preferential Dust Scheme (PDS) (Baddock et al., 2011). These categories included lakes (pans), high-relief alluvial deposits, low-relief alluvial deposits, stony surfaces, sand deposits, loess and low emission surfaces, such as bedrock. The Namib Desert loess deposits consist predominantly of fluvially reworked loess in the ephemeral river valleys (Eitel et al., 2001) and were mapped as part of alluvial deposits as they are not distinguishable at the scale of mapping used in the present study. The study area included for mapping consists of those Landsat tiles used by von Holdt et al. (2017) (Figure 3-1 a). Mapping used a combination of remote sensing data, 1:250 000 geological maps from the Geological Survey of the Ministry of Mines and Energy of Namibia and field observations. The remote sensing data included Google Earth images, Landsat 8 false colour imagery (bands 753) and the SRTM 30-m digital elevation model to distinguish between low- and high-relief, as well as degree of incision of alluvial systems. A total of 2289 source points identified with the aid of Landsat imagery by von Holdt et al. (2017) were classified according to the PDS geomorphic units at a landscape scale. Mapping was done in QGIS v 2.18.12 (QGIS development team, 2016).

The Land Surface Map (LSM) and Sediment Supply Map (SSM) of Parajuli et al. (2014, 2017) were made available as rasters by those authors. The LSM (Parajuli et al., 2014) was originally developed by mapping the Middle East and North Africa region according to 12 land surface types with high-resolution Google Earth Pro images and polygons created as training samples for a global supervised classification which used the maximum likelihood method in ArcGIS, as applied to the global Blue Marble RGB image mosaic. To enable comparison of the two outputs the Parajuli et al. (2014) surface types were reclassified according to the geomorphic units used by Bullard et al. (2011). The original land surface types used in Parajuli et al. (2014) for the LSM are included in supplementary section 3.9.1.

The LSM is used for a qualitative and quantitative comparison with the SSM produced globally by Parajuli et al. (2017).

The SSM combines the size of the upstream catchment area and the surface reflectance captured in the blue band (459-479 nm) from the same Blue Marble mosaic used for the determination of LSM. The upstream catchment is suggested to provide an estimate of the transport and deposition of sediments and highlights areas of sediment accumulation, whereas the reflectance serves as a proxy for highly erodible surfaces such as playas and dunes (Parajuli et al., 2017). The value for the SSM is based on a scale from 0 – 1, with the Bodélé Depression in Chad regarded as the most emissive source with a maximum value of 1.

3.4.2 PI-SWERL dust emission measurements

Dust emission measurements from the PI-SWERL instrument were used to measure the potential for dust emission from different desert landforms (Bacon et al., 2011; Etyemezian et al., 2007; Goossens & Buck, 2009; Sweeney 2008, 2011). The specific methodology and test parameters for the PI-SWERL are presented in von Holdt et al. (2017). At each location of testing, 3 to 10 runs were made at metre intervals along a 10 m linear transect with the number of test runs dependent on the homogeneity of the surfaces within the transect and variability of the emission flux results. The dust emission flux (mg m^{-2} s^{-1}) results were calculated using the following equation from Sweeney et al. (2011):

$$E_f = \frac{\sum_{begin,i}^{end,i} C \; x \; F}{(t_{end,i} - t_{begin,i}) \cdot A_{eff}} \qquad \text{(Eq. 1)}$$

where C is the PM_{10} dust concentration (mg m^{-3}), F is the rate of flow rate of air through the chamber (L s^{-1}), A_{eff} is the test area underneath the PI-SWERL annular ring (m^3), and t is the time (s) at the beginning (t_{begin}, i) and ending (t_{end}, i) of the RPM step test level, i (Sweeney et al., 2011). A total of 23 sites (128 PI-SWERL runs) were based on the source points identified with Landsat imagery by von Holdt et al. (2017) (Figure 3-1 a). Details of the PI-SWERL test sites and landform classifications are given in the supplementary section 3.9.2. Statistical significance was calculated in R (R Development Core Team, 2017).

3.4.3 Surface properties and Boosted Regression Tree (BRT) analysis

Using the surface properties measured at each PI-SWERL field testing site, a BRT model was used to identify the most relevant variables that control surface erodibility, in this case, moisture content, particle size, degree of crusting and mineralogy. This analysis was performed following Elith et al. (2008) using the '*dismo'* package (Hijmans et al., 2016) in R (R Development Core Team, 2017) using a learning rate of 0.005 and a tree complexity of 5. Emission flux (E_f) (Equation 1) representing the overall surface erodibility was used as the dependent/response variable. Predictor variables included particle size, compressive and shear strength to measure the degree of crusting, moisture content and elemental composition to assess the influence of mineralogy. One surface sample was taken to a depth of 0.02 m directly next to where each PI-SWERL run was performed ensuring the surface type was consistent and undisturbed. Further details of the BRT analysis are given in supplementary section 3.9.3.

For particle size analysis, all the samples were air dried at 25°C to a point where their weight became constant and sieved to 1 mm to separate the coarse and fine fractions. The split greater than 1 mm was further sieved to determine the coarse sand and gravel fractions. The <1 mm split was used to determine the particle size distribution by laser diffraction using a Malvern Mastersizer 2000 attached to a Hydro 2000G dispersion unit. The samples were cone and quartered to obtain a representative sample and placed in solution overnight with tap water as dispersant, shaken for half an hour and again for half an hour the next day before measurement. Floating particulate organic matter was scooped out before the samples were introduced and then sonicated for 180 seconds by the Malvern HydroG dispersion unit prior to measurement. Particle size statistics including texture classes, modes, kurtosis, skewness and sorting were calculated using Gradistat software (Blott and Pye, 2001) for use in the BRT model.

The gravel concentration in the surface sediments determined by sieve analysis served as a proxy for the gravel-cover density. These results were confirmed by an unsupervised classification of a surface photograph of each surface with a gravel cover performed in Erdas Imagine 2015-2016 (Leica Geosystems, Atlanta, Georgia, USA). Gravel cover densities of <30 % were classified as low gravel and densities of >30 % as high gravel cover. This distinction was chosen based on the analysis by Wang et al. (2012), where the authors found

that dust emission increases with increasing gravel cover up to a density of 30 %, after which the dust emissions decreased with increasing gravel cover.

The degree of consolidation or crusting of the surface was assessed by measuring both the compressive and shear strength of the surface. Unconfined compressive strength was measured using a Pocket Soil Penetrometer H-4195 and shear strength using a Torvane H-4212 pocket shear vane (Humboldt Mfg. Co., Illinois, USA). At each site a minimum of three measurements of both compressive and shear strength of the surface was taken. If a large difference in individual measurements was encountered, additional measurements were taken to increase representativeness of measurement.

The near-surface volumetric moisture content at the time of PI-SWERL sampling was measured with a Delta-T Devices ML3 ThetaProbe soil moisture sensor. A minimum of three measurements was taken at each PI-SWERL measurement site by inserting the probe to just below the surface (upper 0.02 m). Finally, milled samples of the <1 mm soil fraction were analysed for elemental composition with a Spectroscout energy-dispersive X-ray Fluorescence (XRF) analyser (SPECTRO Analytical Instruments, Kleve, Germany). The instrument was calibrated with a certified standard GBW07312 (National Research Centre for CRMs, Beijing, China) for which technical concentrations were obtained from NOAA Technical memorandum NOS ARCA 68 (1992). The elements measured and included in the analysis were Mg, Al, S, Cl, K, Ca, Ti, Mn and Fe.

3.5 Results

3.5.1 Dust emission scheme mapping and Landsat-derived dust source points

Stony surfaces and bedrock cover extensive areas of the Namib Desert study area (Figure 3-1 b) according to the PDS map. The Namib Sand Sea in the south and the northern Skeleton Coast dune field make up two extensive aeolian sand deposits. In contrast, the lakes and alluvial deposits cover a very small proportion of the area (2% of area, 77% of plumes), but have a higher dust plume density compared to the stony surfaces (27% of area, 22% of plumes) and aeolian sand deposits (15% of area, 0.5% of plumes) based on dust source points from Landsat imagery 1990 to 2016 (von Holdt et al., 2017) (Figure 3-2). Additional details of the landform classification of the dust source points identified by von Holdt et al. (2017)

are given in supplementary section 3.9.4. The representation of the landscape according to the LSM (Figure 3-1 c) is noticeably different from the PDS, with large areas of bedrock and stony surfaces classified as both alluvium (or "fluvial" according to the original LSM scheme) and pans. In addition, a large part of the Namib Sand Sea is classified as stony surface. Relatively small areas of a landscape are responsible for the majority of dust emission (e.g. Gillette, 1999; Lee et al., 2009) which is evident when assigning the dust emission potential to the PDS geomorphic units following Bullard et al. (2011). Alluvial deposits and pans are the highest emitters, sand deposits have low to medium dust emission potential and stony surfaces and bedrock are low potential emitters. (Figure 3-1 d). The colours assigned to low; medium and high emission potential categories follow the colour scheme used in the SSM (Figure 3-1 e) by Parajuli et al. (2017). The SSM highlights the elevated potential of alluvial deposits to emit dust, but when calculated, results in a more extensive alluvial coverage than represented by the PDS scheme.

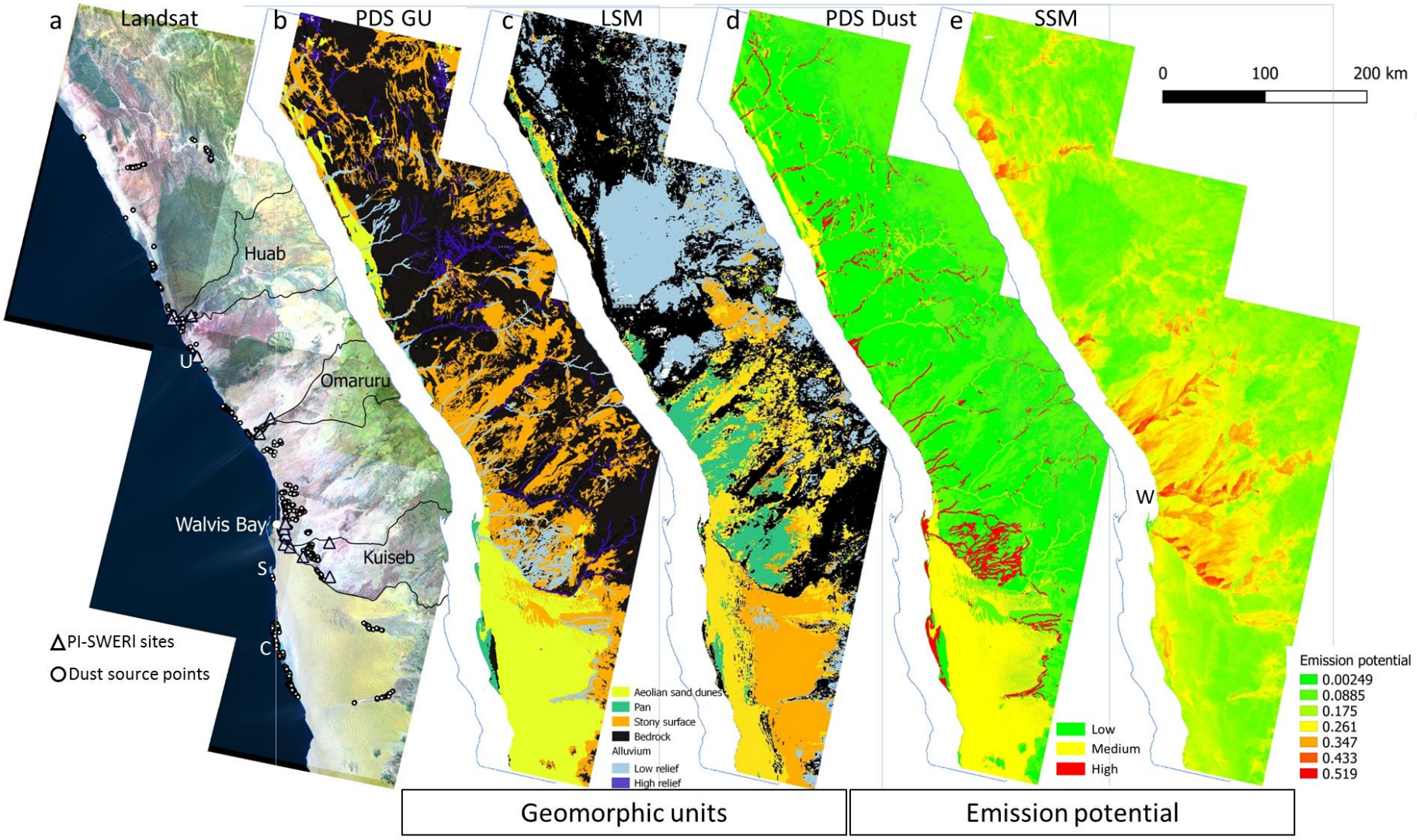
a
Landsat
b
PDS GU
c
LSM
d
PDS Dust
e
SSM
0
100
200 km
Huab
U
Omaruru
Walvis Bay
S
Kuiseb
C
W
PI-SWERI sites
Dust source points
Aeolian sand dunes
Pan
Stony surface
Bedrock
Alluvium
Low relief
High relief
Low
Medium
High
Emission potential
0.00249
0.0885
0.175
0.261
0.347
0.433
0.519
Geomorphic units
Emission potential

Figure 3-1 Geomorphic and emission potential mapping of the Namib Desert. (a) Landsat false-colour image showing the seven tiles included in the Landsat source point analysis, the river catchments and PI-SWERL testing sites (∆), (b) Mapped according to PDS geomorphic categories as per Bullard et al. (2011), PDS GU (c) Parajuli et al. (2017) Land Surface Map (LSM), (d) map of dust emission potential according to PDS categories, PDS Dust (e) Sediment Supply Map (SSM) by Parajuli et al. (2017) showing dust emission potential on a scale from 0 to 1 with the maximum value equated to the Bodélé Depression which is often regarded as the world's most emissive source. In a: U: Ugab pan complex, S: Sandwich Harbour, C: Conception Bay.

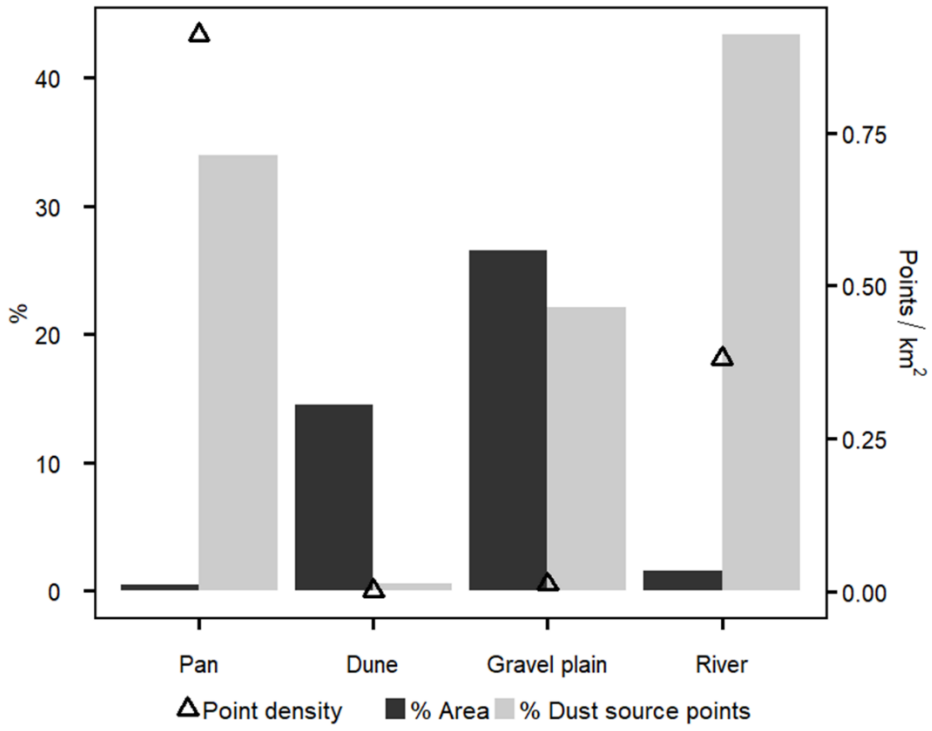

Figure 3-2 Dust source points (%) identified with Landsat situated in different landscapes of the Namib Desert. Pans have the lowest area within the study area (850 km^2), but show the highest density of source points for the small relative area they cover. The gravel plain stony surfaces have the highest area coverage (45,000 km^2), but show a low-density of source points.

3.5.2 Measured emission fluxes

Dust emission at a sub-landscape scale as determined from the PI-SWERL is highly variable. This variability however is not apparent in the mean emission rates when aggregated to a landscape scale because aeolian deposits, stony surfaces and alluvial systems have similar geometric means (Figure 3). Notably, the lakes are significantly different and consistently showed low emissivity during the time they were tested (geometric mean E_f value (geomean) of 0.001 mg m^{-2} s^{-1}). The lakes tested included the Huab pan and Ugab pan (Figure 3-1 a) where significantly less dust was emitted than the other three geomorphic landscape units as quantified by the PI-SWERL (Alluvial deposits geomean: 0.060 mg m^{-2} s^{-1}; Stony surfaces geomean: 0.021 mg m^{-2} s^{-1}; Aeolian deposits geomean: 0.064 mg m^{-2} s^{-1}). Despite the pans not being emissive during PI-SWERL testing, they do contain significant amounts of very fine clastic sediments. The surface of Huab pan consists of knob-like features that are covered by a friable crust layer consisting of a mixture of clastic sediments and salts (supplementary section 3.9.5). This crumb like cover contains a significant proportion of fine material (36 % < 63 µm and 18 % < 10 µm) which could be a source of dust under conditions conducive to emission from sabkhas and playas. The samples from the dunes had no PM_{10} particles present according to the Malvern particle size analysis, but emitted particles <10 µm as measured by the PI-SWERL (supplementary section 3.9.6). This is potentially due fine particles generated by the abrasion of sand grains (Bullard et al., 2004; Crouvi et al., 2008), possibly exacerbated by the rotation of the metal annular ring of the PI-SWERL.

The variability in emission apparent in the stony surfaces and alluvial deposit landform classes could be further resolved by looking at distinct surfaces present within these two broader landform classes. In the case of the stony surface class, a fundamental distinction could be made between pavement surfaces dominated by the presence of coarse lag gravel, and portions of pavement where small channels (c. 0.1 m deep) were found. In turn, the low relief alluvial class could be divided between portions of ephemerally active channel and perched above the channel, valley fill terraces (Figure 3-4). In terms of mean dust emission flux, the river valley fill terraces were the most emissive (geometric mean E_f value: 0.076 mg m^{-2} s^{-1}) followed by the dunes (geomean: 0.064 mg m^{-2} s^{-1}) as well as the gravel plain channels (geomean: 0.030 mg m^{-2} s^{-1}). The river channels (geomean: 0.008 mg m^{-2} s^{-1}), gravel plain stone pavement (geomean: 0.007 mg m^{-2} s^{-1}) and pans (geomean: 0.001 mg m^{-2} s^{-1}) were significantly less emissive, as shown by comparing Figure 3-3 and Figure 3-4.

While Figure 3-4 indicates the influence on observed emission fluxes resulting from landform variability within the broad geomorphological classes used in dust emission potential schemes, the PI-SWERL allows a finer resolution investigation of control on dust emission rate. Categorising the emission fluxes according to the characteristic types of surface found across both the alluvial and stony surface classes illustrates the inherent variability of dust emission at a sub-landform scale (Figure 3-5). The most emissive undisturbed surfaces were unconsolidated sediments or loose erodible material (LEM). The presence of such material was particularly found around small nebkha dunes and interspersed between fluvially deposited crusts within the channels of the gravel plain and the valley fill terraces (Figure 3-4). In Figure 3-5, a distinction between the crusts present on the terraces and channels could be made based on the relative presence of saltators determined by inspection of the surface before a PI-SWERL test. Individual PI-SWERL runs from crusted surfaces, particle size analysis of the crust and sand found on top of the crust and images of the surfaces are given in supplementary section 3.9.7. Figure 3-5 indicates that LEM-dominated surfaces (geomean: 0.442 mg m^{-2} s^{-1}) and those crusts with abundant sand (geomean: 0.342 mg m^{-2} s^{-1}) were significantly more emissive than the other surface types. Gravel-covered surfaces with varying densities of gravel were found predominantly on the gravel plain and in some parts of the river terraces. The low-density gravel pavement (gravel cover < 30%) was significantly more emissive (geomean: 0.063 mg m^{-2} s^{-1}) than the surfaces with a high density of gravel cover (> 30%). High density gravel surfaces (geomean: 0.002 mg m^{-2} s^{-1}) and crusts with no sand (geomean: 0.004 mg m^{-2} s^{-1}) were the lowest emitters. All sample statistics for landscape, landform and surface categories used above are given in supplementary section 3.9.8.

The portability of the PI-SWERL allows rapid, multi-replicate sampling that ensures that the spatial variability in emission flux from a given surface can be measured (King et al., 2011; Sweeney et al., 2011). The same crust within a 10m transect can be largely non-emissive (0.003 mg $m^{-2}s^{-1}$) in the absence of available sand for saltation, but highly emissive (0.646 mg $m^{-2}s^{-1}$) where an abundant supply of saltators is present. Emission rates generated by the PI-SWERL testing of surfaces reflect the relative presence of only those saltators under the instrument footprint, resulting in non-emissive runs on crust where no saltators are present. However, river terraces surrounded by an abundant supply of sand will undergo bombardment by saltation during a high friction velocity wind event. It is likely that the

entire transect will become highly emissive under the continued bombardment of the available saltators and the stockpiles of LEM dispersed between the terraces.

3.5.3 Emission fluxes and relation to land surface classification schemes

The PI-SWERL provides a relative quantification of the dust emission rate from the surface, against which the emission potential of different geomorphic units in surface classification schemes (PDS, SSM) can be compared. Comparing the geometric mean of measured dust emission against the SSM values for the location of each PI-SWERL transect provides a means to assess and contextualise the SSM values (Figure 6). Also represented in Figure 6 is the geomorphic classification as per the PDS scheme by Bullard et al. (2011) and the LSM classification by Parajuli et al. (2014). Determination of the geomorphologic categories between the two different schemes differs considerably, for instance, with LSM classifying three out of the 22 transect locations as bedrock, while PDS identified them as dry lake and alluvial deposits, and LSM classifying further PDS dry lake locations as a stabilised sand deposit and bedrock with sediment.

The PI-SWERL results do not show a clear relationship between the measured dust emission and the SSM values. The SSM values for the entire study area range from a minimum of 0.002 to a maximum of 0.519 with a mean of 0.187, with the peak geometric mean transect emission rate (0.22 mg m^{-2} s^{-1}) corresponding to a moderate SSM value (0.25 mg m^{-2} s^{-1}). Furthermore, a wide range of emissivity (0.002 to 0.22 mg m^{-2} s^{-1}) is seen in the narrow range of SSM values between 0.23 to 0.27. This range covers the LSM categories of stabilised sand deposit, sand deposit on bedrock and bedrock, but correctly classified as predominantly alluvial deposits and some stony surfaces according to the PDS map. The highest SSM value for the PI-SWERL test sites was 0.46, which corresponded to a stony surface with an emission value of 0.013 mg m^{-2} s^{-1}. The high SSM value assigned to this site is potentially due to the high reflectivity of the white quartz gravel that makes up the stony surface, with the LSM classifying it as playa/sabkha according to the classes used by Parajuli et al. (2014). Further high SSM values (> 0.3) mostly occurred within alluvial deposits with emission values of 0.008 to 0.12 mg m^{-2} s^{-1}, with the lowest emission flux value of 0.008 mg m^{-2} s^{-1} associated with the active channels. The locations of the dust source points identified by von Holdt et al. (2017) with Landsat imagery in Figure 1 (a) have SSM values with a range of 0.078 to 0.508 and a mean of 0.245.

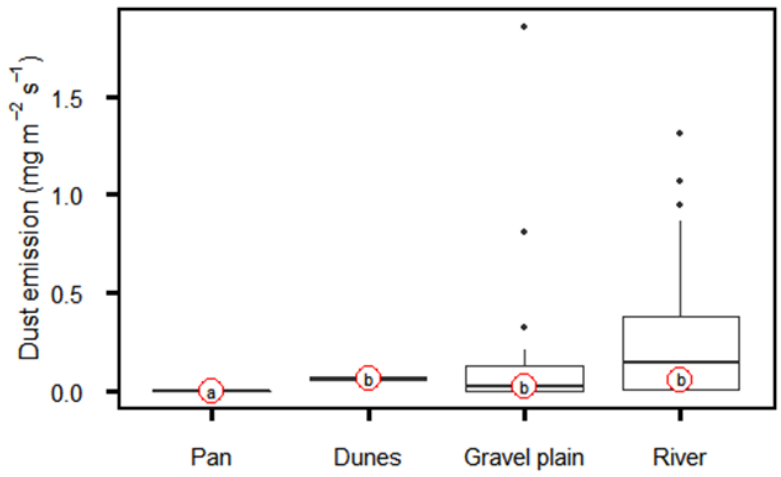

Figure 3-3 Dust emissions from landscape geomorphic units. The dunes, gravel plain and river show no significant difference between the geometric mean of the emissions measured with the PI-SWERL at the landscape level. The landscapes were significantly different to emission results from the pan. Different letters indicate a significant difference between the geometric means of each landscape type as determined using a one-way ANOVA and Tukey's HSD test. The letters are plotted at the geometric mean.

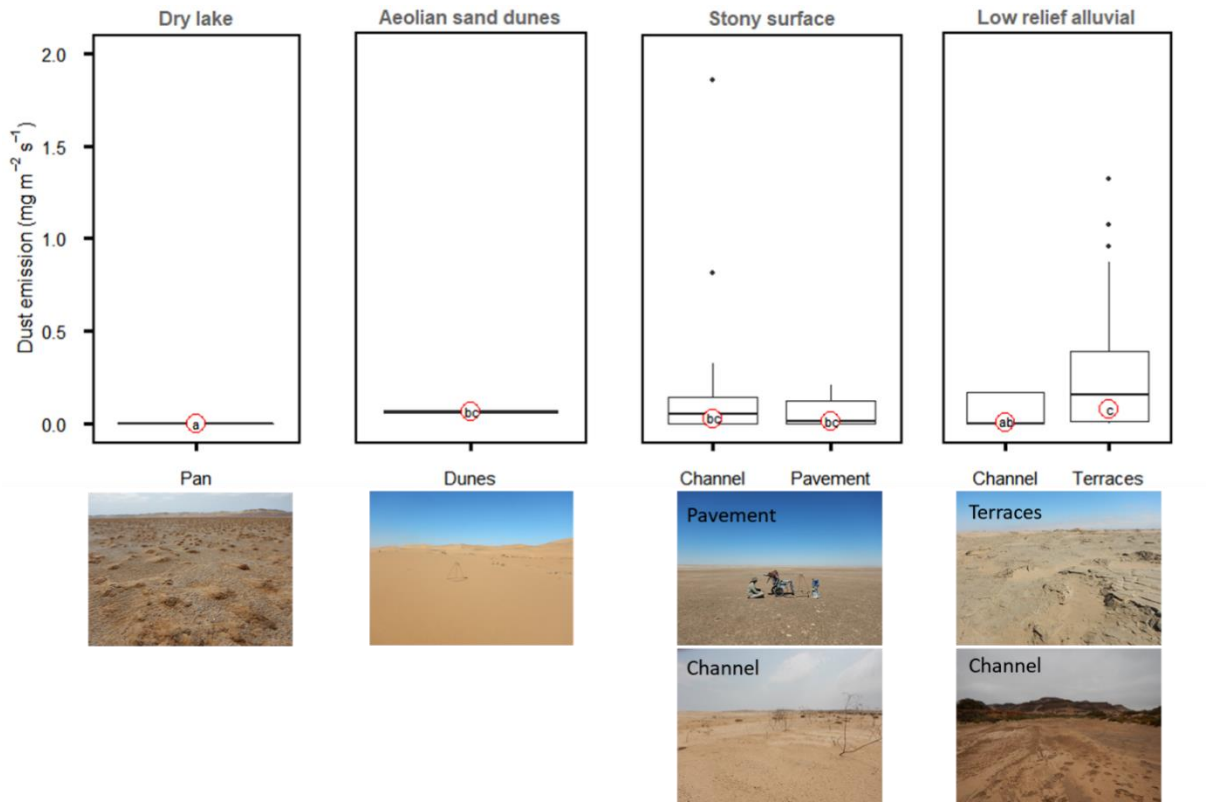

Figure 3-4 Dust emission from landform elements in the stony surfaces and alluvial systems tested with the PI-SWERL. The river terraces proved to be the dustiest in the river. The pan and dunes were not considered at landform level, but are included here for comparison. Letters indicate significant difference determined by one-way ANOVA and Tukey's HSD test and are plotted at the geometric mean of each landform.

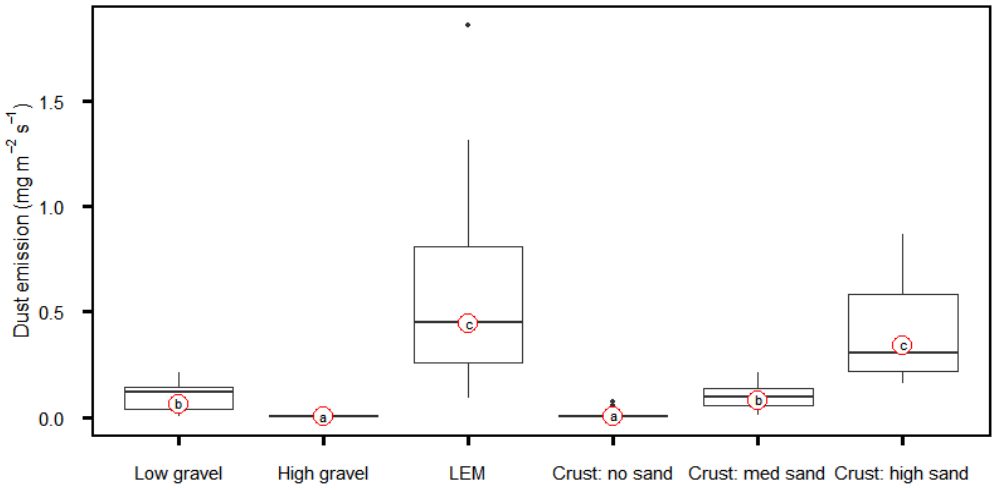

Figure 3-5 Dust emissions from surfaces of the river and gravel plain. LEM (loose erodible material) consists of all unconsolidated sediments. This category incorporates LEM found in between silt crusts of terraces and nebkhas. The stone pavements divided based on the density of the gravel cover, with < 30 % classified as low gravel. The results for depositional crusts were divided based on the availability of saltators based on a visual assessment before the PI-SWERL run. Letters indicate significant difference determined by one-way ANOVA and Tukey's HSD test and are plotted at the geometric mean of each landform.

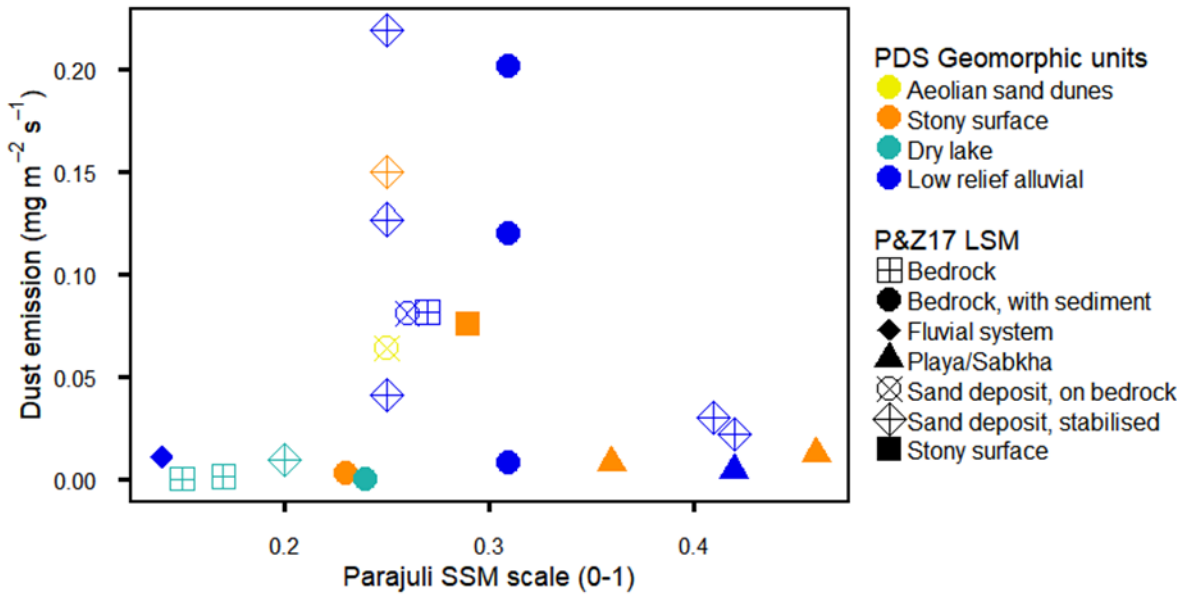

Figure 3-6 Dust emission measured with the PI-SWERL compared to the SSM value at the site of testing. The legend is firstly based on the LSM geomorphic units (shape) and secondly as mapped for this study using the geomorphic categories proposed by the PDS scheme (colour).

3.5.4 Predictors of emission rate as determined by Boosted Regression Tree analysis

The BRT model produced the following variables as the most important predictors for dust emitted during the PI-SWERL runs: gravel cover (%), moisture content (%), kurtosis, very coarse silt fraction (%), very fine sand (%), fine sand (%), compressive strength (kg m^{-2}), Ca (%), Mg (%) and S (%). The relative contribution of each variable to the model is given in Figure 3-7. The partial dependency plots in Figure 3-8 also provide the relationship between the variable in question and the measured dust flux when all other variables are held constant. It is important to look at the trend in these plots and not the actual values, with increasing partial dependence values indicating increased dust emission and decreasing values indicating the opposite. A sudden change indicates a critical threshold at which the dust emission potential changes. Together, the significant predictor variables identified with the BRT explain 70.8 % of the deviance in the dust flux measured with the PI-SWERL.

Based on the BRT analysis, soils layers with a very coarse silt content above 5% and a very fine to fine sand content between 10 and 20% resulting in a platykurtic particle size distribution should indicate areas with potentially increased emission potential. In addition, the density of gravel cover results in an increase in roughness which appears to have a significant influence on reducing emission potential exerted by a gravel content of 15% and above. Moisture has long been regarded as a primary control on dust emission and was also identified as a primary predictor. Calcium and magnesium were also identified as important elements due to the effect that carbonate minerals potentially have on the erodibility of a crusted soil, with some suggesting that it will act to strengthen the crusts by acting as a binding agent (Gillette et al., 1982) and others contending that the calcite will have very little resistance to abrasion (Pye and Tsoar, 1990). Our data seem to support an increase in u^*_t with increasing Ca and Mg content and a subsequent reduction in emissions. The model output

shows excellent predictive capacity (supplementary section 3.9.3). An example of two emission measurements with associated predictor variables are given in supplementary 3.9.9.

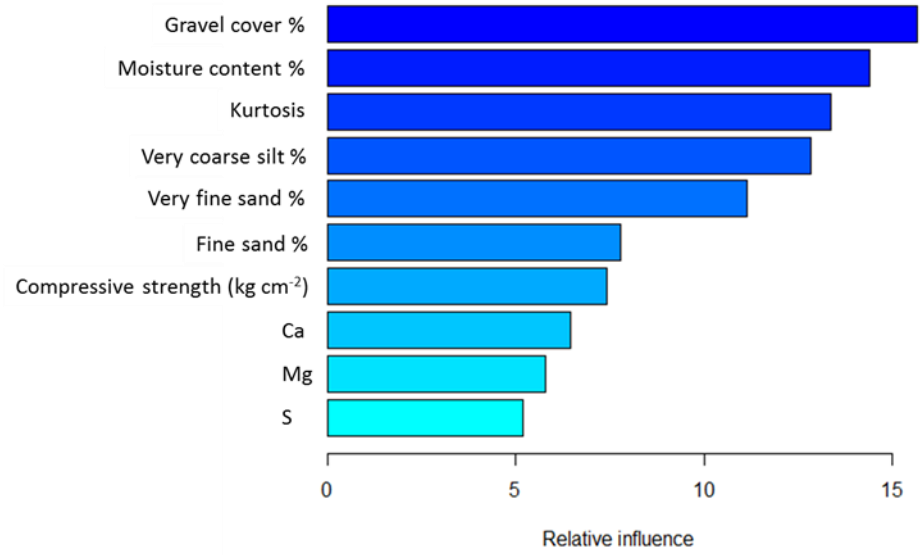

Figure 3-7 Relative importance (%) of the different surface variables in predicting dust emission.

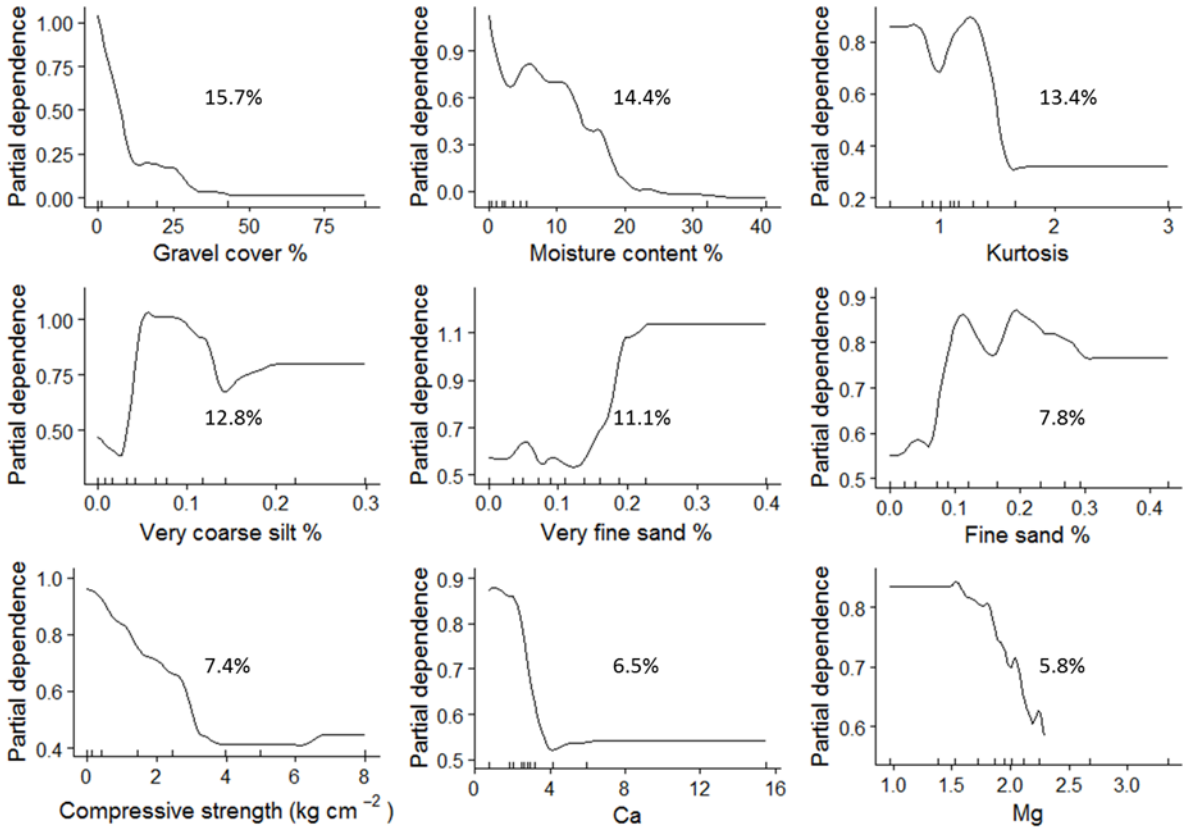

Figure 3-8 Partial dependency plots depicting the relationship between dust emission and each significant variable. The trend rather than the actual values is the important feature in each plot. Increasing partial dependency values indicates an increase in dust flux and decreasing values the opposite.

3.6 Discussion

The recent acquisition of dust source data at the landform scale allows for a validation of the PDS and LSM surface classification schemes and the newly generated global scale SSM product as a means to represent dust emission potential for the Namib Desert. This location represents an ideal region for such a validation study as it is host to a variety of actively emitting landform classes (Vickery et al.; von Holdt et al., 2017). Classifying the dust source points identified with Landsat data by von Holdt et al. (2017) according to the PDS indicates that dust emission from the Namib Desert is highly concentrated, with relatively high densities of plumes found to originate from the alluvial deposits (0.4 points km^{-2}) and dry lakes (0.9 points km^{-2}) (Figure 3-2). Mapping the geomorphic units of the Namib Desert according to the PDS developed by Bullard et al. (2011) shows the limited extent of lakes as dust-producing areas which constitute only 2 % of the total study area which is similar to what Gillette (1999) found. The advantage of the PDS map is that it can represent the landscape in detail because of the high-resolution, user-defined mapping. The disadvantage of this scheme is that it requires detailed inputs to map the landscape, which are not consistently available for all areas, and requires geomorphic units to be identified and created which is prone to subjectivity. The PDS mapping has only been performed for limited areas (e.g. Baddock et al., 2011; Lee et al., 2012) and creating a global PDS map remains a challenge. Using the LSM developed by Parajuli et al (2014, 2017) to map the study area results in an overestimation of the dust emitting alluvial and lake areas (Figure 3-1 c). This is due to the misclassification of several geomorphic units as a result of the supervised technique based on training classes situated in the MENA (Middle East and Africa) region when attempting to create a global geomorphology classification map. Even though a global geomorphology classification map would provide a valuable input to the representation of dust emission, the use of region specific training classes should be exercised with caution. A

further limitation of a qualitative geomorphic mapping scheme, such as the PDS and LSM, involves the representation of a quantified dust emission potential.

A quantified representation of dust emission potential of different landforms in raster format is necessary to incorporate these schemes into dust cycle models. For the PDS this has not been achieved and each geomorphic class is assigned a qualitative categorical indicator based on inferred emission potential. Such an approach does not discriminate between relative emission potential from different regions that act as dust sources. A quantification of the erodibility of the dust emission potential of the LSM land cover categories was attempted by Parajuli et al. (2014) using a correlation between ERA-Interim wind speed at 10 m height and MODIS deep blue AOD at 550 nm. The authors point out that a disadvantage of this approach is the difference in scale between the high-resolution land cover map and the coarser (1° × 1°) correlation map which results in a disconnect between land cover and the emission potential assigned to them. The location of the major Namib Desert dust sources in the low-relief terminal stages of the rivers and sabkhas adjacent to the coast places these dust sources in a difficult position for identification with techniques using aerosol loadings. The use of atmospheric aerosol loading estimates, such as MODIS AOD or TOMS AI to locate dust sources in the Namib Desert may well have specific limitations. For example, detection of dust over bright desert surfaces using ultraviolet, visible or thermal infrared wavelengths is problematic (Baddock et al., 2009; Hsu et al., 2004; Resane et al., 2004). In contrast, the use of MODIS deep blue (MODIS DB) can only be retrieved over bright surfaces and is of limited use over dark ocean surfaces. In addition, TOMS AI does not detect dust from the Namib Desert at low altitude near the coast (Mahowald et al., 2004). Creating an erodibility map from supervised classes situated in a different region and with reliance on emission quantification from satellite retrieved aerosol loadings would likely result in a number of highly emissive dust-producing areas, such as the Namib Desert, being underestimated. Field-

based studies that include PI-SWERL emission measurements from intensely-sampled regions can provide relative dust fluxes, as well as indications of variability, as inputs for the quantification of dust emission scheme mapping such as the PDS and LSM (Supplementary section 3.9.8).

The recently proposed SSM provides a global landscape scale erodibility map with a quantification of dust emission potential by combining both a physical and empirical approach. The use of upstream drainage area represents the supply of sediment and the surface reflectance represents the different sediment characteristics of the land surface types (Parajuli et al., 2017). The SSM dust emission scheme is a novel attempt to represent erodibility of the landscape at a global scale, elegantly tuned to a Bodélé maximum. However, the landform scale assessment of the SSM presented here highlights that there are potential shortcomings in this erodibility map. The dust source points identified with Landsat analysis indicates that most of the dust hot spots in this area are situated in the terminal stages of the rivers as they near the Atlantic Ocean and the coastal sabkhas (von Holdt et al., 2017). The SSM classification however identifies areas with high emission potential significantly upstream of the confirmed dust sources, including areas covering large areas of stony surfaces adjacent to alluvial and lake sources (Figure 3-1 e). Furthermore, rivers that are not significant dust sources, such as the Swakop River (marked W in Figure 1 e) are identified as highly emissive in the SSM. The reduced dust emission from the Swakop River is potentially due to the incised nature of this river combined with less topographic channelling of the high magnitude north-easterly Bergwind compared to other more emissive rivers such as the Kuiseb River. In addition, the lush vegetation sustained by groundwater within many parts of the Namib ephemeral rivers provides significant vegetative roughness to make sediments unavailable for entrainment (von Holdt & Eckardt, 2017). As a result, the high emission potential of alluvial sediment supply is likely to be also overestimated in the SSM. The

influence of vegetation and topographic channelling would not be problematic provided that these variables are adequately parameterised in the dust model, in addition to the preferential dust source areas identified by the dust emission schemes assessed in the present study.

The assessment of SSM values for the locations where dust source points were identified at high-resolution with Landsat and against PI-SWERL dust flux measurements indicate that the SSM scheme does not always relate to the independent measures of dust emission presented here. The mean SSM value for dust source points of 0.245 is just under half the maximum emission value of 0.519 for the Namib region, with only 4.7% of the 2289 dust source points classified in the most emissive category >0.4. Although the Landsat identified dust source points do not provide a continuous numerical quantification of the dust emission potential, this point inventory does identify areas which should be assigned values of high emissivity similar to the method used by Parajuli et al. (2017) in assigning a maximum value of 1 to the Bodélé Depression. In addition, there is no clear relationship between the SSM emission values and PI-SWERL emission results (Figure 3-6). Sites exhibiting high emission rates from the wind tunnel testing were not necessarily classified as potentially highly emissive according to the SSM. The most emissive sites as measured with the PI-SWERL have SSM values ranging from 0.25 to 0.29. The highest SSM value (0.46) associated with the PI-SWERL runs was situated on a quartz stone pavement surface. The mean SSM value for the PI-SWERL sites is 0.28 (± 0.08). In this context, the PI-SWERL provides a quantification of dust emission to compare the dust emission potential from different geomorphic units and offers a means to validate dust emission schemes. Dust emission is highly variable as indicated by the PI-SWERL dust flux measurements (Figure 3-4 and Figure 3-5). The small-scale variability that exists at landscape scale has been seen to exert a clear effect on dust emission, so adequate representation of this variability remains an important yet persistently challenging research goal. The combination of the Landsat dust point source and PI-SWERL

dust flux measurements at landform and sub-landform scale can make contributions in an input and validation sense for landscape scale dust emission schemes.

The PI-SWERL potentially provides a standardised quantification of surface dust emissions however comparison between different studies and regions would require consistency in measured parameters and landform categories. Comparing our results with Sweeney et al. (2011) in the Mojave Desert, USA (referred to from hereon as SW2011) shows agreement between some of the measured landforms (Figure 9). SW2011 tested at the same friction velocity (u^* = 0.56m s^{-1}) as our study. The stony surfaces and dry lakes compare well, whereas the aeolian deposits have good agreement between the geometric means and lower confidence interval, but SW2011 have a much larger upper confidence interval. This is potentially due to SW2011 consisting of more replicates (30 versus 3 for the present study) and their dunes being situated adjacent to a large pan. The dunes tested as part of this study were situated near an ephemeral river (Figure 1 a, south of Kuiseb delta), which would introduce potentially finer material than dunes situated further from such a source. What we classified as a channel within the stony surfaces probably most closely corresponds with a wash as per SW2011, which SW2011 determined to be considerably more emissive (SW2011 Wash geomean: 0.3915 mg m^{-2} s^{-1} vs geomean of channel in present study: 0.030 mg m^{-2} s^{-1}). The gravel plain channels in our study did not have a supply of available sand for saltation at the sites we tested. Our results for crusts in the presence of saltators and LEM correspond well with the wash results from SW2011, which seem comparable from the description provided. The LEM category from this study and the wash from SW2011 were the two most emissive categories and represent a maximum emission value for the two studies. Despite LEM representing a surface type and wash a landform type, the upper limit of emission shows good agreement and again illustrates the importance of landform and surface interpretation.

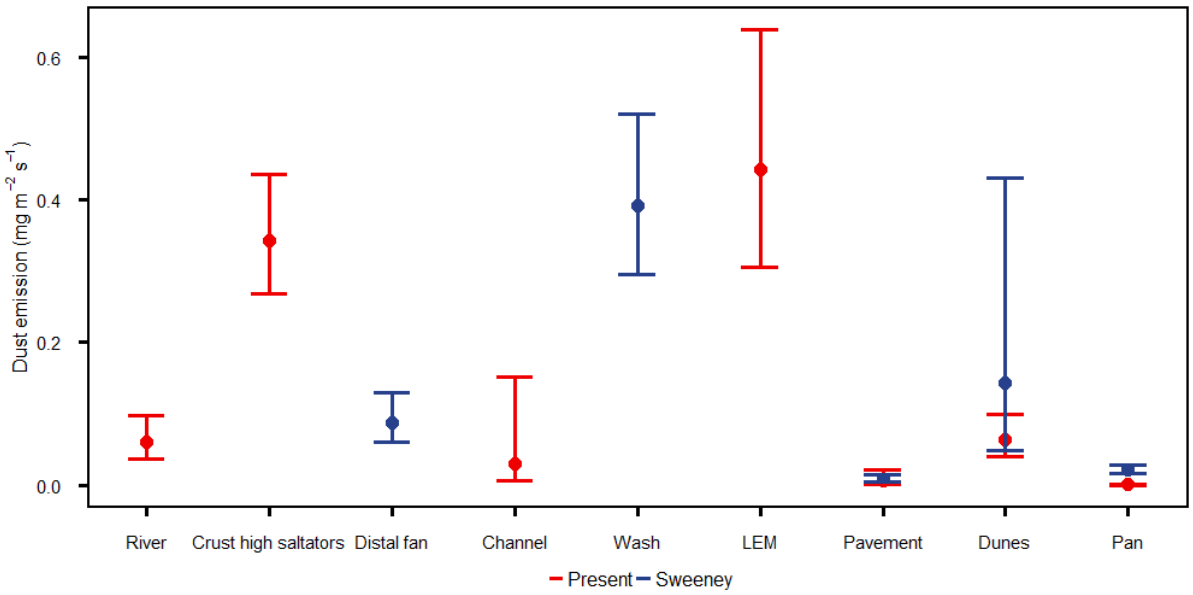

Figure 3-9 Comparison between the present study and result from Sweeney et al. (2011) from the Mojave Desert, USA (both studies attested at $u^* = 0.56 m s^{-1}$). Selected landforms from both studies were chosen for comparison, as well as selected surface types from our study. The pavement and pans show good agreement. The categories with maximum emission values between the two studies (wash for Sweeney et al., 2011 and LEM surface type for our study correspond).

Another potential approach to develop and improve dust emission schemes with small-scale PI-SWERL data is to assess the factors that control the erodibility of the surfaces. This is especially useful for factors that are represented in datasets that are available globally, such as particle size and moisture data. The BRT analysis highlighted the significant variables for PM_{10} dust flux measured with the PI-SWERL at a set friction velocity. The partial dependency plots additionally highlight a critical threshold where dust emission takes place or ceases (Figure 8). An important consideration for this analysis is the choice of variables and the method of measurement. For example, the method of determining moisture content in this study with the use of a moisture probe just below the surface was not ideal. A more accurate reflection of the moisture content would have been obtained by a gravimetric determination of the top 1 cm of the soil surface, which would provide an indication of the soil moisture (%) exerting a primary influence on the erosion threshold (u^*_t). Inclusion of

moisture data points taken from the pans, based on soil moisture measurements from just below and not directly at the surface, likely resulted in a lower predictive ability by the BRT. When the pan data points are excluded, a critical moisture threshold of 2 % is obtained for the tested friction velocity of 0.58 m s^{-1}. This is similar to the threshold of 0.02 g g^{-1} soil moisture obtained by Munkhtsetseg et al. (2016) above which they observed dust emission is significantly depressed. This is also relevant for the environmental conditions at the time of testing. The emissivity of the pans was significantly lower due to the prevailing elevated humid conditions in proximity to the coast at the time of testing, as well as the hygroscopic saline surfaces and shallow water nature of the wet playas (Reynolds et al., 2009; Sweeney et al., 2016). The BRT analysis should also be extended by testing at different friction velocities to determine the threshold at which emission is initiated. Furthermore, by identifying the significant variables, a set of surface characterisation tests can be developed that should be included when measuring emission potential. Combining a standard set of surface characterisation tests and dust flux measurements from different well-known hot spots around the world can be used to substantially improve dust emission schemes.

3.7 Conclusion

Despite improvements in the representation of erodibility by recently proposed dust emission schemes, limitations are apparent in our ability to map dust emission potential as exhibited by independent or assessment efforts of dust potential schemes made in this study. From a Landsat-derived inventory of actively eroding parts of the Namib Desert at a sub-landscape scale combined with the ground-based measurement of dust emission rates of these observed point sources using a PI-SWERL, a qualitative and quantitative evaluation of emission potential classification was performed. Sites for testing with the PI-SWERL wind tunnel was selected from the source point identified with Landsat data for a 25 year period from 1991-

2016. The dust source points and dust emission flux measurements were used to assess proposed dust emission schemes that represent erodibility. The findings here demonstrate that assessment of schemes representing dust emission potential using landform and sub-landform scale data can make a contribution to the improvement of these schemes.

The combination of a physical and empirical based approach used to create the Sediment Supply Map (SSM) is useful at capturing all the relevant factors for erodibility where global data sets are available. The SSM represents sediment supply on the basis of hydrology and surface reflectance, but does not take into account topography or vegetation. As a consequence, alluvial systems as potential high emission areas are identified significantly upstream and more extensive compared to the dust source points identified with the aid of remote sensing. The inclusion of remote sensing data offers the opportunity to capture the dynamic nature seasonality. The representation of dust emission potential on the basis of geomorphic mapping, such as the PDS, has limitations in terms of the inputs necessary to create a global map, as well as to quantify the emission potential.

The determination of significant variables and critical thresholds for dust emission with a Boosted Regression Tree model improves dust emission schemes. The BRT analysis for the Namib Desert highlighted the importance of moisture content, crust strength and particle size characteristics such as kurtosis, the presence of sand and silt and gravel density. This can be done for well-known dust sources around the world. A standardised set of surface characterisation tests combined with dust flux measurements would provide a global data set of relative emission potential.

3.8 Acknowledgements

This research was funded by the National Research Foundation in South Africa as part of research project number: UID 89120. The authors would like to thank Suzette Heath, Peter

Bridgeford, Jo Nield and Ruusa Gottlieb for assistance in the field. Thank you to Michael Cramer for advice on running the BRT and to Martin Hipondoka for his contribution to this study. We thank the Ministry of Environment and Tourism for their support and assistance for the duration of this research. This research was conducted under MET permit number 2076/2015.

3.9 Supplementary section

3.9.1 Land surface Map (LSM) by Parajuli et al. (2014)

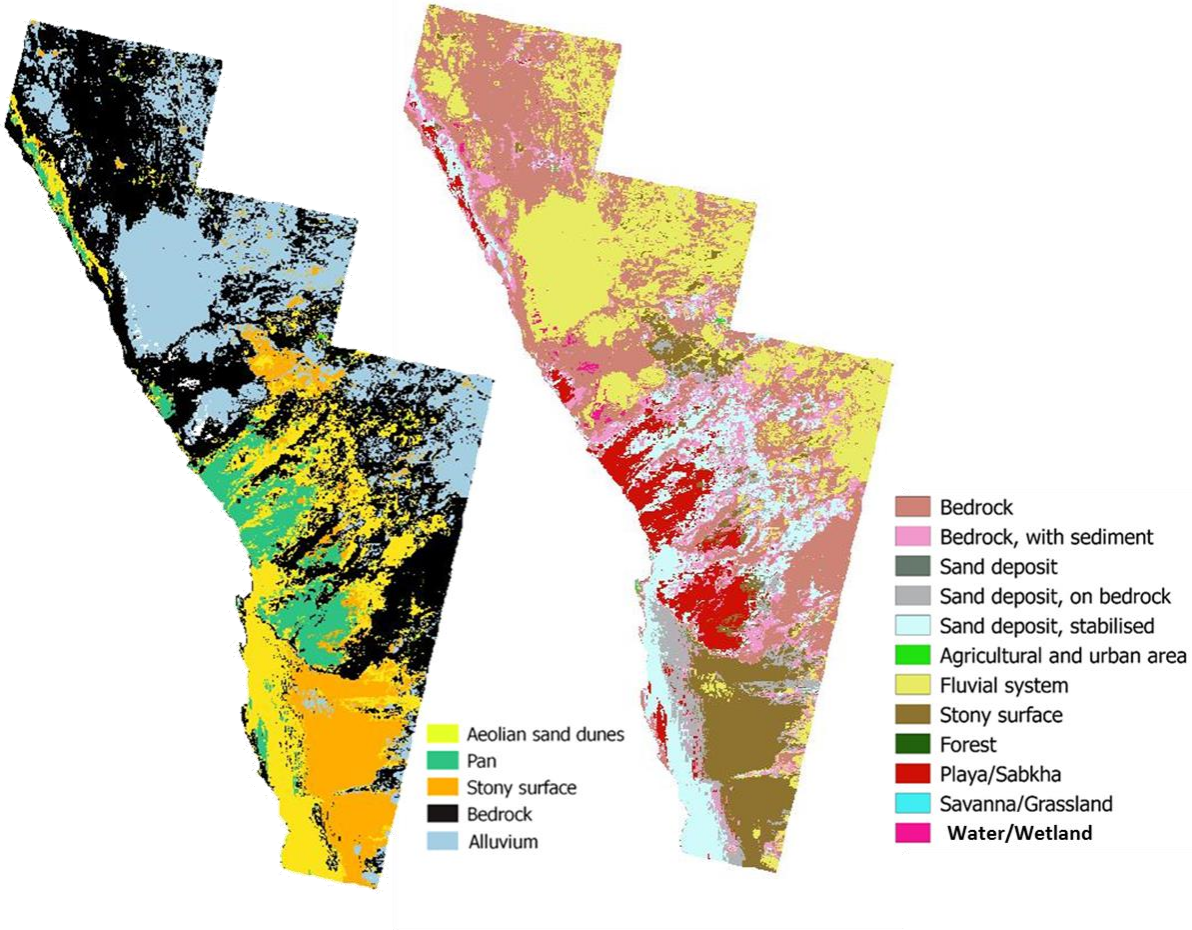

Figure 3-10 Land surface map (LSM) in original classes and colours as done by Parajuli et al. (2014) on right. Classes and colours of LSM as per PDS by Bullard et al. (2011).

3.9.2 PI-SWERL test sites and classifications

Table 3-1 PI-SWERL sites in the Namib Desert

Transect	Geom class PDS	PDS Emission potential	ParajuliSSM	ParajuliLSM	Parajuli LSM legend	Dust emission geometric mean ($mg/m^2/s$)	Latitude	Longitude
Huab1	Low relief alluvial, unarmoured, unincised	High	0.31	2	Bedrock, with sediment	0.2014	-20.8658	13.65378
Huab2	Low relief alluvial, unarmoured, unincised	High	0.31	2	Bedrock, with sediment	0.1201	-20.8655	13.65354
Huab3	Low relief alluvial, unarmoured, unincised	High	0.31	2	Bedrock, with sediment	0.0082	-20.865	13.65121
Huab4	Low relief alluvial, unarmoured, unincised	High	0.27	1	Bedrock	0.0816	-20.8617	13.65111
Huab5	Dry lake, unconsolidated	High	0.17	1	Bedrock	0.0014	-20.8687	13.47703
Huab6	Stony surface	Low	0.15	1	Bedrock	0.0002	-20.8621	13.47654
Huab7	Low relief alluvial, unarmoured, unincised	High	0.14	7	Fluvial system	0.0111	-20.9018	13.45491
Kuiseb1	Low relief alluvial, unarmoured, unincised	High	0.29	8	Stony surface	0.0759	-23.279	14.77142
Kuiseb3	Stony surface	Low	0.46	10	Playa/Sabkha	0.0127	-23.4817	15.04026
Kuiseb4	Bedrock	Low	0.23	2	Bedrock, with sediment	0.0027	-23.1383	15.03611
Kuiseb5	Low relief alluvial, unarmoured, unincised	High	0.25	5	Sand deposit, stabilised	0.2191	-23.0535	14.59137
Kuiseb6	Low relief alluvial, unarmoured, unincised	High	0.25	5	Sand deposit, stabilised	0.1269	-23.0586	14.59672
Kuiseb7	Aeolian sand dunes	Medium	0.25	4	Sand deposit, on bedrock	0.0638	-23.156	14.58164
Kuiseb8	Low relief alluvial, unarmoured, unincised	High	0.26	4	Sand deposit, on bedrock	0.0808	-23.1826	14.6423
Kuiseb9	Stony surface	Low	0.25	5	Sand deposit, stabilised	0.1501	-22.9997	14.581
Oma1	Low relief alluvial, unarmoured, unincised	High	0.41	5	Sand deposit, stabilised	0.0303	-22.0471	14.33467
Oma2	Low relief alluvial, unarmoured, unincised	High	0.42	5	Sand deposit, stabilised	0.0221	-22.0425	14.33474
Oma3	Low relief alluvial, unarmoured, unincised	High	0.42	10	Playa/Sabkha	0.0042	-22.0443	14.33713
Oma4	Low relief alluvial, unarmoured, unincised	High	0.36	10	Playa/Sabkha	0.0083	-21.8919	14.4466
Tumas1	Low relief alluvial, unarmoured, unincised	High	0.25	5	Sand deposit, stabilised	0.0412	-22.9456	14.59727
Ugab1	Dry lake, unconsolidated	High	0.2	5	Sand deposit, stabilised	0.0094	-21.2725	13.70157
Ugab2	Dry lake, unconsolidated	High	0.24	2	Bedrock, with sediment	0.0002	-21.2738	13.70936

3.9.3 Boosted regression tree (BRT) model

3.9.3.1 Model parameters

The BRT model (Elith et al., 2009) was run in R using the gbm.step function within the *dismo* package version 1.1-4 (Hijmans et al., 2016). All PI-SWERL measurements of undisturbed surfaces were included in this analysis (n=128) as the dependent variable and ranged from a minimum emission value of 0.00005 mg m^{-2} s^{-1} to 1.854 mg m^{-2} s^{-1}. A total of 36 variables were included in optimisation and the initial model run using a Gaussian distribution with a learning rate of 0.005, tree complexity of 5, bagging fraction of 0.5 and cross-fold validation of 10. The initial model was then simplified using the gbm.simplify function in *dismo* which drops variables with a relative influence of less than 1.5. The independent variables are listed in Table 3-2.

Table 3-2 Independent variables included in the regression model.

Category	Variable
Particle size analysis	CLAY, COARSE SAND, COARSE SILT, D10, D50, D90, FINE SAND, FINE SILT, Gravel cover, Kurtosis, Mean, MEDIUM SAND, MEDIUM SILT, MODE 1, MODE 2, MODE 3, SAND, SILT AND CLAY, SKEWNESS, SORTING, V COARSE SILT, V FINA SAND, V FINE SILT
Moisture content	Moisture (%) measured with probe within 0.02 m of the surface.
Strength	Compressive and shear strength (kg cm^{-2})
Elemental composition	Al, Ca, Fe, K, Mg, Mn, P, S, Ti (%)

3.9.3.2 Evaluation of predicted values compared to actual values

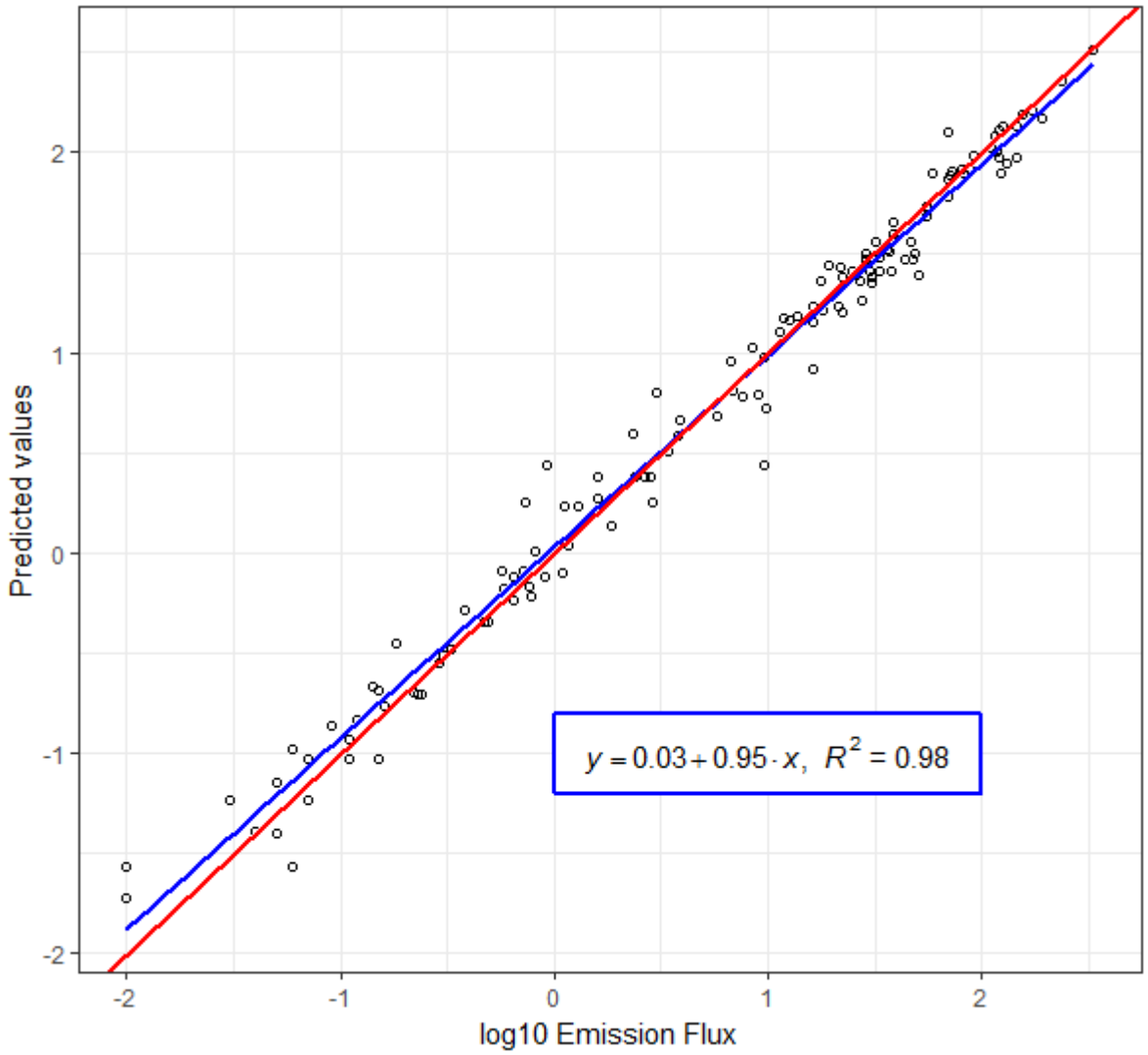

Figure 3-11 Comparison of the BRT model predicted values compared to the actual emission flux values from the PI-SWERL (log10).

3.9.4 Dust source point classification

A certain classification of the landscape units, as set out in Figure 3-2, based on the Landsat imagery analysis were possible for 93% of the 2462 plumes identified from 1991 to 2016. According to this Landsat analysis for the Namib Desert, the largest numbers of plumes were identified in the rivers (991), pans (776) and gravel plain (505). The extent of the area of each of these landscape units are however very different. According to the geomorphic mapping in Figure 3-1 b, the pans cover only 850 km^2 of the study area, the alluvium of the rivers 2600 km^2 and the stony surfaces of the gravel plain covering approximately 45,000 km^2. This results in a high density of points situated in the pans (0.9 / km^2) compared to the river (0.4 / km^2) and the gravel plain (0.01 / km^2) (Figure 3-2). The greatest number of plumes from the pans were identified as originating from the Conception Bay and Meob Bay pan area (37% of pan plumes, marked C in Figure 3-1 a), which covers 450 km^2 in area accounting for more than half of the pan areas of the study site. The next largest pan at Sandwich Harbour covers only 27 km^2 (S in Figure 3-1 a). Although the pans (dry lakes) have a higher density of source points than the rivers (low relief alluvial surfaces), the rivers experienced more dust days (535 for present study area) than the pans (236) according to the analysis of MODIS imagery for the period from 2005-2015 done by von Holdt et al. (2017).

The Landsat data analysis enabled the further identification of 72% of the dust source points down to the landform level (Figure 3-12). For example, the majority of plumes from the rivers originated from the Kuiseb River delta paleo-silt terraces (51 %), these plumes were previously thought to originate from the active delta floodplain (Vickery et al., 2013; von Holdt et al., 2017). In addition, plumes from the gravel plain could be distinguished from those from the adjacent river terraces and plumes from the gravel plain channels (wadis) could be differentiated from those from the stone pavements. The predominance of plumes originating from the interior of the pans, i.e. basins, is a result of the majority of plumes

originating from the vast area of Conception and Meob Bay. The source points identified by Landsat enabled focused ground-based measurements with a PI-SWERL portable wind tunnel. This provided the ability to confirm emissive landform types in cases where they could not be distinguished with certainty with the Landsat imagery, such as valley-fill terraces surrounding the active channel within a river.

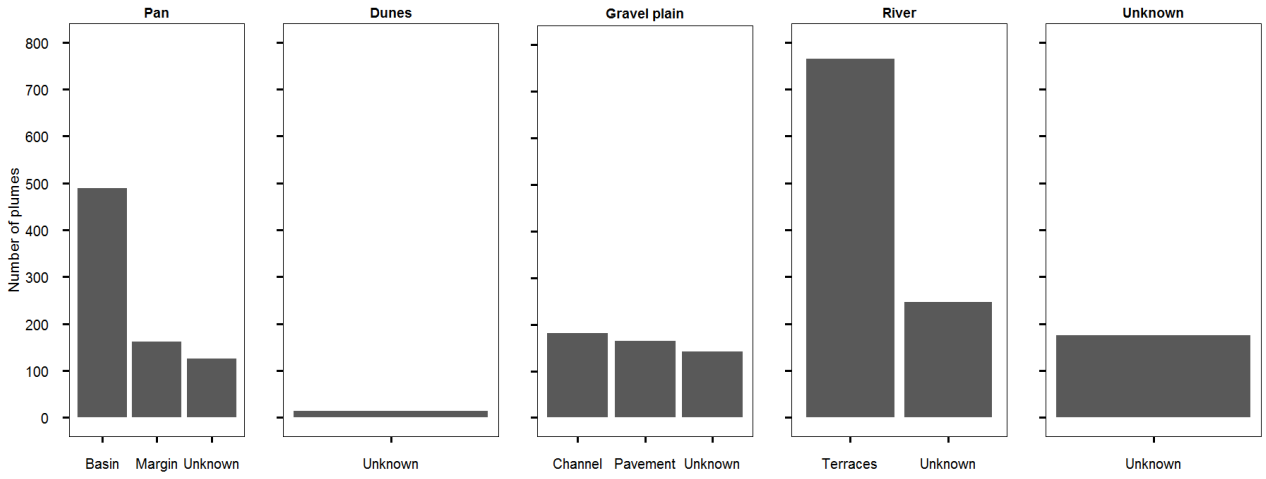

Figure 3-12 Landform classification of dust source points identified with Landsat. 72% of all the source points were classified at the landform scale.

3.9.5 Emissions from pans

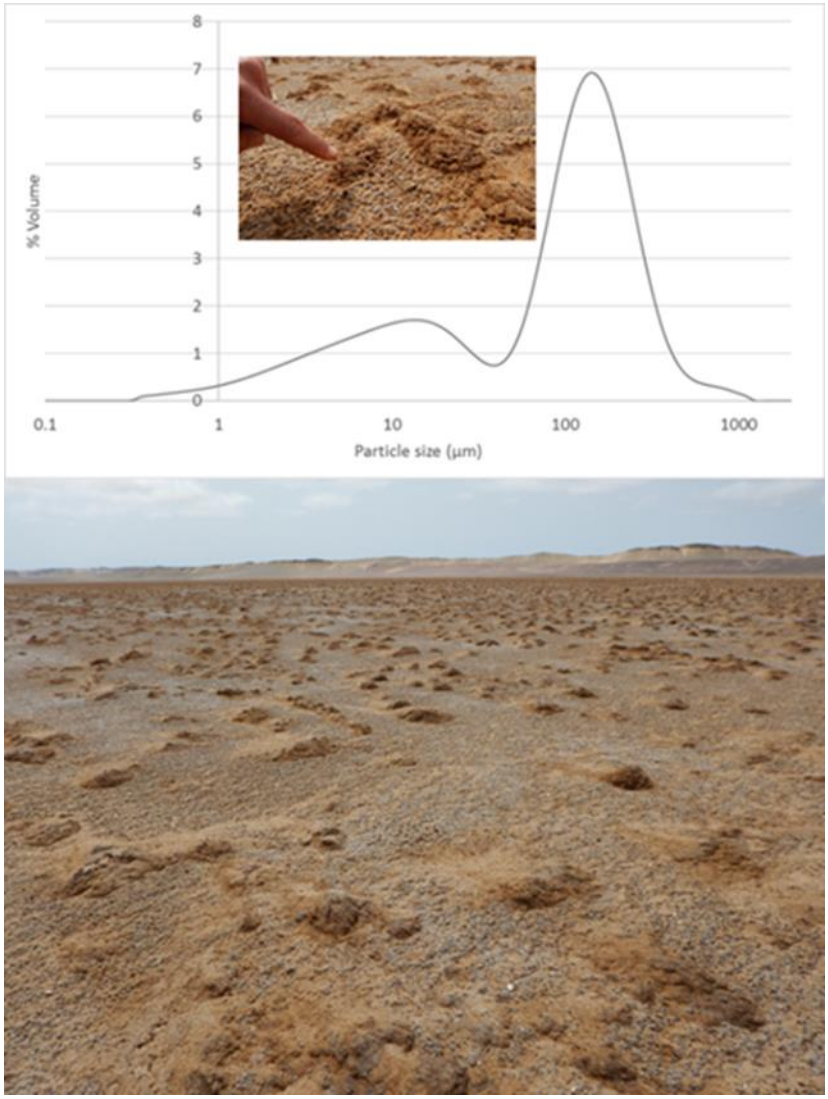

Figure 3-13 Huab pan surface with knobs covered with a crumbly cauliflower texture consisting of a mix of clastic and saline material. A considerable quantity of fines is found within this loose surface covering which can become available for emission with abrasion and saltation under high wind speeds and low humidity.

3.9.6 Emissions from dunes

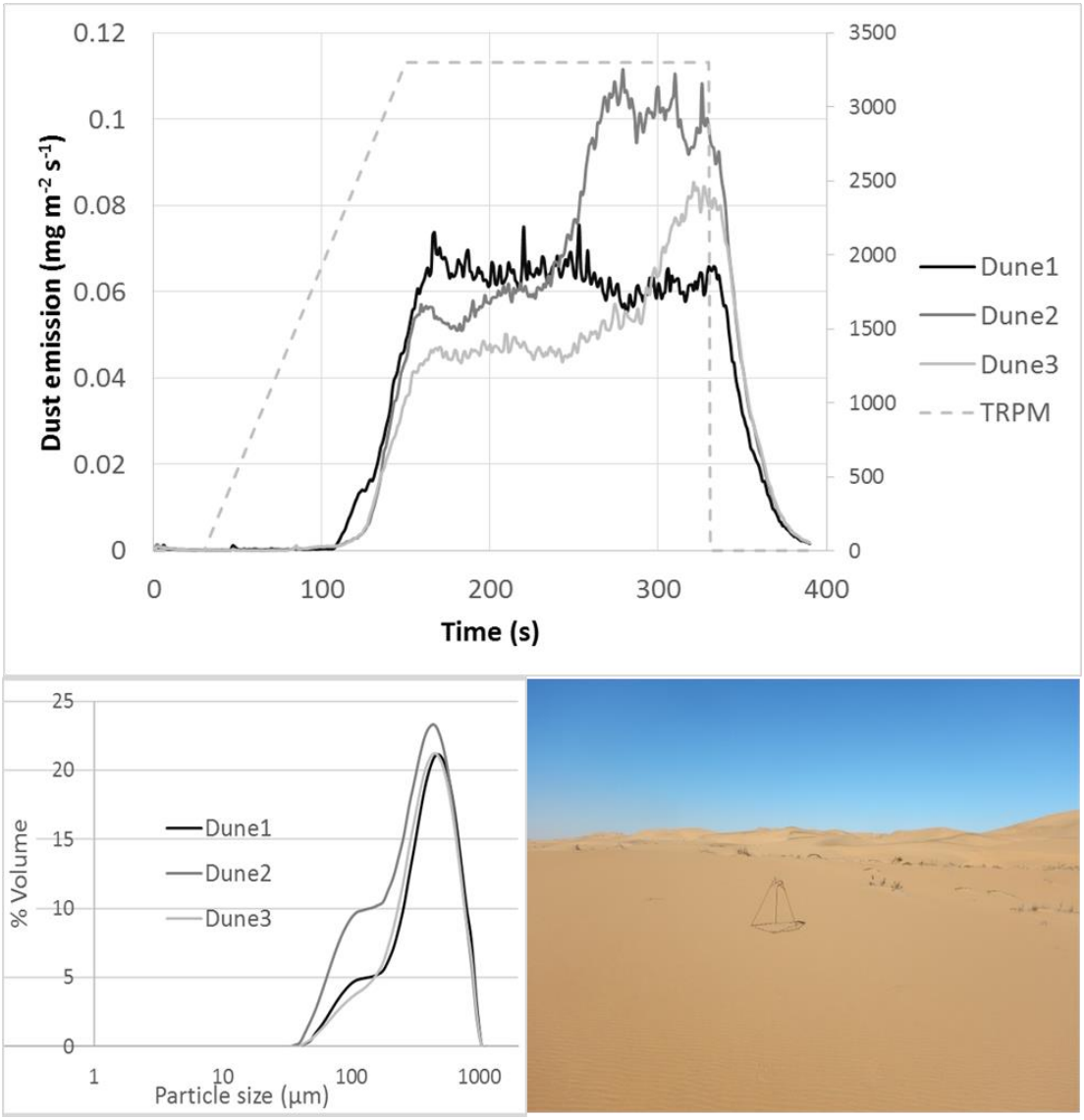

Figure 3-14 The dunes of the Namib Sand Sea PM_{10} dust emission (PI-SWERL runs in a), especially when considering the lack of fine particulates in the surface sediment (b). The PSD corresponds with the PI-SWERL run of the same name. Photo of dunes with 75cm quadrat.

3.9.7 Crusts with saltators present and absent

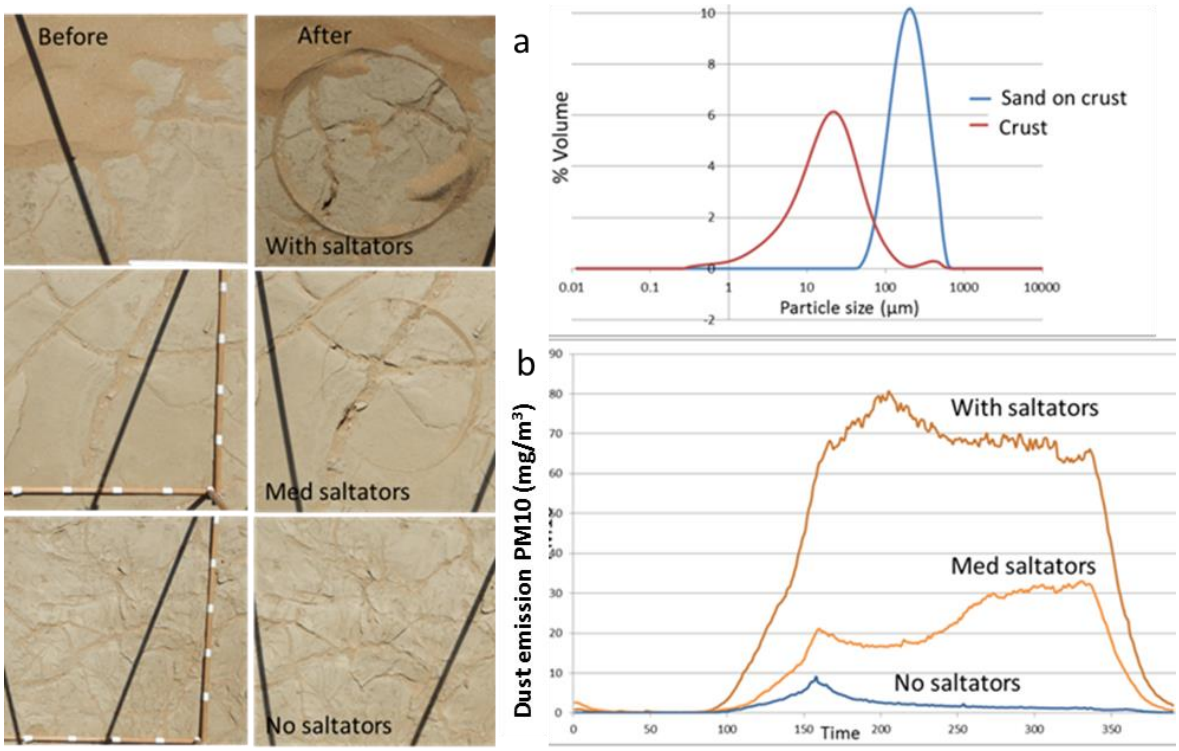

Figure 3-15 Terrace crusts and sand in the Kuiseb River.

(a) The particle size distribution of the silt crust and the sand found on the crust acting as saltators.

(b) Dust emission from the crusted surfaces with different amounts of saltators present. Large quantity of sustained dust emission in the presence of many saltators. Much reduced emission in the presence of limited saltators. Crust with no saltators show a supply limited response, with an initial peak and then a decline to no emission.

3.9.8 Dust emission statistics from different scales

Table 3-3 Dust emission from landscapes, landforms and surfaces

		Dust emission (mg m^{-2} s^{-1})				
	n	Geometric mean	CI low[a]	CI high[b]	Max[c]	Min[d]
Landscape						
River	84	0.060	0.037	0.097	1.314	0.0002
Gravel Plain	24	0.021	0.007	0.059	1.854	0.0003
Dunes	3	0.064	0.041	0.100	0.076	0.534
Pan	17	0.001	0.0004	0.002	0.021	0.00005
Landform						
Terraces	75	0.076	0.047	0.123	1.314	0.0002
River channel	9	0.008	0.001	0.049	0.168	0.0008
Pavement	16	0.007	0.002	0.021	0.213	0.663
Channel	13	0.030	0.006	0.152	1.854	0.0003
Surfaces						
Low gravel	12	0.063	0.027	0.148	0.213	0.0005
High gravel	9	0.002	0.001	0.007	0.015	0.0004
LEM	21	0.442	0.306	0.638	1.854	0.0417
Crust: no saltators	31	0.004	0.003	0.007	0.070	0.0003
Crust: med saltators	13	0.081	0.050	0.132	0.210	0.047
Crust: high saltators	22	0.342	0.268	0.436	0.865	0.158

[a] 95% confidence interval below the mean

[b] 95% confidence interval above the mean

[c] Maximum emissions from unit/surface

[d] Minimum emissions from unit/surface

3.9.9 BRT predictor variables and emissions example

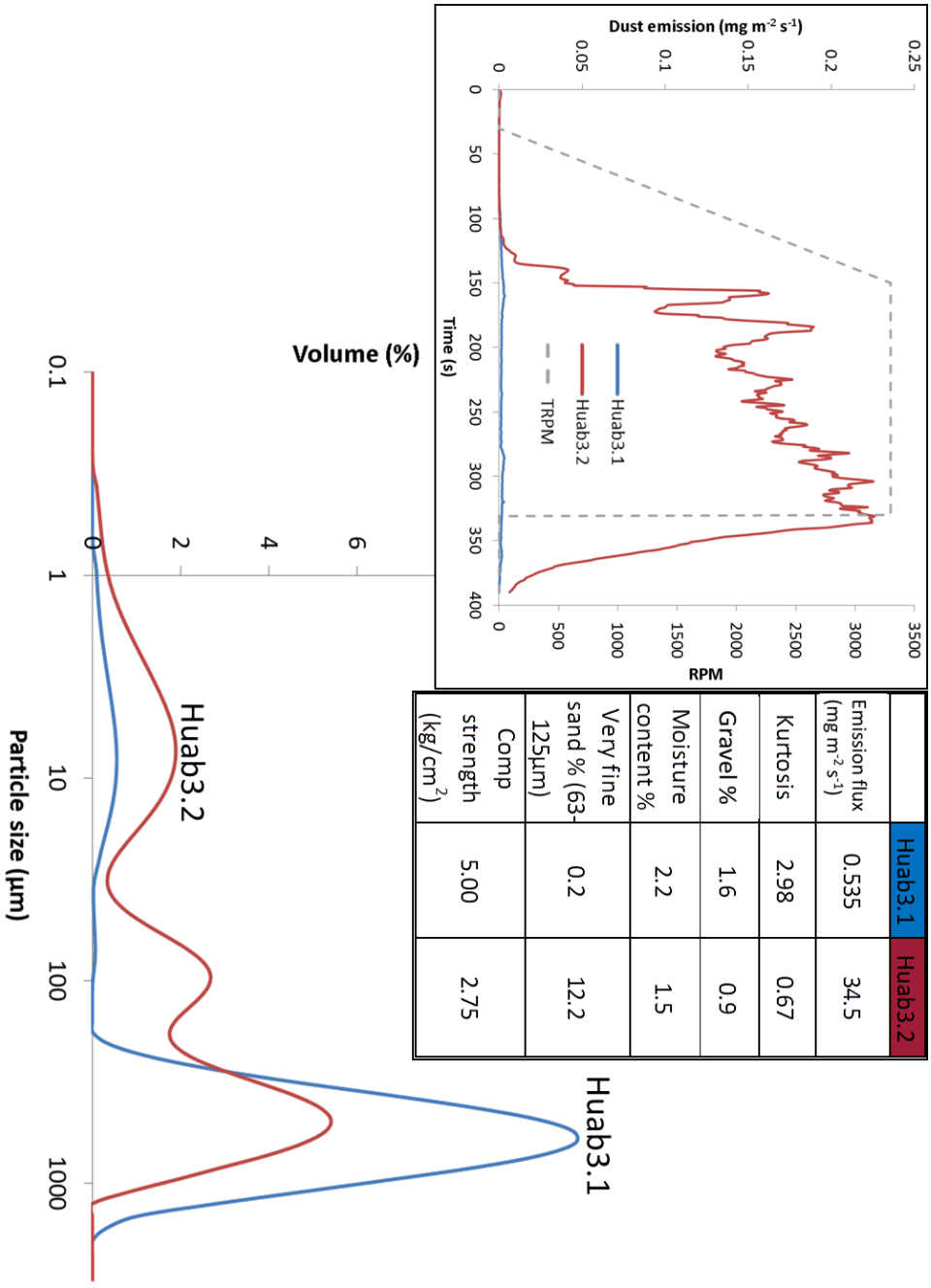

	Huab3.1	Huab3.2
Emission flux (mg m^{-2} s^{-1})	0.535	34.5
Kurtosis	2.98	0.67
Gravel %	1.6	0.9
Moisture content %	2.2	1.5
Very fine sand % (63-125µm)	0.2	12.2
Comp strength (kg/cm^2)	5.00	2.75

Figure 3-16 Two PI-SWERL runs from the Huab River with selected significant variables identified by the BRT analysis.

Figure 3-17 EXTRA IMAGE: PI-SWERL testing on the gravel plain. Photo courtesy of Ruusa Gottlieb.

Chapter 4: Influence of sampling approaches on physical and geochemical analysis of aeolian dust in source regions

4.1 Abstract

The sampling, measurement and characterisation of mineral dust at the source of emission is important for predicting the environmental impacts of dust, as well as providing inputs and validation for the modelling of aeolian dust. Methods used for sampling sediments at the source of emission to characterise dust emission potentially result in very different representations of the emitted dust. We compared three established approaches for sampling and measuring dust emission potential: a BSNE sediment trap, a PI-SWERL wind tunnel, and surface sampling. Individual particle analysis by auto-SEM (QEMSCAN) allowed comparison of the size, shape, mineralogy and elemental composition at a micrometre scale for dust samples collected using the three sampling approaches at a confirmed source in the Namib Desert. The BSNE was inefficient at trapping and/or retaining the fine sediment (<20 µm) and was strongly influenced by atmospheric humidity. Fine mica particles were underrepresented compared to the other sampling methods. The PI-SWERL was not effective in generating particles in the 63-100 µm fraction that was evident in the BSNE and in the surface sediments. The low representation of this fraction results in a significant difference in shape and mineralogy when compared to the BSNE and surface sample results. The surface sampling underrepresents the <20 µm fraction compared to both the PI-SWERL and BSNE. The three sampling methods thus resulted in different representations of the dust emitted at source, with differences in particle size, shape and mineralogy. These differences and the limitations associated with each method are relevant to sampling and characterising dust for

modelling and the determination of the environmental impacts. A more accurate representation of the physical and geochemical properties of aeolian dust emitted at sources would improve out assessment of dust effects. Moreover, a better understanding of the factors that control the emission would improve the accuracy of dust emission models. Field campaigns are crucial for understanding the processes, sources and eventual impacts, but how we interpret results from different sampling and measurement approaches need to be considered carefully.

4.2 Introduction

Mineral aerosols generated from desert regions provide nutrients to both marine and terrestrial ecosystems and affect climate (Knippertz and Stuut, 2014; McTainsh and Strong, 2007; Shao et al., 2011a). The determination of the physicochemical properties of aeolian dust and surface sediments of the sources provides important information regarding the provenance and evolution of dust from emission to deposition. The particle size, mineralogy and shape of the dust are crucial characteristics for understanding the effects that the particles have and the transformations they undergo from source, during transport to the point of deposition. These characteristics are dependent on the sediments at the source of emission and the sampling and measurement approach employed to characterise the emitted dust is a crucial consideration. The correct measurement and parameterisation of these characteristics at source are important for our understanding of the processes involved, the modelling of the dust cycle and assessing the potentialeffects of the dust (Kok et al., 2012; Mahowald et al., 2014).

Particle size is one of the primary determinants of the environmental impact of mineral dust because it has a significant control on sediment erodibility and transport capacity. However, the representation and measurement of the size distribution of aeolian dust samples remain a

challenge (Formenti et al., 2011; Kok et al., 2011a). The particle size distribution (PSD) at the point of emission determines how the dust PSD changes in the atmosphere and consequently how this process is modelled (Mahowald et al., 2014; Shao et al., 2011b; Nousiainen et al., 2009). The emitted aeolian dust PSD is generally thought to depend on the source soil properties, such as particle size distribution, and wind speed (Kok et al., 2011a, 2011b). However, based on empirical observations Mahowald et al., (2014) contended that this applies only to the > 5 μm size fraction and that the size distribution of the emitted dust < 5 μm is independent of soil PSD and wind speed. The coarser dust particles > 5 μm constitute a substantial fraction of the vertical dust flux and have the potential to travel far from the emission source (Ryder et al., 2013). For example, van der Does et al. (2016) sampled sediments along a transect in the Atlantic Ocean, up to 4400 km from the north African source region that had modal grain sizes between 4 and 32 μm. This suggests that the coarser fractions could have significant impacts over much larger distances than previously considered. Field-based methods to sample and measure aeolian dust at source of areas have the potential to provide important information regarding the controls on erodibility and characteristics of the emitted dust.

The mineral and elemental composition are important characteristics that will influence the type of interaction that takes place between the dust particles and the atmosphere, ocean and terrestrial environment (Formenti et al., 2011; Mahowald et al., 2011). For example, dust provides important nutrients such as Fe that affect the biogeochemical cycles of the ocean (Jickels and Moore, 2015; Mahowald et al., 2005), with the quantity and bioavailability of Fe largely determined by the mineralogy of the particles (Journet et al., 2008). Mineral composition, in combination with particle size and shape, also influences the radiative properties of the aerosols that have a direct influence on solar and infra-red radiation because different minerals have different refractive indices (Claquin et al., 1999; Kalashnikova and

Sokolik, 2002; Nousiainen et al., 2009) and an indirect effect on the radiative budget by calcium-bearing minerals acting as cloud condensation and ice nuclei (Laskin et al., 2005; Sullivan et al., 2009). Mineral and chemical compositions of aeolian dust are also useful for investigating sediment provenance (Yang et al., 2007). Dust constitutes a combination of various minerals including clays, quartz, carbonates, feldspars, sulphates and iron oxides (Sokolik and Toon, 1999), with the composition and proportions of the minerals in dust at emission dependent on the mineralogy of the source soil (Journet et al., 2014). An accurate characterisation of the emitted dust at source will improve our prediction of the environmental impacts of the dust.

The settling or sedimentation velocity of the dust particles is also affected by their shape, with flat particles expected to travel further distances than spherical particles for a given velocity (Formenti et al., 2011). Friese et al. (2016) recorded particle sizes up to 250 μm for Saharan windblown sediment sampled 150 km off-shore and related this to the capacity of the platy-shaped mica particles to travel further distances than a spherical particle of equivalent size. The effect of non-sphericity on sedimentation velocity becomes particularly pronounced in combination with size and density. Furthermore, particle shape can also influence the light scattering abilities of the aerosols, with deviations from a spherical shape able to change the light scattering properties of the particles (Kalashnikova and Sokolik, 2002). This factor has important implications for determination of the radiative balance and its effect on climate and for radiances used in remote sensing applications (Formenti et al., 2011; Nousiainen et al., 2009).

A variety of methods have been employed to sample the windblown or wind-erodible sediment at the source of emission. These include windblown sediment samplers on site or downwind of dust sources, including passive samplers such as BSNEs and MWACs (e.g. Dansie et al., 2017a; Fryrear, 1986; Gillette et al., 1997; Hahnenberger et al., 2015; Warren et

al., 2007), resuspension chambers (Engelbrecht et al., 2016), wind tunnel measurements and sampling (e.g. Lafon et al., 2006; Wang et al., 2015; Wang et al., 2017) or using the wind erodible fraction of surface sediments as a proxy for emitted dust (e.g. Battachan et al., 2015; Dansie et al., 2017b; Reynolds et al., 2007; von Holdt and Eckardt, 2017; Wang et al., 2005;). These field studies provide vital information about the characteristics of windblown or wind-erodible sediment from the emission sources. However, the use of different methods could potentially result in the sampling and measurement of fractions with different proportions of particle sizes. For example, the BSNE samplers have been shown to be inefficient at trapping fine particles (<10 μm) (Shao et al., 1993; Sharrat et al., 2007), leading to an overrepresentation of the coarser fractions. This could lead to vastly different suggestions of the physicochemical characteristics of the emitted dust.

Analysis of the size and mineralogy of windblown and surface source sediments has been performed by a large number of studies (e.g. Formenti et al., 2003; Hojati et al., 2012; Rashki et al., 2013). The particle size distributions can be determined by several methods including the measurement of the geometric diameter by coulter counter, or imaging techniques such as optical microscopy; or the optical diameter by laser diffraction (Mahowald et al., 2014). The mineralogy of dust has been determined extensively on a semi-quantitative basis with X-ray diffraction (XRD) for the major mineral phases (e.g. Falkovich et al., 2001; Shi et al., 2005) and the elemental composition quantitatively with X-ray fluorescence spectrometry (XRF) or inductively coupled plasma atomic emission spectroscopy/mass spectroscopy (ICP-AES/ICP-MS) (e.g. Reheis et al., 2009; Trapp et al., 2010, Zhang et al., 2001; Zhuang et al., 2001). These analyses can only discriminate between particle sizes on the basis of physically separated fractions, such as by sieving. Individual particle analysis has been performed with scanning and transmission electron microscopy (SEM and TEM) in combination with energy-dispersive X-ray microanalysis to determine composition and shape (e.g. Engelbrecht et al.,

2009; Jeong et al., 2008), but these techniques generally involve a limited number of particles which are not necessarily representative of the sampled dust. The development of automated SEM for individual particle analysis enables the determination of the size, composition and shape of a statistically significant number of individual particles (e.g. Deboudt et al., 2010; Engelbrecht et al., 2016; Kandler et al., 2007, 2009; Krueger et al., 2003; Reid et al., 2003; Speirs et al., 2008).

In this study, we compared three sampling approaches to measure dust emission potential, namely surface-sediment sampling, windblown dust sampled by BSNE and samples obtained from a PI-SWERL wind tunnel. A high-resolution auto-SEM (QEMSCAN) analysis was used to compare the size, mineral composition and shape of individual particles sampled with each method. We found that the sampling techniques collect quite different fractions of the dust, and we suggest that a consensus approach should be adopted that comprises all three sampling techniques, but at least includes detailed high-resolution sediment analysis.

4.3 Regional setting

The ephemeral river valleys in the Namib Desert are major dust sources in southern Africa, with large plumes visible on satellite imagery as dust is transported over the ocean during strong autumn and winter easterly winds (Vickery and Eckardt, 2013). The Huab river catchment is located in a basement of Upper Proterozoic to Cambrian (2600-1650Ma) Damara Sequence and these are overlain by Carboniferous to Permian (350-250Ma) Karoo Supergroup sediments of fluvio-lacustrine and fluvio-marine origin (Jerram et al., 2000). An angular unconformity, with a gap of up to 120 Ma, exists between the Karoo Supergroup and the deposition of the Etendeka Group (c. 133Ma) (Figure 4-1) which marks the separation of Africa from South America. This group includes the fluvial and aeolian units of the Cretaceous Etjo Formation, intruded and covered by the volcanic flood basalts of the

Etendeka Igneous Province (Jerram et al., 1999). The Damara Sequence provides schists, granites and marbles. The Karoo Supergroup adds shales, siltstones and mudstones and the Etendeka contribute basalt, andesite and the sandstone of the Etjo formation.

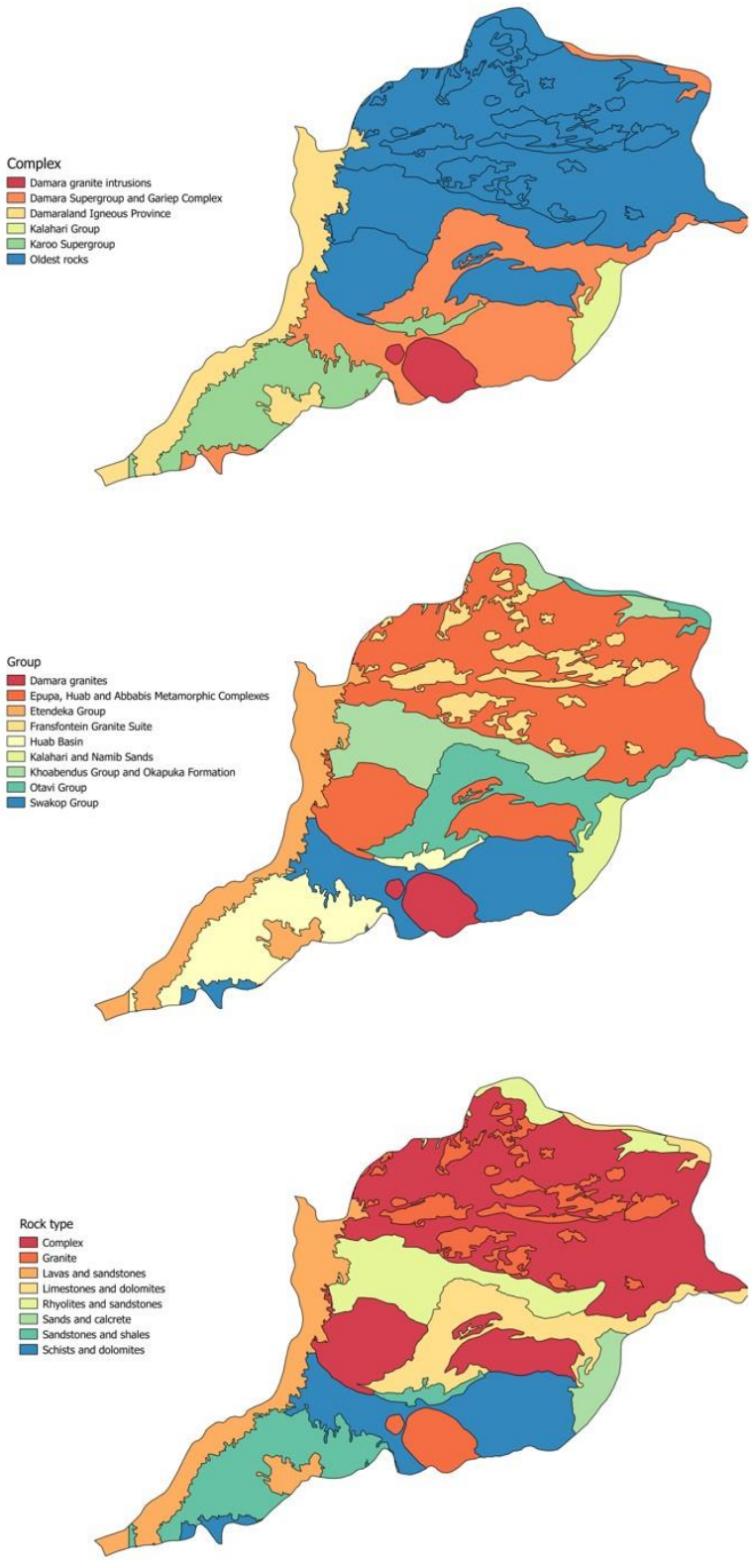

Figure 4-1 Geology of the Huab catchment in terms of Complex, Group and main rock types.

The Huab River is one of the most emissive rivers in this system according to analyses of remote sensing, with consistent emission sites situated within the river at an upstream section and the terminal stages in the delta, as well as from the pans situated to the north and south (Vickery and Eckardt, 2013; von Holdt et al., 2017). Dust emission tests with the PI-SWERL confirmed the high emission potential of the Holocene fluvial valley silt terraces (von Holdt et al., 2017), with no flood events recorded on these fill sediments for the last c.600 years from an OSL chronology done by Thomas et al. (2017). In addition, Dansie et al., 2017a confirmed the emission potential of this river with ground-based measurements from seven stations situated within the river. These measurements included monitoring of dust concentrations with a combination of a DustTrak DRX aerosol monitor and meteorological conditions with an automatic weather station. In addition, windblown sediment samples were collected with a tower of BSNE traps. Dansie et al. (2017a, b) highlighted the fertilisation potential of the surface and windblown sediments collected with the BSNEs from the Huab with elevated levels of bioavailable Fe, P and N. von Holdt et al. (2017) measured the emission potential of the landforms of this system with a PI-SWERL wind tunnel, which identified the nebkhas and paleo silt terraces with available mobile sand as significant sources of emission.

4.4 Methods

4.4.1 Field sites and measurements

Dust emission measurements with a Portable In-Situ Wind ERosion Lab (PI-SWERL) wind tunnel (Etyemezian, 2007, Sweeney 2008, 2011, Goossens and Buck, 2009, Bacon et al., 2011, von Holdt et al., 2017) were carried out at seven sites within the Huab River system, including the Huab Pan and the adjacent gravel plain. These sites were chosen based on the

remote sensing analysis of dust sources by Vickery et al. (2013) and von Holdt et al. (2017). The sites included the main geomorphic units within the dust-producing area of the river system, which included the valley fill and delta terraces (four sites: Huab 1, 2, 4, 7), the river channel (one site, Huab 3), gravel plain (one site: Huab 5) and Huab pan to the north of the river (one site: Huab 6) (Figure 4-2). All measurements were carried out as a ramp test up to 3300 rpm (120 seconds to reach target rpm) and a runtime at the maximum rotation speed of 180 seconds. The seven sites consisted of 5 to 10 runs spaced at least 1 m apart on a transect line (Figure 4-3). Surface samples were taken adjacent to the position of each PI-SWERL run and consisted of a grab sample of the top 0.02 m ensuring that the surface type and material remained consistent with the tested surface. PI-SWERL exhaust samples were taken from two measurement runs that had high dust emissions and were sampled by placing a plastic bag over the exhaust to capture entrained sediment. These runs were situated on the river valley and delta fill terraces (Huab East and Huab West on Figure 4-2).

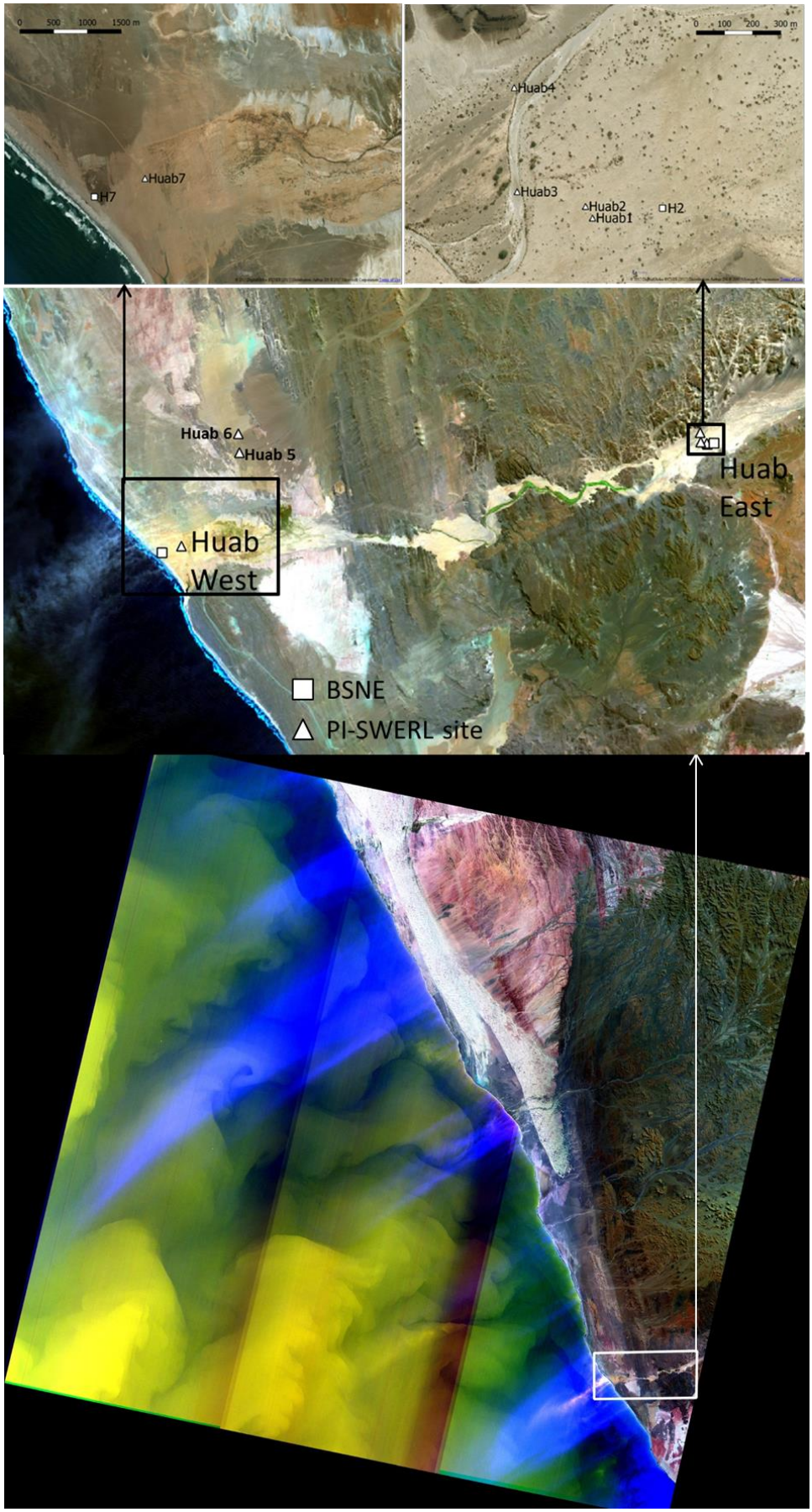
0 500 1000 1500 m
Huab7
H7
0 100 200 300 m
Huab4
Huab3
Huab2
Huab1
H2
Huab 6
Huab 5
Huab West
Huab East
BSNE
PI-SWERL site

Figure 4-2Test sites in the Huab River system. PI-SWERL test sites are marked with triangles from Huab 1-7 and are located in the following landform types: Huab 1,2, 4 on valley fill terraces, Huab 3 within the active channel, Huab 5 on the gravel plain and Huab 6 on Huab Pan. BSNE samples were obtained from sites marked with squares at Huab West and Huab East. Top images obtained from Bing Aerial imagery (Microsoft Bing, 2017). The middle image is the Landsat 8 false colour image (bands 7,5,3) for 21 July 2013. The bottom image shows potential upwelling during the north-east Bergwind event captured by Landsat 8 on 21 July 2013. Stacked image created with a shortwave infrared (7) and the two thermal infrared bands (10,11). This event occurred while the BSNEs were deployed.

Figure 4-3 PI-SWERL site within the Huab active channel (Huab 3). Each site consisted of a minimum of 5 runs along a transect (marked with blue rope). PI-SWERL wind tunnel on the buggy on the left and grid for taking surface photos.

Two towers with BSNE samplers were erected in proximity to these highly emissive sites (squares in Figure 4-2). The BSNE samplers are wedge-shaped traps based on the design by Fryrear (1986) and were placed at four heights: 0.25 m, 0.47 m, 0.89 m and 1.68 m (Table 4-1). The surface, BSNE and one PI-SWERL sample from Huab West were split by cone and quartering to obtain subsamples for XRF, particle size and QEMSCAN analysis. There was not enough sample from the PI-SWERL exhaust sample at Huab East for XRF (4.4.2) analysis. Only QEMSCAN (4.4.3) was performed on this exhaust sample. The three sample types will be referred to as surface, BSNE and exhaust samples. The two sites (Huab East and West) are situated 17 km from each other in the most downstream section of the river where the long-range transport of sediments by floods generated in the highlands provide the supply of material that can be entrained by the wind. Localised deposition of sediments occur infrequently in this low rainfall stretch of the river (Figure 1-4). As a result, the sediments at the two study sites are predominantly derived from the same geology.

Table 4-1 Sample details from the surface, BSNE and PI-SWERL exhaust.

Sample ID	Sample location	Height (m)	Collection start and end date
BSNE E*	East (H2 number 3)	0.89	07/07/2013-01/08/2013
BSNE E*	East (H2 number 4)	1.68	07/07/2013-01/08/2013
BSNE W	West (H6 number 3)	0.89	09/07/2013-03/08/2013
Surface E	East	-0.02 to 0**	18/09/2015
Exhaust E	PI-SWERL run East	0.25***	18/09/2015
Surface W	West	-0.02 to 0**	18/09/2015
Exhaust W	PI-SWERL run West	0.25***	18/09/2015

*These sample results were combined "BSNE E" because there was no significant variation. The sample locations H2 and H6 correspond with those from Dansie et al. (2017a).

**Surface sample of top 2 cm

***PI-SWERL exhaust height

4.4.2 XRF

The elemental composition of all surface and BSNE samples and one PI-SWERL exhaust sample were analysed with a Spectroscout energy-dispersive X-ray Fluorescence (XRF) analyser (SPECTRO Analytical Instruments, Kleve, Germany). There was insufficient material for the second exhaust (East) sample to be analysed. The instrument was calibrated with a certified standard GBW07312 (National Research Center for CRMs, Beijing, China) for which technical concentrations were obtained from NOAA Technical memorandum NOS ARCA 68 (1992). This analysis was performed to validate the auto-SEM-EDS (QEMSCAN) results.

4.4.3 QEMSCAN (Auto-SEM-EDS analysis)

The samples were analysed using a FEG QEMSCAN 650F and accompanying software, iDiscover^{TM} with the aim of determining the size, mineralogy and shape of the individual particles. A description of QEMSCAN can be found in Gottlieb et al., 2000 and Goodall et al., 2005. The surface samples were screened over a 250 and 63 µm sieve. The two fractions <63 µm and 63-250 µm were analysed separately, but the results are aggregated when referring to Surface East or West samples. The Exhaust and BSNE samples were analysed without screening. A subsample was further split by rotary micro splitter to obtain approximately 0.2 g of material for analysis by the QEMSCAN system. The samples were mounted with two different techniques: one method used a traditional SEM top mount using SEM glue and another using the routine resin mounting technique used with the QEMSCAN. The quantitative results presented were from the resin mounted samples. The SEM photographs were used from the top glue mounting technique. Methodological consideration and comparison of results from the glue versus the resin mount are presented in supplementary section 4.8.1. The mounting technique has a significant influence on the

results. Thus the choice of the mounting technique should be carefully considered. Vickery (2014) used the top mounting technique due to saline nature of the samples. For this study, halite was expected in significant quantities for the coastal site as it is situated within a sabkha environment, but the XRF analysis revealed a maximum concentration of 2% chlorine in the BSNE West sample, 1.5% in Surface West and 0.8% in the Exhaust West sample. Due to the methodological consideration set out in supplementary section 4.8.1, it was decided to use the resin mount technique and therefore only it will be described here. The samples were mixed with graphite in a 2:1 (sample: graphite) ratio to ensure maximum dispersion and to aid with electron conductivity. This mixture was then added to resin and stirred vigorously in a figure of eight pattern to ensure complete mixing and random orientation of all particles. The sample moulds were placed in a vacuum chamber for 10 minutes and then again for 5 minutes, breaking the vacuum in between to release any trapped air bubbles. The moulds were cured overnight in a pressure pot and the blocks removed for polishing the next day. The blocks were polished in a series of grinding and polishing steps and inspected with an optical microscope to ensure there are no plucked or cracked grains and to ensure a smooth surface. The blocks were carbon coated and placed in a vacuum cupboard overnight before analysis.

Samples were scanned at 2 µm/pixel for a minimum of 2 hours which yielded approximately 10000 – 60000 individual particle images per sample. This provided a large enough number of randomly oriented particles for a comparative assessment of particle size. All particles were categorised into the following size fractions: <5, 5-10, 10-20, 20-63, 63-125, 125-150, 150-350 and >350 µm using the calculated equivalent circle diameter (ECD) of the measurement of the flat, cross-sections of the particle (Little, 2016; Ralph and Kurzydlowski, 1997).

4.5 Results

4.5.1 Particle size distributions

A total of 171104 particles were scanned for all the samples from Huab West and East providing the size, mineralogy, elemental composition and shape of each particle scanned at 2 µm per pixel resolution, providing an effective resolution of 2.75 µm. The particle size distributions based on the total area of pixels in each size bin of the surface, exhaust, and BSNE samples for both sites are different among the three sampling methods (Figure 4-4). For the East site, this is the case for most of the size fractions, with the Surface and BSNE showing a maximum in the 20-63 µm size bin and the Exhaust a maximum in the 10-20 µm bin. In addition, the proportions of the sample differ within the smaller size bins (Table 4-2). The concentration of particles in the finer fractions of the Exhaust E sample is due to the selective entrainment of these smaller particles. The BSNE E, on the other hand, appeared to be less effective in trapping particles in the <20 µm fraction. At Huab West, all the samples have a maximum in the 20-63 µm bin, similar to the Surface and BSNE East samples. The Exhaust West sample has a significantly larger proportion within the 10-20 µm bin, whereas the BSNE West sample has a larger proportion in the < 10 µm fraction. This BSNE appears to be more efficient at trapping particles in the finest size classes. The number size distribution illustrates the predominance of the <10 µm fraction for the exhaust and surface samples at the East site (greater than 95%), whereas the BSNE sample only has 63.7% <10 µm and 96.1% < 63 µm. The samples from the West site all have a number size distribution of at least 98 % <63 µm, with the BSNE having the largest number of particles in the smallest size class (38% < 5 µm). The number distribution of the Exhaust East and BSNE West sample follow the same trend. The mineralogy of the samples all have varying combinations of minerals, but the contribution of mica to the BSNE West and Exhaust East sample is

markedly different from the other samples. The mica makes up the largest proportion of all the size fractions in these two samples. The PI-SWERL emission flux results for all the sites tested in the Huab are given in supplementary section 4.8.2 as boxplots per site. In addition, the emission flux results for the individual runs for the exhaust samples in the east and west in supplementary section 4.8.2.

Table 4-2 Percentages of samples on an area basis in selected size fractions based on QEMSCAN analysis

	<5 µm	<10 µm	<20 µm	<63 µm	<100 µm
Surface W	0.7	4.3	16.2	70.8	88.4
Exhaust W	1.4	11.0	47.1	99.4	100.0
BSNE W	2.8	16.5	38.1	90.3	99.5
Surface E	3.3	12.2	19.7	48.6	68.9
Exhaust E	5.9	33.9	69.2	94.3	98.5
BSNE E	2.3	13.1	28.4	68.2	93.2

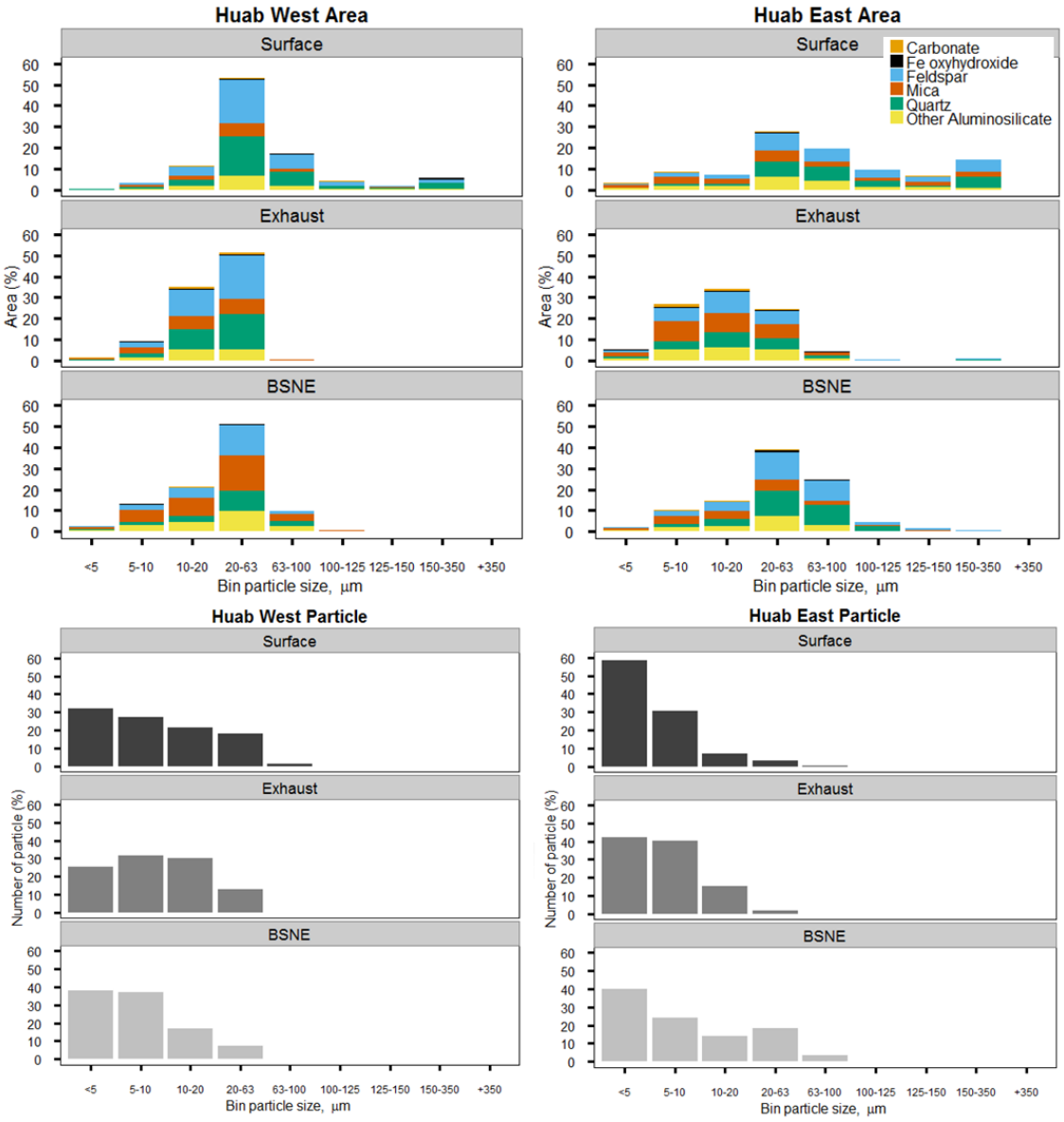

Figure 4-4 Comparison of particle size on the basis of area (top) and number (bottom) of particles from the QEMSCAN on y-axis. Particles are placed in size bins based on the equivalent circle diameter (ECD) of each measured particle.

4.5.2 Mineralogical comparison

The dust and surface sediments consist of a mixture of minerals consisting of predominantly feldspar, quartz, mica, other aluminosilicates such as the alteration products epidote and chlorite and low to medium-grade metamorphic rocks such as amphibole and pyroxene, iron oxihydroxides, titanium minerals, carbonates and clay minerals. The distribution of the individual minerals per size class further highlights the differences in mica content (Figure 4-5). The BSNEs ability to catch mica differed between the two sites with the BSNE in the east not being effective at trapping mica in the <20 µm fraction. In contrast, the BSNE in the west trapped proportionately more mica than collected from the PI-SWERL or available in the surface sediments. Mica was the dominant mineral in the <5 and 5-10 µm size fractions for all the samples, but contributed more to the total size class mineralogy for the BSNE W (7.0 %) and Exhaust East (12.0 %), compared to the other samples (1.3-4.6 %). The Exhaust East sample also had a higher carbonate content in the 5-10 µm fraction compared to the trend in the total size distribution.

The ratio between feldspar and quartz remained consistent across all samples, but the mica showed large variations as indicated by the total mineralogy (Figure 4-6). Mica had the largest contribution for the Exhaust East and BSNE West sample. The mineral distribution for these two samples were very similar, including the other aluminosilicates, suggesting that the material captured by BSNE West originated from the surfaces found further upstream in the river towards the east. The BSNE East sample was relatively depleted in mica compared to the surface and exhaust sample, indicating that the mica was not being trapped by this sampler. The BSNE sampler sediments in the west was damp (probably due to frequent fog-events) when it was collected, which could explain why this BSNE successfully trapped mica. In contrast, the BSNE East sampler did not experience wet conditions.

The sediments cannot be regarded as fully dispersed because some agglomerations were present in all the samples despite dispersion during sample preparation that resulted in the disaggregation of most clusters. The amount of agglomerated particles was determined by measuring the number of pixels within the particle that were classified as background, i.e. no mineral data recorded for that pixel. The image grid (Figure 4-7) distinguishes between agglomerated particles (those with more than 15% background pixels) and non-agglomerated particles having less than 15% background pixels. The percentages of agglomerated particles were sufficiently low for all the samples (<3.9%), except for the Surface East 63-250 µm fraction which had 6.3% agglomerations. A distinction should be made between agglomerations of finer particles (Figure 4-8 BSNE W) and finer particles cemented onto larger particles (Figure 4-8 BSNE E). These particle images were taken from a top mounted sample, with undispersed aggregates. The agglomerations of finer particles should be regarded as being classified in the wrong size class, whereas the cemented particles are in the correct size bin but have the ability to produce finer particles. The agglomerated particles were included in the analysis as they did not make up a significant quantity of the sample. Furthermore, all the samples underwent the same mounting procedure and agitation and are therefore comparable. The percentage of agglomerated particles for all the samples is given in supplementary 4.8.2.

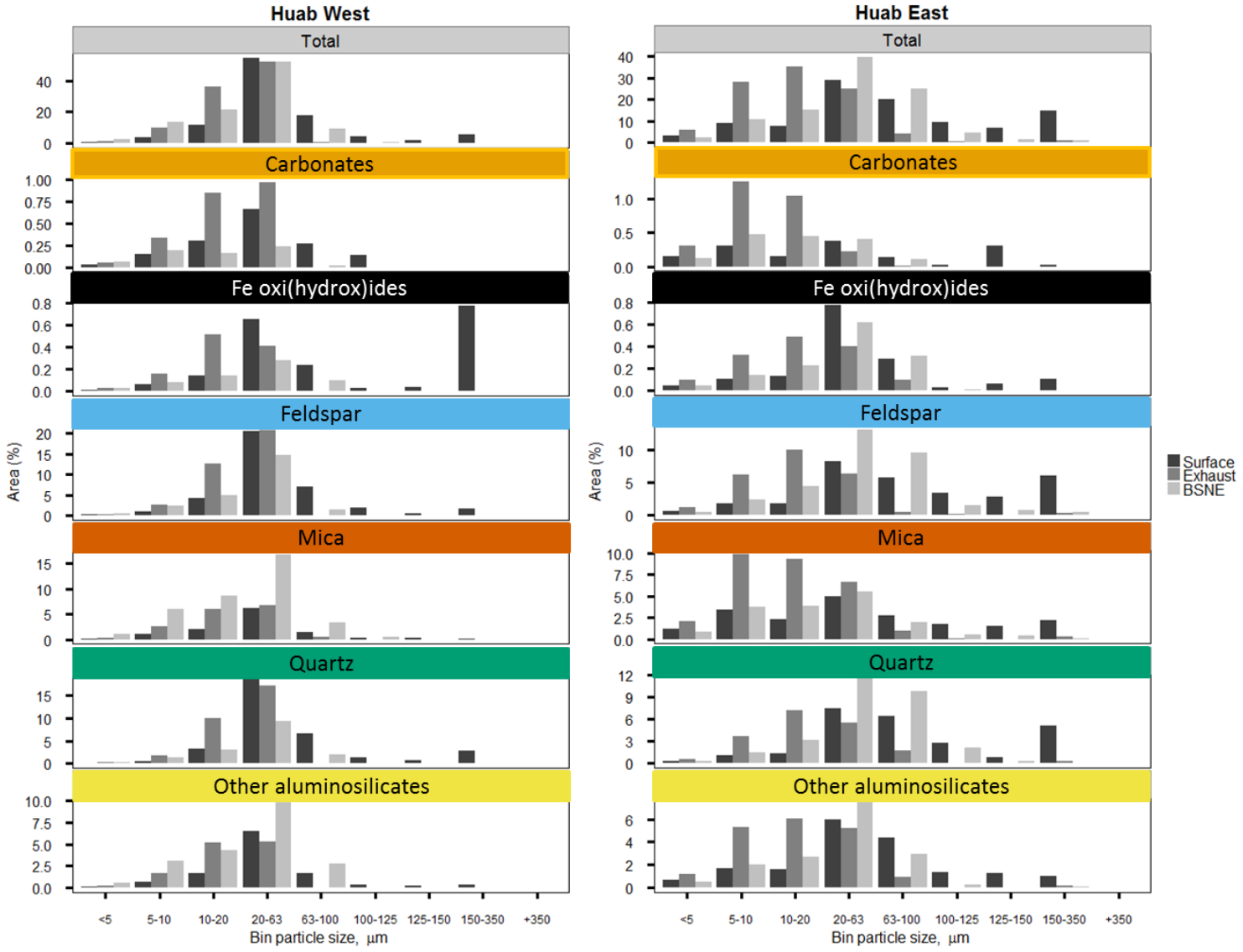

Figure 4-5 The distribution of the minerals within each size bin. The mineral distributions follow the same trend as the total size distributions, with a few notable exceptions such as the concentration of the Fe oxihydroxides in the 10-20 µm bin for the Exhaust West sample and the mica and carbonates in the <20 µm bin for the Exhaust East sample.

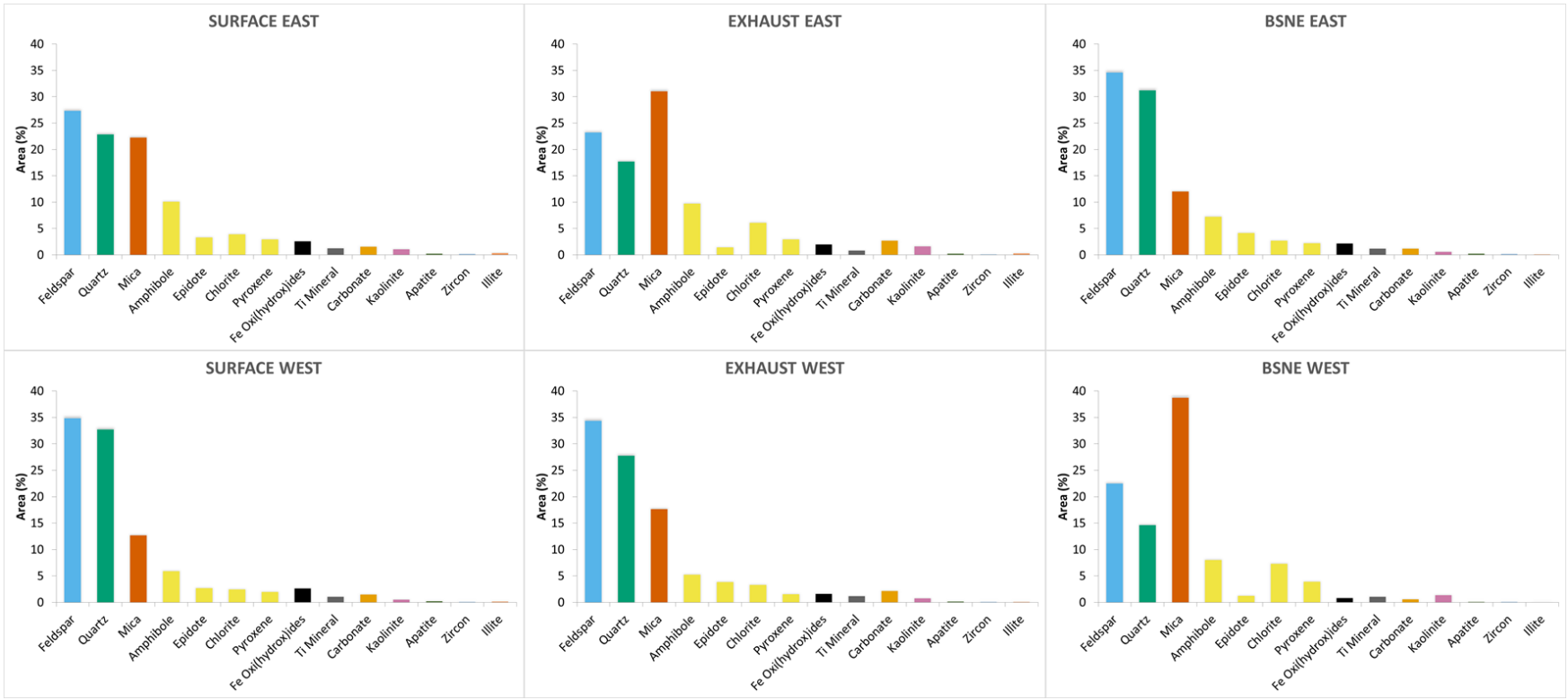

Figure 4-6 The total mineral distribution for each sample. Feldspar, quartz and mica are the predominant minerals. The Exhaust East sample is dominated by mica compared to the reduced quantity in the BSNE East sample. In contrast, the BSNE West sample is dominated by mica, with much less mica in the Exhaust sample. The other aluminosilicates for the BSNE West and Exhaust East show a similar trend. The carbonates and Fe oxihydroxides are depleted in the BSNE West compared to the Exhaust East sample

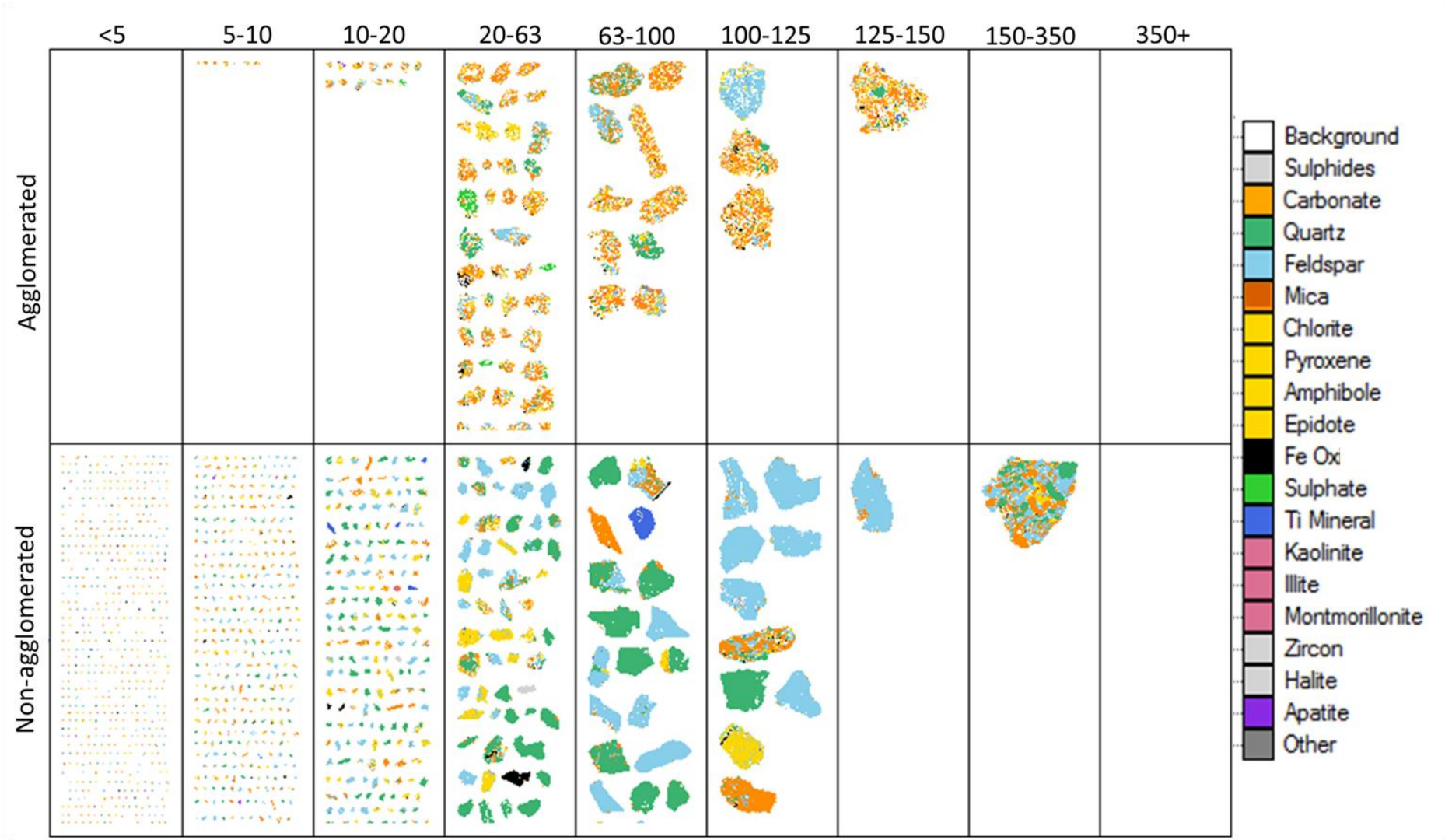
<5
5-10
10-20
20-63
63-100
100-125
125-150
150-350
350+
Agglomerated
Non-agglomerated
Background
Sulphides
Carbonate
Quartz
Feldspar
Mica
Chlorite
Pyroxene
Amphibole
Epidote
Fe Oxi
Sulphate
Ti Mineral
Kaolinite
Illite
Montmorillonite
Zircon
Halite
Apatite
Other

Figure 4-7 Agglomerated versus non-agglomerated particles for Exhaust East sample. The particles were separated based on the amount of background contained within the scanned area (15% in above grid). All agglomeration values are given in Table S1. Note that not all particles are displayed in this grid and a visual comparison of quantity cannot be made. The non-agglomerated fraction has many particles than the non-agglomerated sample.

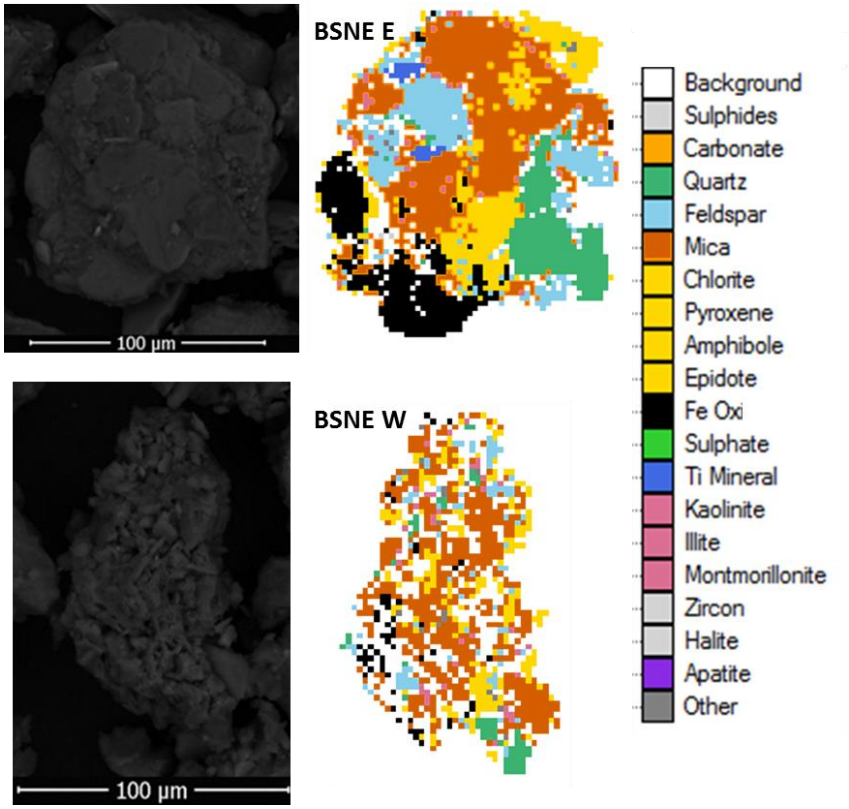

Figure 4-8 SEM image and false colour image of particle consisting of various minerals from a top mounted sample. BSNE E is an example of a larger particle with fine particles cemented to it and the BSNE W particle is an agglomeration of finer particles with a high proportion of background pixels identified within the particle image.

4.5.3 Elemental distributions

The elemental deportment of Fe, Ca and P within the size classes indicates that these elements are concentrated in the wind erodible fraction (Figure 4-9). The Fe is mainly associated with Fe oxihydroxides, mica and other aluminosilicates, with minor amounts associated with feldspar, titanium minerals and the clays kaolinite (0.001-0.005%) and illite (0.001-0.007%). The minor contribution to the iron from the feldspar, clays and Ti minerals is not from structural Fe, but from Fe closely associated with these minerals. The Fe oxihydroxides consist mostly of geothite (α-FeO(OH)) and a goethite-clay interface. The Fe oxihydroxides and clays are only superficially explored in this study as both these mineral groups need special consideration in the experimental design. Calcium is predominantly associated with the Fe and calcium-rich aluminosilicates, feldspar and carbonates predominantly as calcite. Minor amounts of Ca are present in titanium minerals, apatite and clay minerals (0.00006-0.0001%). Only BSNE West and Exhaust East have Ca present in the form of sulphate, predominantly as gypsum. Phosphorous was only associated with apatite. Dansie et al. (2017b) suggested that most of the phosphorous contained in the ephemeral rivers in the Namib is derived from the geology and potentially accumulated in sediments in the lower reaches of the ephemeral rivers as they flow through the desert due to the decrease in vegetation to utilise this nutrient.

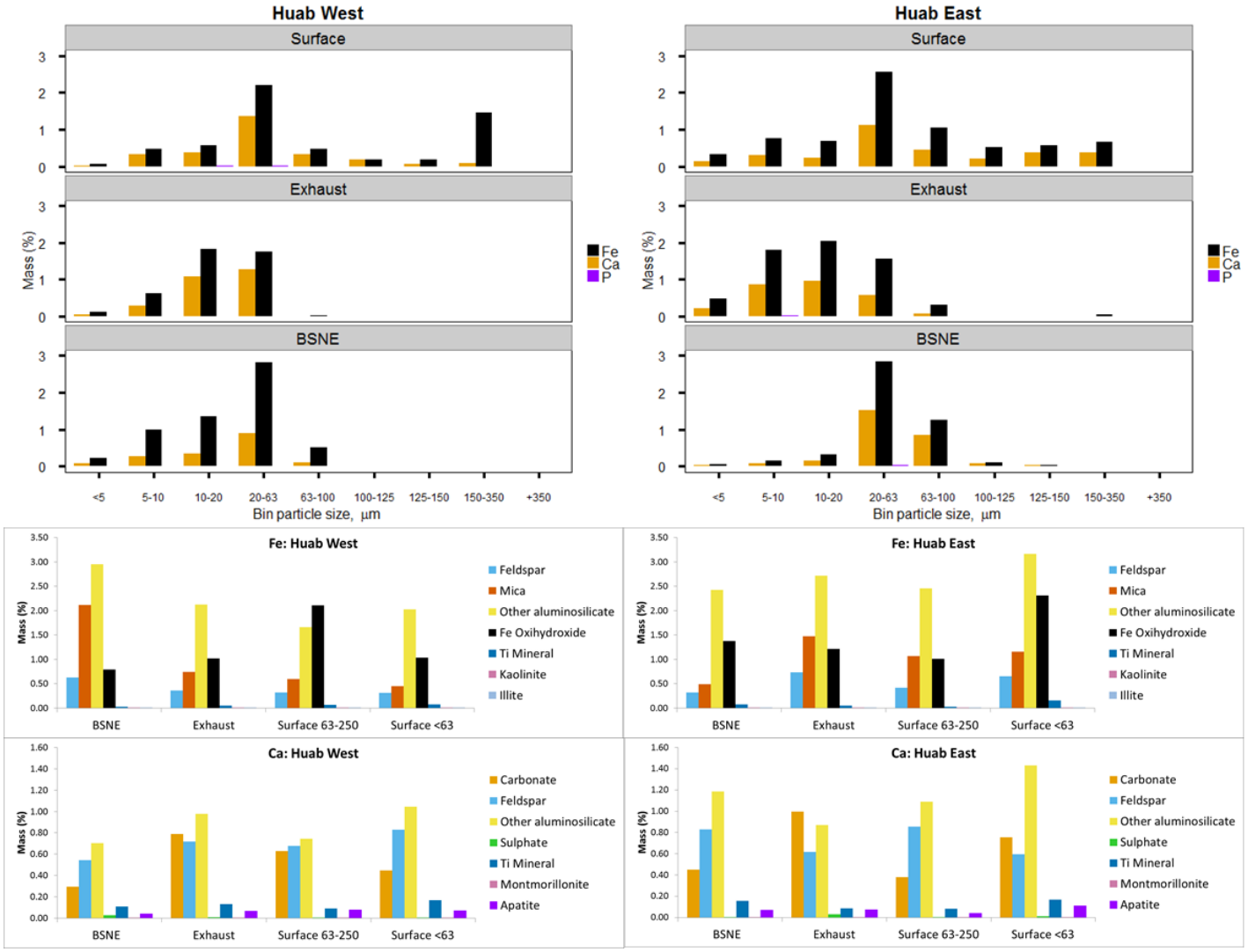

Figure 4-9 Element deportment of Fe, Ca and P within size classes (top) and Fe and Ca within different minerals present in all size classes (bottom). The surface samples for elemental deportment within the minerals show the coarse and fine fraction separately. For the size classes: the Fe and Ca for Huab East are concentrated in the <63 µm fraction compared to the 20-100 µm in the BSNE East.

4.5.4 Shape characteristics

The shape analysis classifies the majority of particles for all sampling methods and both sites as sub-angular to angular based on the number of particles classified according to the roundness criteria for the >5 μm fraction (Figure 4-10). The overall distributions of all the samples follow the same pattern, with a maximum in the sub-angular (0.4-0.6) class. The shape classification for the surface and exhaust samples is consistent at both sites. The BSNEs show important differences that correspond with the size and mineral data. Particles collected in the East BSNE are less angular compared to the other samples at the site. In contrast, particles collected in the West the BSNE are more angular, with a larger contribution in the angular and less in the sub-rounded category. This confirms the greater efficacy of the West BSNE to trap mica relative to the East BSNE. The elongated and angular class is dominated by platy micas (evident on particle inset in Figure 4-10).

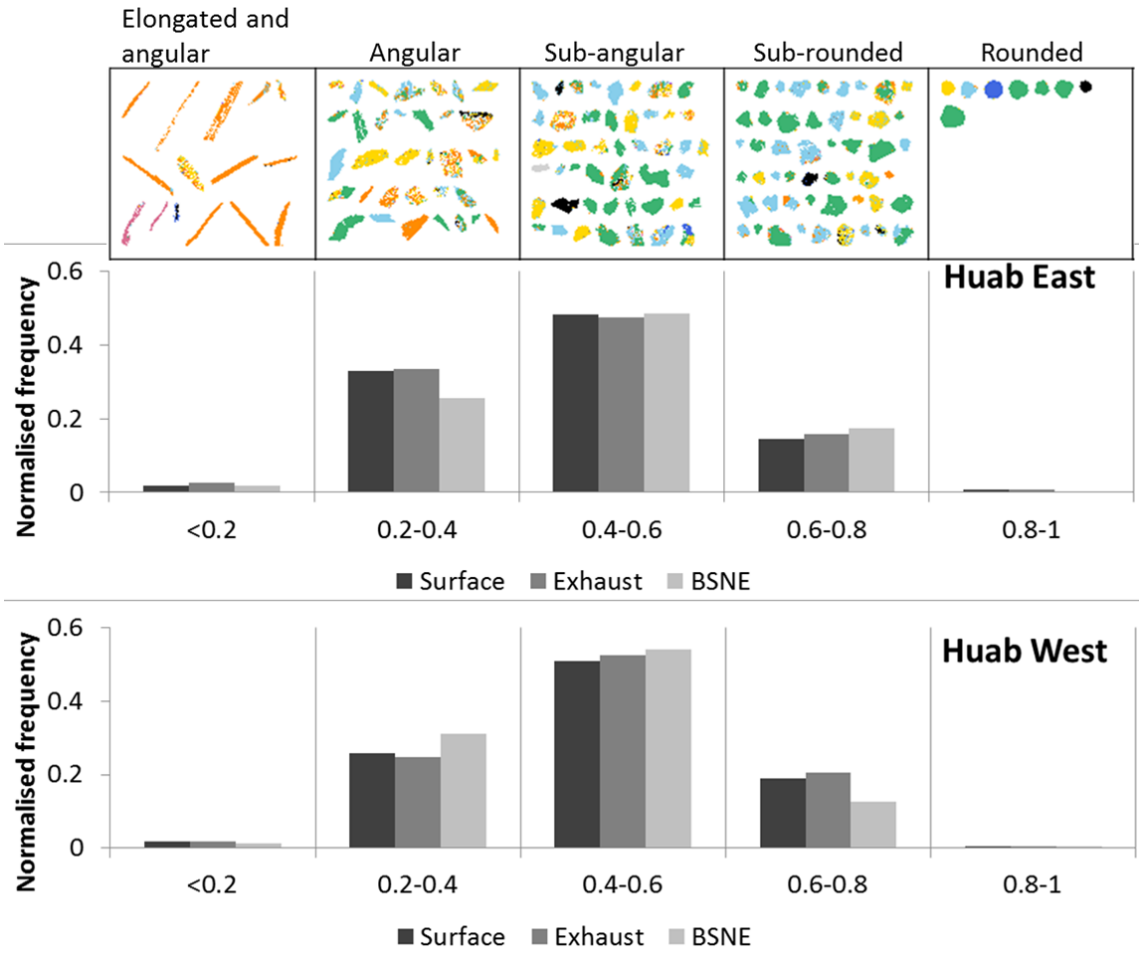

Figure 4-10 Roundness distributions for the three sampling methods at the two sites for the >5 µm fraction. Most of the particles clustered in the angular to sub-angular classes. The angular class for the BSNE confirms the smaller contribution from platy mics to BSNE East and the larger contribution to BSNE West. The inset above is the 20-63 µm fraction for sample BSNE East. Roundness can only be determined for the >5 µm at the scanning resolution of 2 µm/pixel used for this study.

4.5.5 Elemental tracers

The ratios of elemental concentrations for these two sites provide important detail in terms of dust emitted from this source, as well as comparing the different methods of measuring and sampling dust (Figure 4-11). The Si/Al ratio is not regarded as a good tracer for dust due to the low variability around 2.3, except for the diatomite rich dust from the Bodélé depression which approaches 4 (Formenti et al., 2011). The values for the Huab dust are all higher than 3. The ratios that include the particles >63 µm are all elevated due to the higher quartz content of the sand size fraction. This is also evident from the mineralogical size distribution in Figure 4-5. The Exhaust West 0-63 µm has an elevated value due to the increased quartz content of the 20-63 µm fraction, whereas the 0-10 µm fraction contains significantly less quartz. This result is to be expected for this site where the sediments have undergone extensive weathering to the terminal stages of fluvial transport resulting in resistant quartz dominating the coarser fractions. The 0-10 µm fraction consistently has the lowest Si/Al ratios with the exception of the Surface West sample. The Si/Al ratios of BSNE West and Exhaust East have similar values and follow the same trend.

The Fe/Al ratio has a much broader range than the other tracers and all the samples fall within the range previously reported for North African and Asian dust (Formenti et al., 2011). The increase in the Fe content of the sand-sized fractions of the Surface samples is most likely due to Fe oxihydroxide coatings on the sand grains. The Exhaust and BSNE West, as well as the BSNE East, have elevated Fe/Al ratios in the 0-10 µm fraction. The Exhaust East dust sample has very little variation across the different fractions. The elevated Fe/Al ratio in the BSNE West sample is possibly due to the high mica (predominantly Fe rich biotite) content relative to feldspar and quartz.

Although Ca is mainly regarded as a tracer for carbonates, the elemental deportment (Figure 4-9) indicates a substantial contribution of Ca from the aluminosilicate minerals. The Ca/Al for the Huab falls within the lower part of the range of other reported values (Formenti et al., 2011) and is consistent, except for BSNE West and the <63 µm fraction for Surface East that have lower values. The BSNE West sample has the lowest overall carbonate content (0.67%). In contrast, the sample from Exhaust East has a carbonate content of 2.7%. The carbonate contribution for all the samples does not exceed 3% and therefore does not contribute extensively to the composition of the samples. The K/Al ratio is above the ranges previously reported (Formenti et al., 2011) probably due to the increased mica content. The BSNE West sample has K/Al ratios substantially above the other samples as a result of the highest mica concentration in this sample across all size fractions. The elevated value for the BSNE East 0-10 µm fraction is due to the predominance of mica and potassium-rich feldspar ($KAlSi_3O_8$ ≈30% of total Feldspar) within this fraction. Overall, however, overall this sample is relatively depleted in mica compared to the other East samples (Figure 4-6).

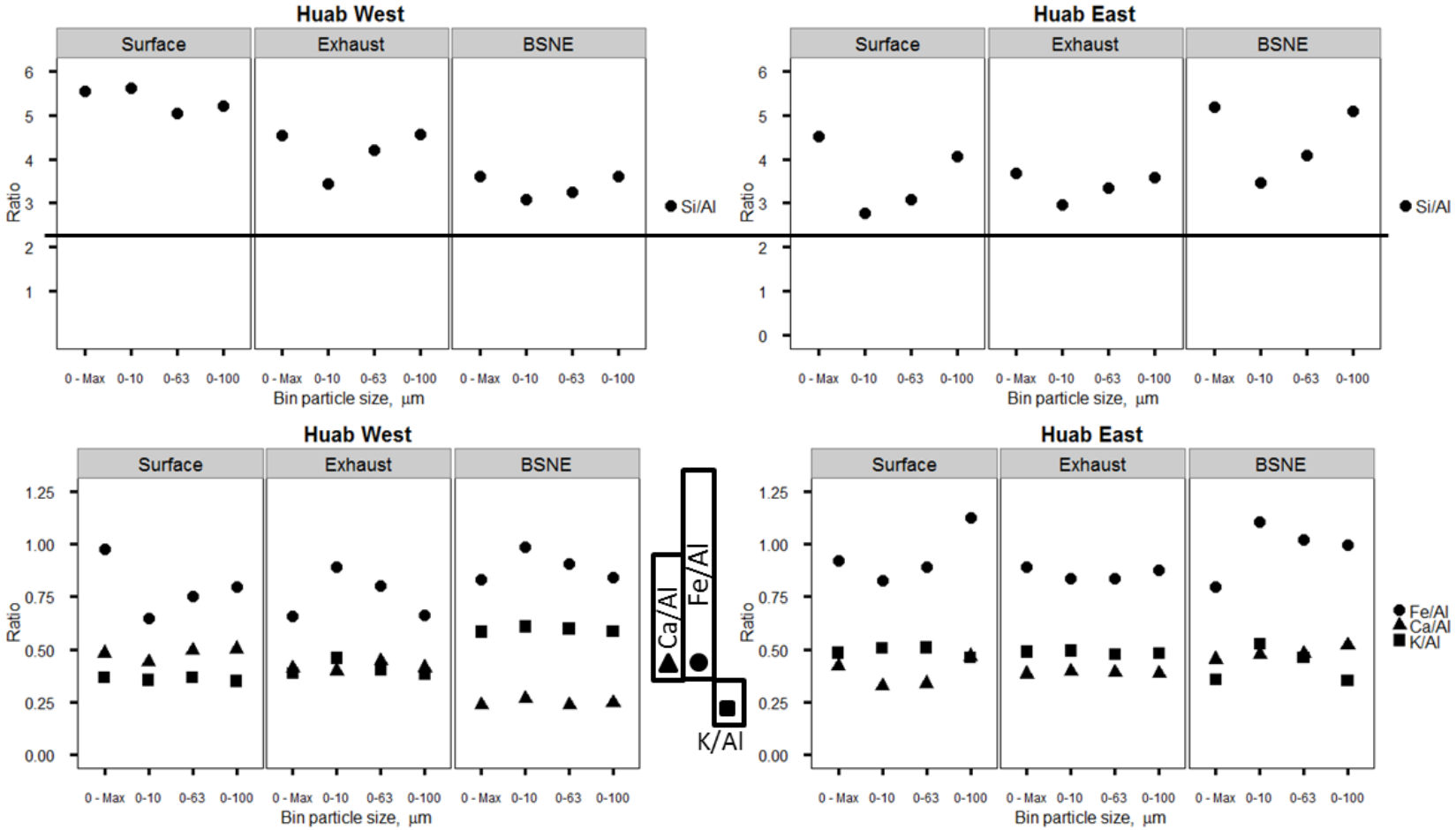

Figure 4-11 Selected elemental parameters for Huab dust and source sediments. Typical ranges of Fe/Al, Ca/Al and K/Al reported in previous studies (Formenti et al., 2011) indicated in between the West and East plots, whereas the Si/Al typically is invariant around 2.3 as indicated by line. Si/Al has been shown to have limited capability to distinguish source regions because of its low variability (normally around 2.3). The elevated levels for the Huab are particularly pronounced with inclusion of the sand-sized fractions.

4.6 Discussion

The three different sampling methods tested here produced different characterisations of dust at the source of emission. The particle size distributions of the three sampling approaches show significant differences resulting in variations in the mineralogy and shape of the particles. In addition, the BSNE and PI-SWERL collections depend on the prevailing environmental conditions at the time of collection. Both these sampling methods were affected by the high atmospheric humidity near the coast and the BSNE additionally by the predominantly south-westerly onshore winds.

The BSNEs at the two sites had varying abilities to trap the fine windblown sediment. The BSNE in the East was ineffective at trapping the finest fractions (<20 µm). The BSNE sampler is known to be inefficient at trapping dust in the fine fractions, being most efficient for particle sizes of >30 µm (Mendez et al., 2011) with efficiencies of between 10% (Sharrat et al., 2007) and 40% (Shao et al., 1993) reported for the <10 µm fraction. The BSNE at the eastern site appeared to be particularly inefficient at trapping very fine mica <20 µm when compared to the Exhaust East sample. In contrast, the BSNE sampler in the west on the coast was more efficient at trapping finer particles, particularly in the <10 µm fractions. Dansie et al., 2017a similarly found that the BSNE West had the smallest median diameter of 26.83-27.13 µm of all the sampling sites in the Huab. The authors suggested that this result is due to a combination of fluvial and aeolian processes, with ephemeral flows progressively resulting in the deposition of finer material downstream and dust emitted from upstream areas progressively becoming finer as gravitational settling of the larger particles takes place. However, it is likely that the improved ability of this sampler to trap the finer fraction is due to the humid conditions at this site. The increased ability to retain fine particles within the sampler could be due to the moisture creating a physical crust of the trapped sediments at the

bottom of the sampler, preventing re-entrainment of the sample, or alternatively, the wetting of the sediments changing the aerodynamics of the sampler and thereby increasing its ability to trap fines. The BSNE has a simple, cheap and robust design, but moisture is a problem when sampling windblown sediment, especially when trapping saline particles that can easily dissolve, with some researchers constructing rain hoods to protect the samples in the traps (Shao et al., 1993). The fog precipitation and sea spray is, however, more difficult to control. The inability to trap the finest fractions or the modification of the sampler due to environmental conditions would result in incorrect and inconsistent representations of windblown sediments.

Using surface samples as a proxy for emitted dust results in an underestimation of the <20 µm fraction relative to the PI-SWERL. At both the east and west site, the PI-SWERL have higher quantities of dust in these fractions due to the preferential entrainment of the finer particles. The PI-SWERL exhaust sample in the east also preferentially entrained more mica compared to the surface sample. Moreover, the measurement of the platy mica particles in the <10 µm fraction by the DustTrak light scattering laser photometer mounted on the PI-SWERL may have further influenced the result. Mica would significantly alter the size distribution obtained with laser diffraction, potentially due to its capacity for light-scattering, the large number of particles per unit volume and the non-spherical nature of the particles (Hayton et al., 2001). The ability to sample from the PI-SWERL (Bacon et al. 2011; Wang et al. 2017) provides the opportunity to directly compare the surface sediments with what is entrained from that surface in addition to the < 10 µm dust flux measurements. The surface sediment sampling appears to underestimates the fines, whereas the PI-SWERL appears to overestimate the fines. The underestimation of the fine fraction in the surface sample would increase as the particle sizes (up to 2 mm) used for analysis increases.

The overestimation of the fines by the PI-SWERL is possibly due to the interaction of the metal annular ring and the entrained particles that result in a fully dispersed particle size distribution. This condition is beneficial inasmuch as the < 10 µm measured by the DustTrak would measure the fully dispersed, ultimate size distribution and the maximum quantity of dust released in this size fraction. On the other hand, as suggested by Vickery (2014), this could also result in the excessive abrasion and rounding of particles which could result in higher dust emission than what is realistic and additionally changing the particle characteristics. The abrasion and rounding of particles were not found to be the case in the present study. However, the friction velocity used for testing by Vickery (2014) was significantly higher (5300rpm) than the present study (3300rpm). The friction velocity of this testing (3300rpm for u* = 0.55 - 0.58ms^{-1}) equates to a wind speed of approximately 8 ms^{-1} when adjusted for surface roughness (Etyemezian et al., 2014) and represents an important threshold at which saltation is initiated (Fryberger, 1979; Stout, 2007). The analysis of remote sensing data for Namib confirms the initiation of dust emission at this friction velocity, with wind velocities above this threshold consistently producing dust (von Holdt et al., 2017).

PI-SWERL sampling on the gravel plain and pan was severely affected by the humid conditions at the coast and resulted in these landforms being non-emissive despite it being apparent from the remote sensing analysis by Vickery et al. (2013) and von Holdt et al. (2017) that they can be emissive. The dust emission from the playas and sabkhas of the Namib Desert appear to depend on the interplay between surface and groundwater, a combination of saline and clastic sediments and the presence of sand for saltation. Reynolds et al. (2007) and Sweeney et al. (2016) emphasised the importance of hydrology of pans to dust emission. In the Namib Desert, the relative humidity from the coastal environment and frequent fog precipitation provides potentially important surface hydrological components to the dust emission processes from these saline sources. Clastic sediment deposited from

surrounding areas provides additional fines that become available for entrainment when conditions are conducive for emission. This factor is especially the case for the Huab settings, where sediment from the river appears to be deposited onto the playa surface with the south-west winds. The playas and sabkhas of the Namib Desert are highly variable in terms of hydrology, composition, and surface roughness. Consequently, dust emission from these landforms warrants further investigation. Environmental conditions at the time of measurement play a crucial role in the emissivity of the different landforms and the performance of the testing methods necessitates more frequent sampling.

The Huab sediments sampled by all three methods consisted of particles made up of a mixture of minerals derived from the weathering of the local metamorphic geology within the catchment. The combination of the different rock types within the catchment makes for a rich mixture of minerals reflected in the sediments derived from these rocks. The internally mixed mineralogy of these particles is not unique. Falkovich et al. (2001) reported that only 10% of the particles in their study were composed of a single mineral. The auto-SEM (QEMSCAN) is a useful technique to analyse the complex mineralogy combined with shape and size for individual particles. It offers the ability to determine the characteristics of a statistically significant number of particles. However, careful consideration has to be given to the purpose of the analysis and therefore the experimental design. This is especially relevant to the study of dust since the analysis of clay minerals and Fe, both as oxihydroxides and associated with clays (Journet et al., 2008), requires sample preparation and measurement techniques specifically designed to target those components. This includes mounting technique, top versus resin mount; scanning resolution and rate; beam intensities and compiling the user-defined mineral list. The analysis of clay minerals requires an interactive approach to correctly identify the type as the scan progresses (personal communication, Gaynor Yorath). In the present study, kaolinite was identified as the most prominent clay mineral, which is in

contrast to previously reported predominance of illite (Heine and Völkel, 2010; Claquin et al., 1999). A more detailed study of the clay minerals would confirm the clay mineral composition. Although the resin mount appeared to result in minimal agglomerations, this warrants further investigation to determine the effect of mounting technique on the dispersion of the sample.

This analysis provides important detailed information about the potential ecological and atmospheric impacts of dust from the Namib as a source of dust. The high mica content and fine particle sizes and angular shape of these particles will influence solar radiation. In addition, the mica particles appear to have surface coatings of finer particles cemented onto them. The weathering of iron-rich biotite and clay minerals adhered on the mica could result in an increased concentration of Fe associated with these particles that can travel further distances than more spherical particles of equivalent size as noted by Friese et al. (2016). The Fe is concentrated in the wind erodible fraction as Fe oxihydroxides, within the aluminosilicates, the titanium minerals and to a lesser extent the clay minerals. The Fe in the clay minerals has been proposed by Journet et al. (2008) to be most soluble and as a result more bioavailable than from the other mineral associations.. The Fe associated with the clay minerals as part of this study has 0.01% for BSNE W, 0.008% for Exhaust East and 0.008% for Surface East, whereas the other samples have concentrations of 0.003-0.004%. These concentrations further confirm the origin of BSNE West sediments from the Huab East site. In addition, Dansie et al., (2017a) reported bioavailable Fe concentrations in the BSNE windblown sediments of 0.00055% and 0.00071% within the surface sediments, values that are an order of magnitude lower than the Fe associated with the clays. The association of this bioavailable Fe with the various mineral components of the dust needs to be confirmed with an experimental design specifically aimed at this aspect of the dust particles. The inability of the BSNE sampler to trap fine particles might underestimate the nutrient content of the dust,

especially the bioavailable Fe content delivered to the ocean (Dansie et al., 2017a). In contrast, the modification of the sampler by moisture might have the unintended consequence of improving the ability to trap fines but would result in a sample that is no longer representative of the dust load.

4.7 Conclusion

The three different sampling methods tested here produced different characterisations of dust at the source of emission. The particle size distributions of the three sampling approaches show significant differences, which results in variations in the mineralogy and shape of the particles. BSNEs are known to be less efficient at catching smaller particle sizes, especially at higher wind speeds, which possibly result in an underestimation of the quantity of emitted dust in these fractions. Similarly, using a surface sample to represent dust emission potential could also result in an underestimation of the fines, specifically the <20 μm fraction. This will result in a misrepresentation of the influence of the dust, including a potential underestimation of the nutrient content contained within the sediments. On the other hand, environmental conditions influenced the BSNEs ability to trap fine particles. However, as the BSNE sampler can no longer be regarded as isokinetic, it could result in an overestimation of the dust load.

Sampling from the PI-SWERL has been done successfully as part of this study and previous studies, but the alteration of particles by the rotating ring needs further investigation. The exhaust was not intended for sampling with the design of the wind tunnel, but the determination of fluid and particle flow would provide potentially important insight into the dynamics of this instrument which can be achieved with a Particle Image Velocimeter (PIV) system. The analysis of flow dynamics will also be of benefit for the assessment of the

saltation sensors fitted to the inside of the hood. Results from these sensors have not been widely used due to the experimental nature of this addition. The ability to test the emission potential of a surface at a set friction velocity and obtain a physical sample of the entrained sediments provides the potential to formulate more accurate characterisations of dust emission at source. In addition, measurements undertaken with this instrument are also significantly affected by environmental conditions, such as relative humidity, which is important to consider and report.

The auto-SEM (QEMSCAN) enabled the determination of individual particle size, shape, mineral and elemental composition of the mineral dust and surface sediments to enable a comparison of the three different methods assessed in this study. As previously shown, this technique has the ability to provide important data regarding emitted dust, particularly in combination with techniques that can go to sub-micron resolution such as TEM (Transmission electron microscope), such as performed by Kandler et al. (2007). The analysis and measurement parameters should be carefully designed to fit the research question.

4.8 Supplementary section

4.8.1 Sample preparation and method for the QEMSCAN analysis

The auto-SEM individual particle analysis was done by QEMSCAN (Quantitative Evaluation of Minerals by SCANning electron microscopy). The QEMSCAN is one of the systems available for performing this type of analysis. The instrument used in this analysis belongs to the Centre for Minerals Research at the University of Cape Town where it has been mainly applied process mineralogy research. The conventional mounting technique used for most of the research is a resin mount. Vickery (2014) used this instrument to analyse sediments from Makgadikgadi Pan in Botswana and used a top mounting technique by sprinkling sediment on double-sided tape stuck to an old resin block. This method was used because of the saline nature of the samples and the concern over the dissolution of the salts if mounted in resin (halite contents of >18%). For the present study with samples from the ephemeral rivers both the top mount and resin mount techniques were used and are described in the following section.

4.8.1.1 Mounting procedure

The samples were prepared initially with a top-mount procedure following Vickery (2014), but using SEM glue instead of double-sided tape. However, it became apparent during the scanning of the samples that the microscope was preferentially scanning flat particles (Figure 4-12 and Figure 4-13). The scanning of the very coarse sediments of the Frisbee fallout trap from Walvis Bay (right panel Figure 4-12, but not reported on in this study) fared even worse and resulted in only a small portion of the sample and particles being scanned. The same is the case for samples consisting of very fine particles (Figure 4-14). In addition, the distribution of particles on the top resulted in many particles touching and highly skewed size

distributions. This was not the case with the resin mounted samples, where minimal particles were touching. The field scan images are displayed live as the microscope is scanning and are not available on completion of the scan. The images of field scans included here were screenshots taken during the analysis.

A comparison of the elemental composition between the two mounting procedures and an XRF analysis provides validation for the choice of the mounting technique (Figure 4-15 and Figure 4-16). The difference in mineralogy between the glue and resin mounted samples confirms the preference for the microscope to scan flat surfaces, with much higher mica content in the glue compared to the resin (Figure 4-16).

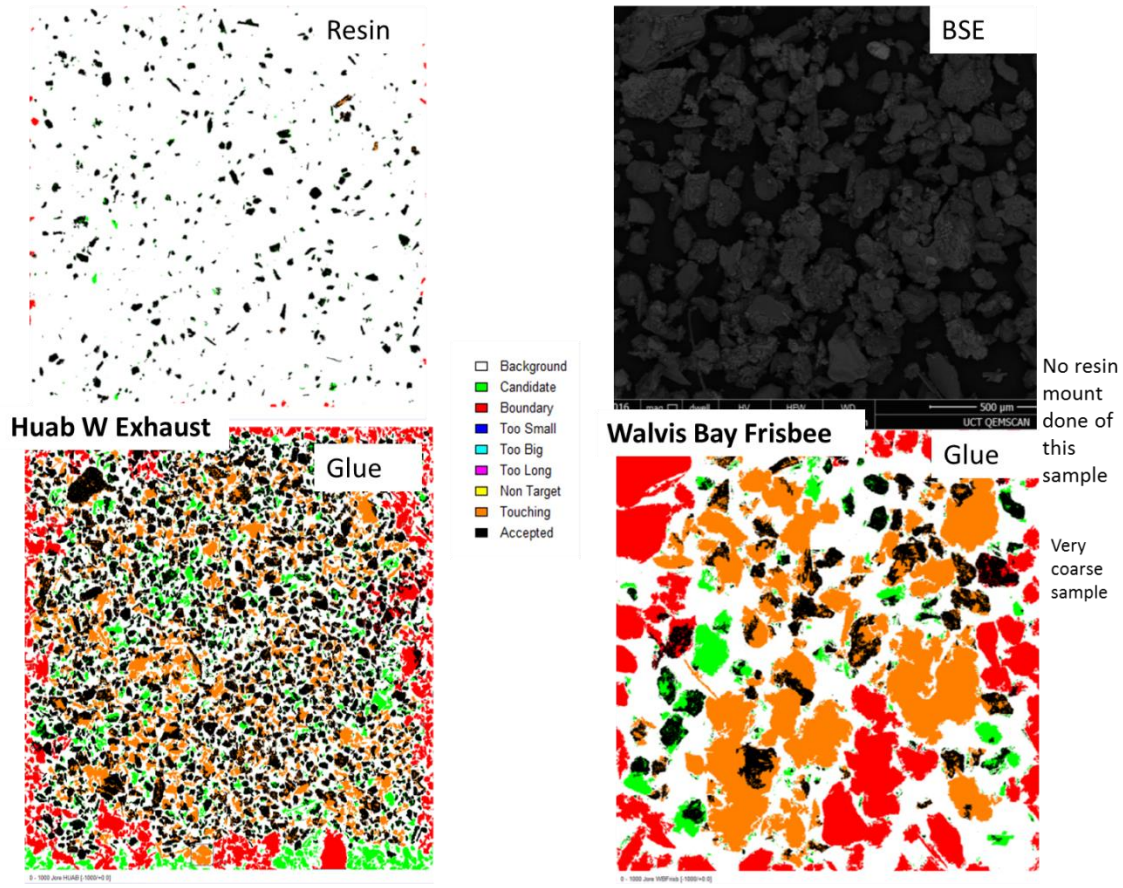

Figure 4-12 False colour images of scanned particles taken live as microscope scanned. Huab W Exhaust top left image shows field scan of resin mounted particles and bottom left the glue mounted sample. Black coloured particles are accepted particles, with orange and red not accepted as they are touching or on the boundary. Green denotes particles that were initially flagged as potential candidate particles, but that were not scanned. The Walvis Bay Frisbee sample was not repeated with a resin mount, but the preferential scanning of selected parts of the particles was even more striking.

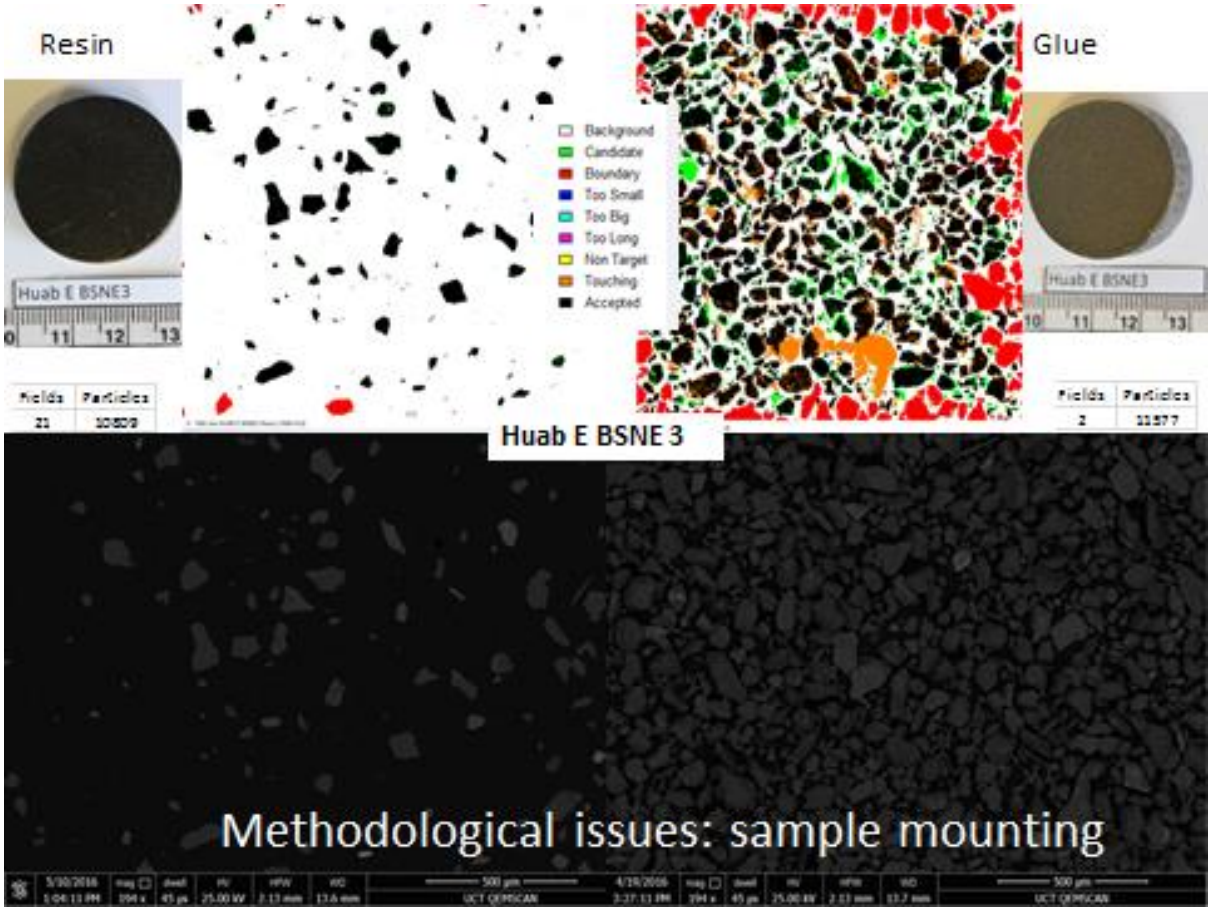

Figure 4-13 Resin (left) versus top glue mounted (right) samples for Huab E BSNE 3. The bottom images are SEM images of the respective scanned fields.

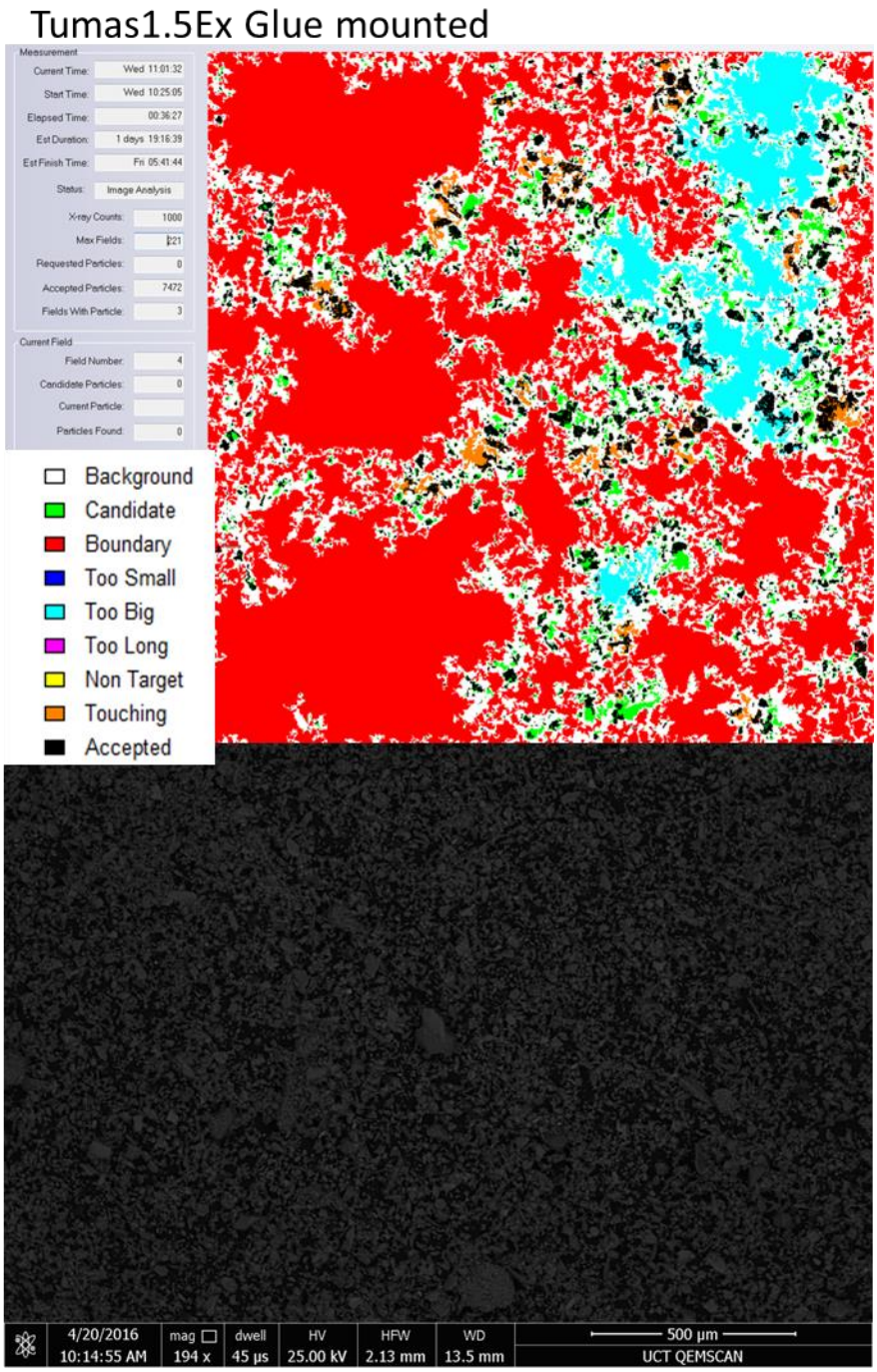

*Field view and BSE figures above are from different fields

Figure 4-14 Field scan of sample consisting of very fine particles. Too many touching particles result in it being identified as one particle with the red indicating that the particle exceeds the boundaries.

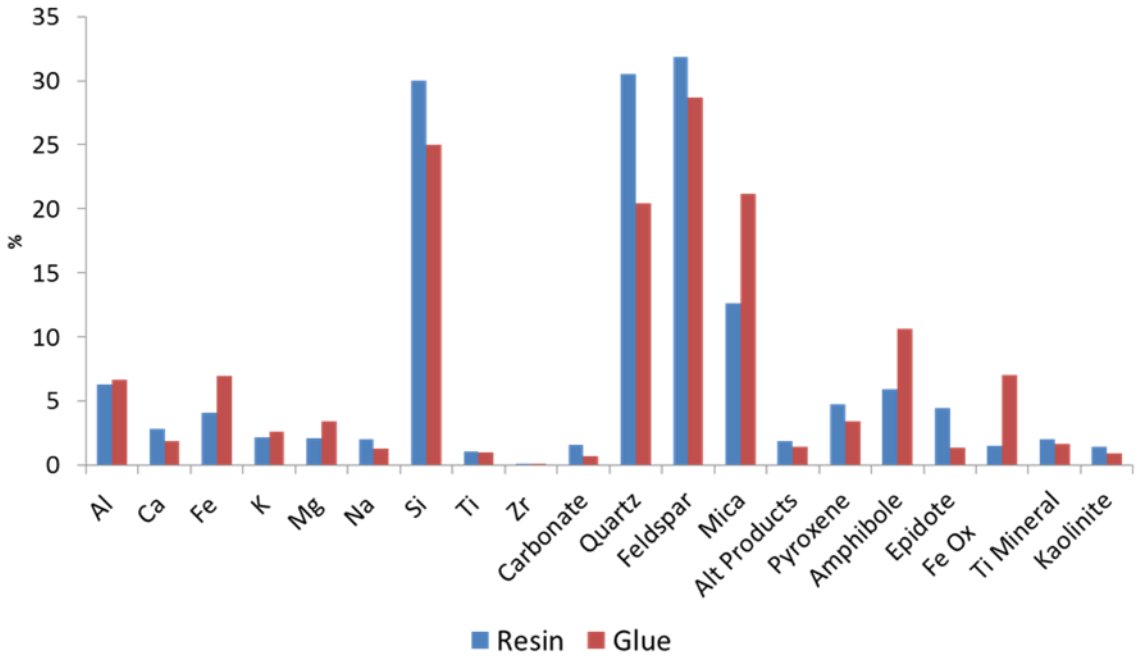

Figure 4-15 Comparison of selected elements and minerals between the resin mounted and glue mounted samples analysed with the QEMSCAN for Huab E BSNE.

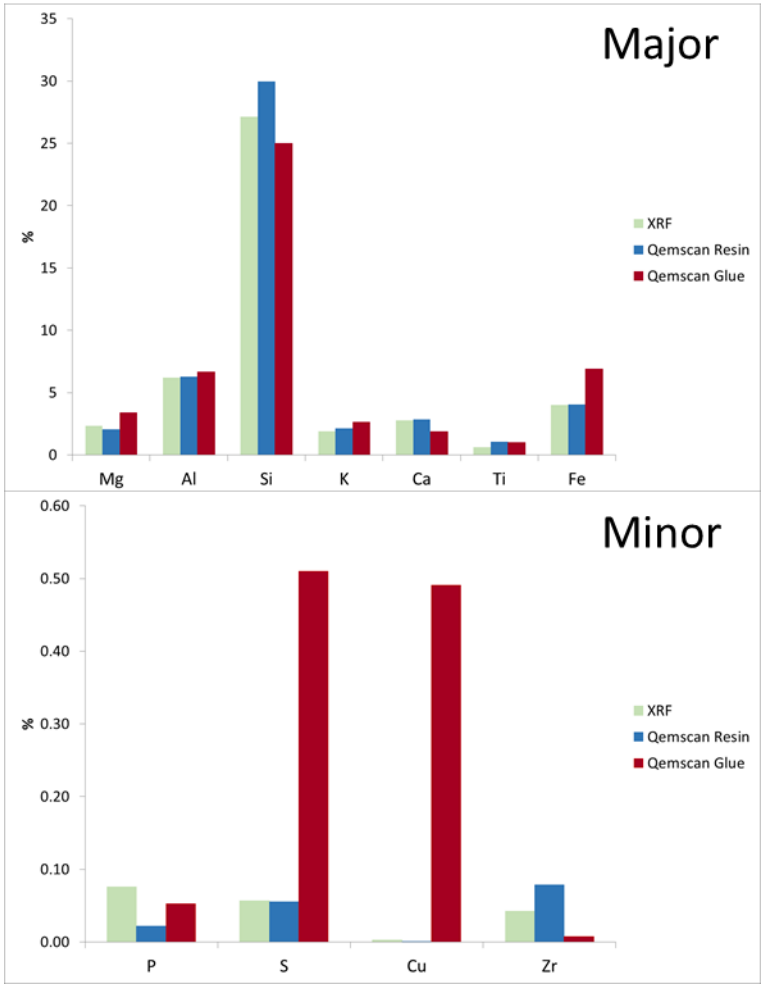

Figure 4-16 Comparison between the two different mounting techniques analysed with the QEMSCAN and XRF.

4.8.2 PI-SWERL results

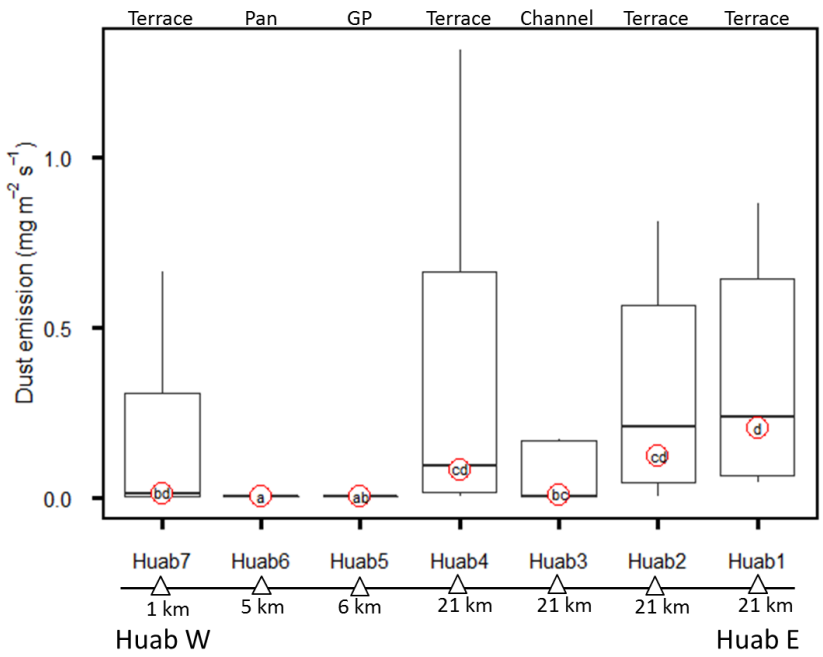

Figure 4-17 Emission potential of the Huab River. PI-SWERL emission flux results from seven transects within the river system from west to east. Locations are given in Figure 1 and distances from the coast given below emission results. The terraces were the most emissive landforms from nebkhas and paleo silt crusts in the presence of mobile sand. The active channel was not as emissive as the terraces. Samples for auto-SEM analysis were taken from Huab 1 and 7 and are referred to from here as Huab East and Huab West. GP refers to gravel plain.

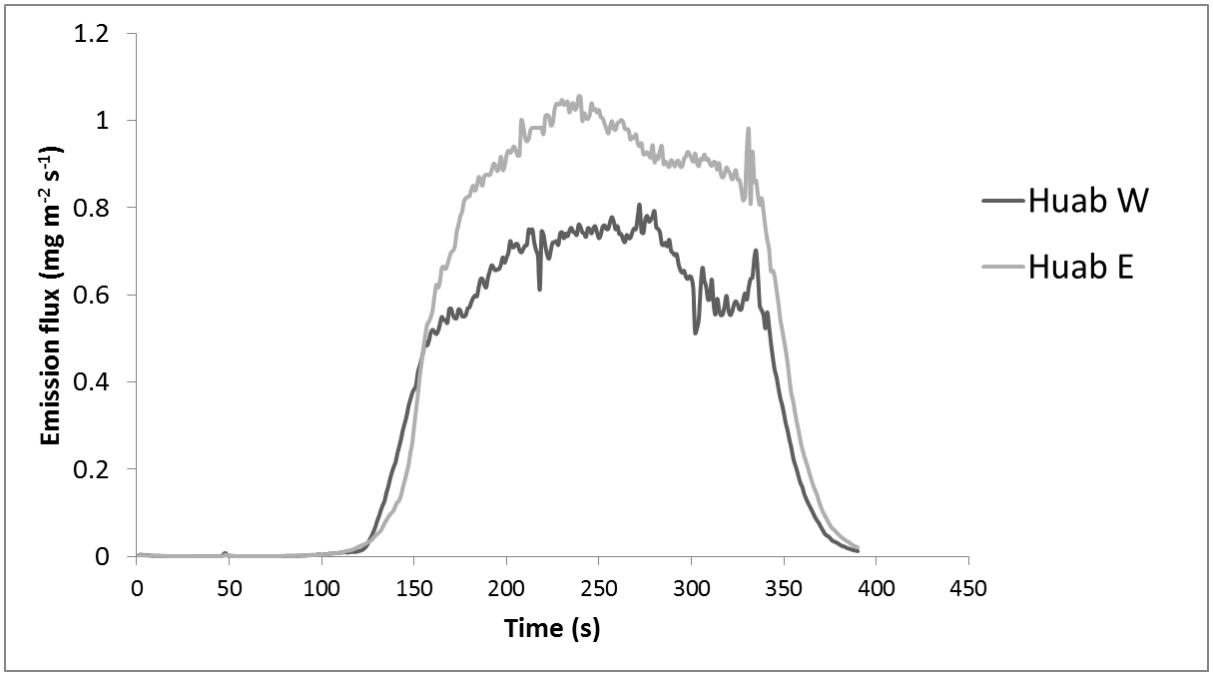

Figure 4-18 Emission flux results for PM_{10} from the PI-SWERL runs for the exhaust samples at the east and west sites. The east site produced higher PM_{10} emissions (1.05 mg m^{-2} s^{-1}) compared to the western site (0.8 mg m^{-2} s^{-1}), but the western site produced a larger quantity of particles in the >10 µm fraction (sample mass: 6.00 g versus 0.52 g for the eastern site

4.8.3 Degree of agglomeration for QEMSCAN analysis

Table 4-3 Amount of agglomerated particles within each sample (%). Agglomerated particles were those that had 15% or more background area pixels within the particle.

Sample	All	0-63 µm	63-250 µm
Surface East		1.8	6.3
Exhaust East	3.3		
BSNE East	2.7		
Surface West		3.9	0.4
Exhaust West	0.4		
BSNE West	2.3		

Figure 4-19 EXTRA IMAGE: The upstream Huab River with paleo silt terraces as main dust emission source. Photo courtesy of Frank Eckardt.

Chapter 5: Conclusion

The aim of this study was to use a multiscaled approach to accurately identify and characterise the small-scale dust sources within the Namib Desert by using a combination of remote sensing, field-based measurements and laboratory testing. In addition, I aimed to investigate whether the connections among the various spatial scales can be used to (1) improve our understanding of dust emission processes, (2) characterise dust, and (3) provide input and validation for the modelling of dust emission. The objectives addressed in the three technical chapters were formulated to address this aim and are discussed below.

5.1 Objective 1: Identification of dust sources at high-resolution

This study used the increased spatial resolution of Landsat multispectral images to investigate dust emission sources within the study area in the Namib Desert at a landform scale, providing a more accurate identification than previously achieved with remote sensing data. More than 2000 Landsat images available online for the study region from 1971 to 2016 were examined and 40 images of dust events were found for the period from 1989 to 2016. These images provided 30 m (15 m for Landsat 7 and 8) resolution and enabled the identification of point sources of dust emitted from specific landforms. The spatial resolution of Landsat provided a significant improvement on dust source identification achieved with 250 m resolution MODIS imagery to date, that involved substantial subjective interpretation of the location of the plume origin within the landscape (Lee et al., 2009). The accurate placement

of dust source points within landforms was used to guide fieldwork, which guided tests on the emitting surfaces.

The images with dust events found over a period of 25 years provided a long-term record of how some source areas remain consistent for the duration of the study period and how others changed following significant anthropogenic modifications to the hydrological systems. The study did not assess the short-term daily to seasonal temporal dynamics of the dust sources due to the 16-day overpass of the satellite. The focus of this study was on the spatial dynamics of the sources and only limited consideration was given to meteorological drivers associated with dust emission. The manual nature of this investigation is a major drawback which involved significant operator involvement. An automatic screening of images and dust detection should be attempted in any future endeavours for other parts of the world involving high-resolution satellite imagery, including other data sources such as from the Sentinel program operated by the European Space Agency (https://sentinel.esa.int/web/sentinel/home).

5.2 Objective 2: Emission potential and surface characteristics at source

Dust emission potential and surface characterisation were carried out at 23 sites targeting the dust source points identified from Landsat imagery. Dust emission potential measured with a PI-SWERL wind tunnel from both emissive and non-emissive surfaces indicated variability in emission potential within recurrently emitting landforms. Surface characterisation of the surfaces tested with the wind tunnel included measurements of sediment supply characteristics that play a potential role in the erodibility of the surfaces. Using the dust flux measurements and surface characterisation tests in a Boosted Regression Tree (BRT) analysis identified the most significant variables that influence dust emission. These results can be

expanded on to ensure the most relevant variables are tested during field testing, ideally providing standardisation amongst test methods.

This study further used dust source points identified with Landsat and ground-based emission measurements to assess proposed dust emission schemes. Mapping according to the Preferential Dust Scheme (PDS) proposed by Bullard et al. (2011) provided the first high-resolution map of the geomorphic units of the Namib and is particularly suited to classifying the small-scale dust emission sources. The PDS for the study area was used to compare the global scale Land Surface Map (LSM) proposed by Parajuli et al. (2014) generated by a supervised classification with training classes situated in the MENA region (Middle East and North Africa). The LSM did not represent the Namib study area well and the comparison highlighted the shortcomings of applying training classes from one specific region to the whole world. These data were further used to assess the most recent global scale dust emission scheme proposed by Parajuli et al. (2017), the Sediment Supply Map (SSM). Although the SSM provides one of the best representations of dust emission potential to date, it still shows significant shortcomings in overestimating dust emission in many of the ephemeral river systems of the Namib, especially in the upstream catchment areas.

The portable nature and ease of use of the PI-SWERL provide the ability to test many more locations and surfaces than conventional wind tunnels. This study tested at one friction velocity to simulate a wind speed likely to initiate saltation. Testing at different friction velocities would further refine the characterisation of the surfaces and their thresholds for emission. These tests would also provide a link between dust events captured on satellite imagery, wind data such as reanalysis data, the thresholds of the surfaces that emit dust and important surface factors that promote or suppress dust emission. Other environmental factors such as relative humidity should also be taken in to account. Dust emission is affected by moisture even at very low moisture contents (Munkhtsetseg et al., 2016) and especially so for

hygroscopic saline dust sources such as playas and sabkhas. The pans tested as part of this study were not emissive due to the high relative humidity experienced at the coast for the duration of the fieldwork. For saline dust sources, the ability to vary relative humidity would provide important data on thresholds and the mechanisms involved in dust emission. Analysis techniques such as in-situ XRD (Fischer et al., 2016) to measure mineral-phase changes with variation in temperature and humidity would provide further details regarding the mechanisms of dust emission from saline sources.

The PM_{10} fraction has been conventionally regarded as the most important fraction for global-scale modelling of dust and as such has dictated the design of the PI-SWERL measurable size fraction (Etyemezian et al., 2007). However, particles larger than PM_{10} can have significant ecosystem and environmental impacts and travel longer distances than previously thought (Friese et al., 2016) and should therefore also form part of the testing regime. The modification of the PI-SWERL to additionally measure and sample sizes greater than PM_{10} will provide valuable information on the dust emitted from source regions. The interaction between the annular ring of the PI-SWERL and the entrained particles should be investigated to see the degree of modification that they undergo and how this affects the results. This could be achieved with a Particle Image Velocimeter (PIV).

An ongoing challenge for the representation of dust source mapping is the inclusion of anthropogenic sources. Ginoux et al. (2012) and Parajuli et al. (2014) included an anthropogenic dust source category in their mapping of preferential dust source areas but only mapped agricultural and urban areas. The Namib study area does not consist of extensive areas of cultivated agricultural lands or extensive urban areas, but it has and continues to experience significant disturbance and modification due to mining, water extraction and tourism. The provision of water for urban and mining purposes has resulted in substantial modifications to the river systems within the Namib Desert. In addition, vast areas

of stony surfaces undergo disruptions due to extensive mining and tourism operations (Eckardt and White, 1997; Wassenaar et al., 2013). The dust source points identified with Landsat data provide a long-term record of how the sources have changed following significant modifications to the river flow due to water management practices. The increased resolution of the imagery provides the ability to identify dust emission from the stony surfaces of the gravel plain following construction activities, including the building of a water pipeline to ensure the supply of water from an increasingly stressed aquifer.

The PDS scheme proposed by Bullard et al. (2011) does not have a category for anthropogenic modification or disturbance. The importance of this factor in this study area shows that it is essential to incorporate modification and disruption of natural systems when mapping or modelling dust emission. The modification and disruption of normal fluvial dynamics indirectly affect dust emission providing a handoff between fluvial and aeolian processes (Koven and Fung, 2008). Ginoux et al. (2012) classified global dust source areas as either natural (hydrologic) or anthropogenic. The Namib consists of sources that can be classified as both natural and anthropogenic, a combination that seems to have resulted in increased dust emissions. This study did not incorporate a specific category for anthropogenic dust source areas, but this classification should be done in a manner which is achievable on a global scale. The recognition of source areas where emission dynamics have been changed due to modification requires detailed local knowledge, which is only achievable with high-resolution landform mapping and/or field studies. While this study did not attempt to quantify the contribution of anthropogenic induced dust emission from the Namib, including the degree of disruption to the stony surfaces of the gravel plains and their contribution to the dust load, it is evident that assessment of the contribution by human influences on the dust emission dynamics is essential for the accurate representation of dust sources. This assessment should extend beyond a category for only agricultural areas.

5.3 Objective 3: Dust sampling and characterisation

What we regard as dust is an important consideration for characterising dust emission at source. The third objective of this study was to compare three different established methods of measuring and sampling dust at the source of emission by analysing the sediments with a QEMSCAN auto-SEM system. This analysis provided size, mineralogy and morphology data at a micrometre scale for a statistically significant number of individual particles and a detailed characterisation of the source sediments from one of the dustiest ephemeral rivers in southern Africa. This study shows that the method used to sample dust at the source of emission can result in very different representations of dust-particle properties. The BSNE and surface sampling potentially underestimate and the PI-SWERL potentially over-estimate the finer fractions. The distance of the sampling from the source also influences the characteristics of the trapped dust as the entrained sediment load undergoes continual transformation due to gravitational settling of particles increasing with distance from source (Baker and Jickells., 2006; Mahowald et al., 2014). The accurate identification of dust emission source points allowed the sampling to take place as close as possible to the actual surfaces that emit dust. This study did not attempt to ascertain what the true representation of emitted dust looks like and consequently which method should represent the gold standard. This study did, however, reveal three different characterisations of the dust sampled with three different approaches at the source of emission. This result highlights the importance of the accurate characterisation of emitted dust for the modelling of the dust cycle.

An important consequence of the different methods used to sample dust and the resulting characterisation is the conclusions we draw on the nutrient and fertilisation potential of the dust to downwind ecosystems. The different methods would apparently result in different

concentrations of potential nutrients within the sampled dust. This finding has far-reaching implications on the possible environmental impacts of the dust, potentially resulting in either over or underestimation of such impacts. This study did not target specific elements, but mainly investigated the overall composition of the sediments. Furthermore, this study used samples from the field and only used three different sampling approaches. A more detailed look possibly under more controlled conditions and involving more sampling methods would provide more detailed and accurate characterisation of the dust emitted at source. Lastly, the analysis of the sediments with a technique such as a QEMSCAN should be designed for specific elements in mind. A nutrient such as bioavailable iron requires specific experimental design and test parameters, such as scanning resolution, electron beam intensity and mounting procedures.

This study has made an important contribution towards connecting dust emission dynamics across different spatial scales. By using remote sensing imagery with a resolution capable of identifying dust sources at the landform scale and using this to target field-work and analysis down to the grain scale an important connection has been established between field-based process data and the identification and modelling of dust source areas (Figure 5-1). This study made a contribution towards our understanding of dust emission processes and inputs for modelling purposes specifically at the landscape, surface and particle scale, with the landform-scale dust source point identification predominantly providing the bridge between large-scale modelling and small-scale processes. The replication of this approach in other regions of the world could provide significant improvements in the manner in which we study and represent dust emission sources globally.

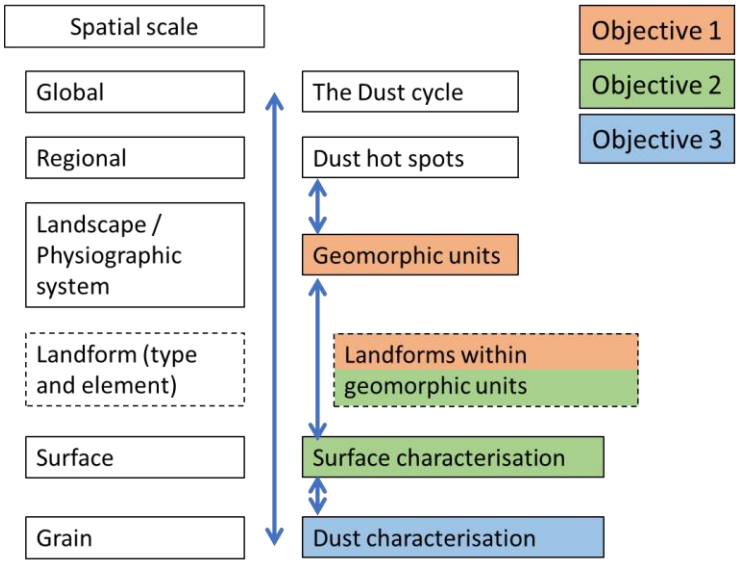

Figure 5-1 Spatial scales at which dust is investigated and the linkages provided by this study.

5.4 Potential future objectives

This study shows that the ability to accurately identify dust emission source points and connect them to ground-based testing provides important validation of dust emission schemes representing an erodibility factor to test their accuracy and improve efforts to model dust emission. In addition, the use of a BRT model using the emission testing and surface characterisation data to determine the significant factors for erodibility and identifying critical thresholds initiating dust emission holds promise for the incorporation of these factors and thresholds into dust emission schemes. The BRT model was used to make inference about the most significant predictors of dust emission processes at the surface to particle scale. This analysis could be replicated in other parts of the world and extended to a predictive BRT model (Elith et al., 2008) to predict the dust emission source areas based on the most significant variables determined with an inference BRT.

This method of modelling significant factors and the interactions between them to predict dust sources has great potential for mapping erodibility at a global scale. The inclusion of areas in the BRT model other than the Namib study area would undoubtedly improve the model and potentially overcome the limitations of the LSM and SSM, which are based on a specific region or a single geomorphic unit such as large inland draining basins with the Bodélé Depression as an example. The approach used by Parajuli et al. (2017) in devising the SSM using the upstream catchment area combined with empirical surface reflectance data from the MODIS blue-band provides a way forward in successfully creating a global erodibility map.

The advantage of using a predictive BRT is that all potential variables representing both physical aspects of the landscape and empirical data from remote sensing can be included in the model. This can include all aspects previously used to devise dust emission schemes representing erodibility, including topographic, hydrological and geomorphic factors (Zender et al., 2003). Remote sensing data can be included that incorporate all multispectral bands, including algorithms based on various bands such as the contrast between the red and deep blue bands used by Ginoux et al. (2012). In addition, soil layers which are now available at 250 m resolution (Batjes et al. 2017; Hengl et al., 2017) should also be included as potential predictor variables based on the inference BRT performed as part of objective 2. Categorical variables can also be included, which allows the incorporation of mapping efforts such as the PDS and LSM where available, which will examine the success of such mapping schemes to predict dust emission. The model will assess the importance of the predictor variables and only use those that make a significant contribution to explaining the deviance and predict the presence of dust. A preliminary predictive BRT run for the study area found that 53% of the deviance in the model was explained by the PDS scheme. This result attests to the highly

successful classification of dust emission provided by this high-resolution geomorphic mapping (the preliminary BRT is included in Appendix section 7.2).

Chapter 6: References

Abuduwaili, J., Liu, D., Wu, G., 2010. Saline dust storms and their ecological impacts in arid regions. Journal of Arid Land, 2(2), 144–150.

Ashpole, I. and Washington, R., 2013. A new high-resolution central and western Saharan summertime dust source map from automated satellite dust plume tracking. Journal of Geophysical Research: Atmospheres, 118(13), 6981-6995.

Bacon, S. N., McDonald, E. V., Amit, R., Enzel, Y., Crouvi, O., 2011. Total suspended particulate matter emissions at high friction velocities from desert landforms. Journal of Geophysical Research: Earth Surface, 116(3), 1–17.

Baddock, M. C., Bullard, J. E., & Bryant, R. G., 2009. Dust source identification using MODIS: A comparison of techniques applied to the Lake Eyre Basin, Australia. Remote Sensing of Environment, 113(7), 1511–1528.

Baddock, M. C., Gill, T. E., Bullard, J. E., Acosta, M. D., & Rivera Rivera, N. I., 2011. Geomorphology of the Chihuahuan Desert based on potential dust emissions. Journal of Maps, 7(1), 249–259.

Baddock, M. C., Ginoux, P., Bullard, J. E., & Gill, T. E., 2016. Do MODIS-defined dust sources have a geomorphological signature? Geophysical Research Letters, 43(6), 2606–2613.

Bagnold, R.A., 1941. The Physics of Blown Sand and Desert Dunes. Methuen, London, 265

Baker, A.R. and Croot, P.L., 2010. Atmospheric and marine controls on aerosol iron solubility in seawater. Marine Chemistry, 120(1), 4-13.

Baker, A.R. and Jickells, T.D., 2006. Mineral particle size as a control on aerosol iron solubility. Geophysical Research Letters, 33(17).

Batjes, N.H. 2017. *Overview of procedures and standards in use at ISRIC WDC- Soils*. DOI: 10.17027/isric-wdcsoils.20170001.

Belnap, J. and Gillette, D.A., 1998. Vulnerability of desert biological soil crusts to wind erosion: the influences of crust development, soil texture, and disturbance. Journal of Arid Environments, 39(2), 133-142.

Bhattachan, A., D'Odorico, P. and Okin, G.S., 2015. Biogeochemistry of dust sources in Southern Africa. Journal of Arid Environments, 117, 18-27.

Blott, S.J. and Pye, K., 2001. GRADISTAT: a grain size distribution and statistics package for the analysis of unconsolidated sediments. Earth surface processes and Landforms, 26(11), 1237-1248.

Brindley, H., Knippertz, P., Ryder, C., Ashpole, I., 2012. A critical evaluation of the ability of the Spinning Enhanced Visible and Infrared Imager (SEVIRI) thermal infrared red-green-blue rendering to identify dust events: Theoretical analysis. Journal of Geophysical Research Atmospheres, 117(7), 1–20.

Bryant, R.G., Bigg, G.R., Mahowald, N.M., Eckardt, F.D., Ross, S.G. 2007. Dust emission response to climate in southern Africa. Journal of Geophysical Research. 112(D9):1–17.

Bryant, R. G., 2013. Recent advances in our understanding of dust source emission processes. Progress in Physical Geography, 37(3), 397–421.

Buck, B.J., King, J. and Etyemezian, V., 2011. Effects of salt mineralogy on dust emissions, Salton Sea, California. Soil Science Society of America Journal, *75*(5), 1971-1985.

Bullard, J. E., & Livingstone, I., 2002. Interactions between aeolian and fluvial systems in dryland environments. Area, 34(1), 8–16.

Bullard, J. E., McTainsh, G. H., 2003. Aeolian–fluvial interactions in dryland environments: examples, concepts and Australia case study. Progress in Physical Geography, 27(4), 471–501.

Bullard, J.E., Mctainsh, G.H., Pudmenzky, C. 2004. Aeolian abrasion and modes of fine particle production from natural red dune sands : an experimental study. Sedimentology. 51:1103–1125.

Bullard, J., Baddock, M., McTainsh, G., Leys, J., 2008. Sub-basin scale dust source geomorphology detected using MODIS. Geophysical Research Letters, 35(August), 1–6.

Bullard, J. E., Harrison, S. P., Baddock, M. C., Drake, N., Gill, T. E., McTainsh, G., & Sun, Y., 2011. Preferential dust sources: A geomorphological classification designed for use in global dust-cycle models. Journal of Geophysical Research, 116(F4), F04034.

Chappell, A., Warren, A., O'Donoghue, A., Robinson, A., Thomas, A. and Bristow, C., 2008. The implications for dust emission modelling of spatial and vertical variations in horizontal dust flux and particle size in the Bodélé Depression, Northern Chad. Journal of Geophysical Research: Atmospheres, 113(D4).

Chavez, P. S., Mackinnon, D. J., Reynolds, R. L., & Velasco, M. G., 2002. Monitoring dust storms and mapping landscape vulnerability to wind erosion using satellite and ground-based digital images. Arid Lands Newsletter, 51(51), 1–8. Retrieved from http://ag.arizona.edu/oals/ALN/aln51/chavez.html

Chepil, W.S. and Woodruff, N.P., 1963. The physics of wind erosion and its control. Advances in agronomy, 15, 211-302.

Claquin, T., Schulz, M. and Balkanski, Y.J., 1999. Modelling the mineralogy of atmospheric dust sources. Journal of Geophysical Research: Atmospheres, 104(D18), 22243-22256.

Crouvi, O., Amit, R., Enzel, Y., Porat, N. & Sandler, A. 2008. Sand dunes as a major proximal dust source for late Pleistocene loess in the Negev Desert , Israel. Quaternary research. 70:275–282.

Dansie, A.P., Wiggs, G.F.S., Thomas, D.S.G. and Washington, R., 2017a. Measurements of windblown dust characteristics and ocean fertilization potential: The ephemeral river valleys of Namibia. Aeolian Research, 29, 30-41.

Dansie, A.P., Thomas, D.S.G., Wiggs, G.F.S. and Munkittrick, K.R., 2017b. Spatial variability of ocean fertilising nutrients in the dust-emitting ephemeral river catchments of Namibia. Earth Surface Processes and Landforms.

Dansie, A.P., Wiggs, G.F.S. and Thomas, D.S.G., 2017c. Iron and nutrient content of wind-erodible sediment in the ephemeral river valleys of Namibia. Geomorphology, 290, 335-346.

Deboudt, K., Flament, P., Choël, M., Gloter, A., Sobanska, S. and Colliex, C., 2010. Mixing state of aerosols and direct observation of carbonaceous and marine coatings on African dust by individual particle analysis. Journal of Geophysical Research: Atmospheres, 115(D24).

Dusek, U., Frank, G.P., Hildebrandt, L., Curtius, J., Schneider, J., Walter, S., Chand, D., Drewnick, F., Hings, S., Jung, D. and Borrmann, S., 2006. Size matters more than chemistry for cloud-nucleating ability of aerosol particles. Science, 312(5778), 1375-1378.

Dee, D.P., Uppala, S.M., Simmons, A.J., Berrisford, P., Poli, P., Kobayashi, S., Andrae, U., Balmaseda, M.A., Balsamo, G., Bauer, P. and Bechtold, P., 2011. The ERA-Interim reanalysis: Configuration and performance of the data assimilation system. Quarterly Journal of the royal meteorological society, 137(656), 553-597.

Department of Water Affairs., 1995. Omdel Dam State Water Scheme. Retrieved from http://www.namwater.com.na/images/data/The Omdel Dam.pdf

Department of Water Affairs and Forestry, 1991. Water Resource Development for Walvis Bay: Assessment of expected impacts of the proposed water resource development options, possible mitigation measures, information requirements and recommendations.

Eckardt, F. D., Soderberg, K., Coop, L. J., Muller, A. A., Vickery, K. J., Grandin, R. D., Jack, C.,Kapalanga, T.S., Henschel, J., 2013. The nature of moisture at Gobabeb, in the central Namib Desert. Journal of Arid Environments, 93, 7–19.

Eckardt, F. D., Kuring, N., 2005. SeaWiFS identifies dust sources in the Namib Desert. International Journal of Remote Sensing, 26(19), 4159–4167.

Eckardt, F. D., Washington, R., Wilkinson, M. J., 2001. The origin of dust on the west coast of Southern Africa. Palaeoecol. Afr., 27, 207–219.

Eckardt, F. and White, K., 1997. Human induced disruption of stone pavement surfaces in the central Namib desert, Namibia: observations from Landsat Thematic Mapper. International Journal of Remote Sensing, 18(16), 3305-3310.

Eitel, B., Blümel, W.D., Hüser, K. and Mauz, B., 2001. Dust and loessic alluvial deposits in Northwestern Namibia (Damaraland, Kaokoveld): sedimentology and palaeoclimatic evidence based on luminescence data. Quaternary International, 76, 57-65.

Elith, J., Leathwick, J.R. & Hastie, T. 2008. A working guide to boosted regression trees. Journal of Animal Ecology. 77(4):802–813.

Engelbrecht, J.P., McDonald, E.V., Gillies, J.A., Jayanty, R.K.M., Casuccio, G. and Gertler, A.W., 2009. Characterizing mineral dusts and other aerosols from the Middle East—part 1: ambient sampling. Inhalation toxicology, 21(4), 297-326.

Engelbrecht, J.P., Moosmüller, H., Pincock, S., Jayanty, R.K.M., Lersch, T. and Casuccio, G., 2016. Mineralogical, chemical, morphological, and optical interrelationships of mineral dust re-suspensions. Atmospheric Chemistry & Physics, 16(17).

Etyemezian, V., Nikolich, G., Ahonen, S., Pitchford, M., Sweeney, M., Purcell, R., Gillies, J. & Kuhns, H. 2007. The Portable In Situ Wind Erosion Laboratory (PI-SWERL): A new method to measure PM10 windblown dust properties and potential for emissions. Atmospheric Environment. 41(18):3789–3796.

Etyemezian, V., Gillies, J.A., Shinoda, M., Nikolich, G., King, J. and Bardis, A.R., 2014. Accounting for surface roughness on measurements conducted with PI-SWERL: Evaluation of a subjective visual approach and a photogrammetric technique. Aeolian Research, 13, 35-50.

Falkovich, A.H., Ganor, E., Levin, Z., Formenti, P. and Rudich, Y., 2001. Chemical and mineralogical analysis of individual mineral dust particles. Journal of Geophysical Research: Atmospheres, 106(D16), 18029-18036.

Field, J. P., Breshears, D. D., Whicker, J. J., 2009. Toward a more holistic perspective of soil erosion: Why aeolian research needs to explicitly consider fluvial processes and interactions. Aeolian Research, 1(1–2), 9–17.

Field, J.P., Belnap, J., Breshears, D.D., Neff, J.C., Okin, G.S., Whicker, J.J., Painter, T.H., Ravi, S., Reheis, M.C. and Reynolds, R.L., 2010. The ecology of dust. Frontiers in Ecology and the Environment, 8(8), 423-430.

Fischer, N. and Claeys, M., 2016. Phase changes studied under in situ conditions—A novel cell. Catalysis Today, 275, 149-154.

Formenti, P., Elbert, W., Maenhaut, W., Haywood, J. and Andreae, M.O., 2003. Chemical composition of mineral dust aerosol during the Saharan Dust Experiment (SHADE)

airborne campaign in the Cape Verde region, September 2000. Journal of Geophysical Research: Atmospheres, 108(D18).

Formenti, P., Schütz, L., Balkanski, Y., Desboeufs, K., Ebert, M., Kandler, K., Petzold, A., Scheuvens, D., Weinbruch, S. and Zhang, D., 2011. Recent progress in understanding physical and chemical properties of African and Asian mineral dust. Atmospheric Chemistry and Physics, 11(16), 8231-8256.

Friese, C.A., van der Does, M., Merkel, U., Iversen, M.H., Fischer, G. and Stuut, J.B.W., 2016. Environmental factors controlling the seasonal variability in particle size distribution of modern Saharan dust deposited off Cape Blanc. Aeolian Research, 22, 165-179.

Fryberger, S.G., 1979. Dune forms and wind regimes. In: McKee, E.D. (Ed.), A study of Global Sand Seas. USGS Professional paper 1052, 137-169.

Fryrear, D.W., 1986. A field dust sampler. Journal of Soil and Water Conservation, 41(2), 117-120.

GCS, 2011. Nampower coal-fired power station baseline report. Hydrogeological, geotechnical, soils and water supply. Namibian Power Corporation (Pty) Ltd, Windhoek, Namibia. Available on: www.gcs-sa.biz.

Gillette, D., Adams, J., Endo, A. & Smith, D. 1980. Threshold Velocities for Input of Soil Particles Into the Air by Desert Soils. Journal of Geophysical Research. 85:5621–5630.

Gillette, D.A. Adams, J., Muhs, D. and Kihl, R., 1982. Threshold friction velocities and rupture moduli for crusted desert soils for the input of soil particles into the air. Journal of Geophysical Research, 87(C11), p 9003.

Gillette, D.A., Fryrear, D.W., Gill, T.E., Ley, T., Cahill, T.A. and Gearhart, E.A., 1997. Relation of vertical flux of particles smaller than 10 μm to total aeolian horizontal mass flux at Owens Lake. Journal of Geophysical Research: Atmospheres, 102(D22), 26009-26015.

Gillette, D. A., 1999 A qualitative geophysical explanation for “hot spot” dust emitting source regions, Contrib. Atmos. Phys., **72**, 67– 77.

Gillette, D., Ono, D. and Richmond, K., 2004. A combined modelling and measurement technique for estimating windblown dust emissions at Owens (dry) Lake, California. Journal of Geophysical Research: Earth Surface, 109(F1).

Gillies, J. A., 2013. Fundamentals of Aeolian Sediment Transport: Dust Emissions and Transport - Near Surface. Treatise on Geomorphology (Vol. 11). Elsevier Ltd.

Ginoux, P., Chin, M., Tegen, I., Prospero, J.M., Holben, B., Dubovik, O. and Lin, S.J., 2001. Sources and distributions of dust aerosols simulated with the GOCART model. Journal of Geophysical Research: Atmospheres, 106(D17), 20255-20273.

Ginoux, P., Garbuzov, D. and Hsu, N.C., 2010. Identification of anthropogenic and natural dust sources using Moderate Resolution Imaging Spectroradiometer (MODIS) Deep Blue level 2 data. Journal of Geophysical Research: Atmospheres, 115(D5).

Ginoux, P., Prospero, J.M., Gill, T.E., Hsu, N.C. and Zhao, M., 2012. Global-scale attribution of anthropogenic and natural dust sources and their emission rates based on MODIS Deep Blue aerosol products. Reviews of Geophysics, 5*0*(3).

Goldewijk, K.K., 2001. Estimating global land use change over the past 300 years: the HYDE database. Global biogeochemical cycles, 15(2), 417-433.

Goodall, W.R., Scales, P.J. and Butcher, A.R., 2005. The use of QEMSCAN and diagnostic leaching in the characterisation of visible gold in complex ores. Minerals Engineering, 18(8), 877-886.

Goossens, D., 2004. Effect of soil crusting on the emission and transport of wind-eroded sediment: field measurements on loamy sandy soil. Geomorphology, *58*(1), 145-160.

Goossens, D. and Buck, B., 2009. Dust emission by off-road driving: Experiments on 17 arid soil types, Nevada, USA. Geomorphology, 107(3), 118-138.

Goossens, D. and Buck, B., 2011. Gross erosion, net erosion and gross deposition of dust by wind: field data from 17 desert surfaces. Earth Surface Processes and Landforms, *36*(5), 610-623.

Gottlieb, P., Wilkie, G., Sutherland, D., Ho-Tun, E., Suthers, S., Perera, K., Jenkins, B., Spencer, S., Butcher, A. and Rayner, J., 2000. Using quantitative electron microscopy for process mineralogy applications. JoM, 52(4), 24-25.

Gottlieb, R.T. 2018 The contribution of fog to the moisture and nutritional supply of *Arthraerua leubnitziae* in the central Namib Desert, Namibia. Master's thesis, University of Cape Town, Cape Town, South Africa (submitting corrections).

Goudie, A.S. and Middleton, N.J., 2006. *Desert dust in the global system*. Springer Science & Business Media.

Goudie, A. S., 2014. Desert dust and human health disorders. Environment International, 63, 101–113.

Goudie, A. and Viles, H., 2015. Climate. In *Landscapes and Landforms of Namibia* (37-46). Springer Netherlands.

Grini, A., Myhre, G., Zender, C.S. and Isaksen, I.S., 2005. Model simulations of dust sources and transport in the global atmosphere: Effects of soil erodibility and wind speed variability. Journal of Geophysical Research: Atmospheres, 110(D2).

Hahnenberger, M., & Nicoll, K., 2014. Geomorphic and land cover identification of dust sources in the eastern Great Basin of Utah, U.S.A. Geomorphology, 204, 657–672.

Hahnenberger, M. and Perry, K.D., 2015. Chemical comparison of dust and soil from the Sevier Dry Lake, UT, USA. Atmospheric Environment, 113, 90-97.

Hayton, S., Nelson, C.S., Ricketts, B.D., Cooke, S. and Wedd, M.W., 2001. Effect of mica on particle-size analyses using the laser diffraction technique. Journal of Sedimentary Research, 71(3), 507-509.

Heine, K. and Völkel, J., 2010. Soil clay minerals in Namibia and their significance for the terrestrial and marine past global change research. Afr Study Monogr 40: 31–50

Hojati, S., Khademi, H., Cano, A.F. and Landi, A., 2012. Characteristics of dust deposited along a transect between central Iran and the Zagros Mountains. Catena, 88(1), 27-36.

Haustein, K., Washington, R., King, J., Wiggs, G., Thomas, D.S.G., Eckardt, F.D., Bryant, R.G. and Menut, L., 2015. Testing the performance of state-of-the-art dust emission schemes using DO4Models field data. Geoscientific Model Development, 8, 341-362.

Heinze, C., 2009. Spatial planning for off-road driving areas – Pros and cons of environmental regulations A case study in a semi-arid environment, Namibia, Enschede, The Netherlands: International Institute for Geo-Information Science and Earth Observation (MSC Thesis)

Hengl, T., Leenaars, J.G., Shepherd, K.D., Walsh, M.G., Heuvelink, G.B., Mamo, T., Tilahun, H., Berkhout, E., Cooper, M., Fegraus, E. and Wheeler, I., 2017. Soil nutrient maps of Sub-Saharan Africa: assessment of soil nutrient content at 250 m spatial resolution using machine learning. Nutrient Cycling in Agroecosystems, 109(1), 77-102.

Herman, J. R., Bhartia, P. K., Torres, O., Hsu, C., Seftor, C., & Celarier, E., 1997. Global distribution of UV-absorbing aerosols from Nimbus 7/TOMS data. Journal of Geophysical Research, 102(D14), 16911

Hijmans, R.J., Phillips, S., Leathwick, J. and Elith, J., 2016. dismo: species distribution modelling.–R package ver. 1.0-15.

Huang, J., Ge, J. & Weng, F. 2007. Detection of Asia dust storms using multisensor satellite measurements. Remote Sensing of Environment. 110(2):186–191.

Huntley, B. J. (ed)., 1985. The Kuiseb Environment: the development of a monitoring baseline. Foundation for Research Development, CSIR, Pretoria, 146

IPCC. 2013. Climate Change 2013: The Physical Science Basis. Contribution of Working Group I to the Fifth Assessment Report of the Intergovernmental Panel on Climate Change. (V. B. and P. M. M. (eds. . Stocker, T.F., D. Qin, G.-K. Plattner, M. Tignor, S.K. Allen, J. Boschung, A. Nauels, Y. Xia, Ed.), Cambridge University Press, Cambridge, United Kingdom and New York, NY, USA.

Iwahashi, J. and Pike, R.J., 2007. Automated classifications of topography from DEMs by an unsupervised nested-means algorithm and a three-part geometric signature. Geomorphology, 86(3), 409-440.

Jacobson, P. J., Jacobson, K. N., & Seely, M. K. 1995. *Ephemeral rivers and their catchments: sustaining people and development in western Namibia*. Desert Research Foundation of Namibia.

Jacobson, P. , Jacobson, K. , Angermeier, P., Cherry, D., 2000. Hydrologic influences on soil properties along ephemeral rivers in the Namib Desert. Journal of Arid Environments, 45(1), 21–34.

Jeong, G.Y., 2008. Bulk and single-particle mineralogy of Asian dust and a comparison with its source soils. Journal of Geophysical Research: Atmospheres, 113(D2).

Jerram, D., Mountney, N., Holzförster, F. and Stollhofen, H., 1999. Internal stratigraphic relationships in the Etendeka Group in the Huab Basin, NW Namibia: understanding the onset of flood volcanism. Journal of Geodynamics, 28(4), 393-418.

Jerram, D.A., Mountney, N.P., Howell, J.A., Long, D. and Stollhofen, H., 2000. Death of a sand sea: an active aeolian erg systematically buried by the Etendeka flood basalts of NW Namibia. Journal of the Geological Society, 157(3), 513-516.

Jickells, T.D., An, Z.S., Andersen, K.K., Baker, A.R., Bergametti, G., Brooks, N., Cao, J.J., Boyd, P.W., Duce, R.A., Hunter, K.A. and Kawahata, H., 2005. Global iron connections between desert dust, ocean biogeochemistry, and climate. Science, 308 (5718), 67-71.

Jickells, T. and Moore, C.M., 2015. The importance of atmospheric deposition for ocean productivity. Annual Review of Ecology, Evolution, and Systematics, 46, 481-501.

Journet, E., Desboeufs, K.V., Caquineau, S. and Colin, J.L., 2008. Mineralogy as a critical factor of dust iron solubility. Geophysical Research Letters, 35(7).

Journet, E., Balkanski, Y. and Harrison, S.P., 2014. A new data set of soil mineralogy for dust-cycle modelling. Atmospheric Chemistry and Physics, 14(8), 3801-3816.

Jung, E. and Shao, Y., 2006. An intercomparison of four wet deposition schemes used in dust transport modelling. Global and Planetary Change, 52(1), 248-260.

Kalashnikova, O.V. and Sokolik, I.N., 2002. Importance of shapes and compositions of wind-blown dust particles for remote sensing at solar wavelengths. Geophysical Research Letters, 29(10).

Kandler, K., Benker, N., Bundke, U., Cuevas, E., Ebert, M., Knippertz, P., Rodríguez, S., Schütz, L. and Weinbruch, S., 2007. Chemical composition and complex refractive index of Saharan Mineral Dust at Izana, Tenerife (Spain) derived by electron microscopy. Atmospheric Environment, 41(37), 8058-8074.

Kandler, K., Schütz, L., Deutscher, C., Ebert, M., Hofmann, H., Jäckel, S., Jaenicke, R., Knippertz, P., Lieke, K., Massling, A. and Petzold, A., 2009. Size distribution, mass concentration, chemical and mineralogical composition and derived optical parameters of the boundary layer aerosol at Tinfou, Morocco, during SAMUM 2006. Tellus B, 61(1), 32-50.

Kaufman, Y. J., Tanré, D., Dubovik, O., Karnieli, A., & Remer, L. a. (2001). Absorption of sunlight by dust as inferred from satellite and ground-based remote sensing. Geophysical Research Letters, 28(8), 1479–1482.

King, J., Etyemezian, V., Sweeney, M., Buck, B. J., & Nikolich, G., 2011. Dust emission variability at the Salton Sea, California, USA. Aeolian Research, 3(1), 67–79.

Kjeldsen, K. K., Mortetyeensen, J., Bendtsen, J., Lennert, K., & Rysgaard, S., 2014. Mapping erodibility in dust source regions based on geomorphology, meteorology, and remote sensing. Journal of Geophysical Research: Earth Surface, 119(6), 1310–1321.

Knippertz, P., and Stuut, J. B. W., 2014. Mineral dust: A key player in the earth system. Mineral Dust: A Key Player in the Earth System, 1–509.

Kohfeld, K.E., Reynolds, R.L., Pelletier, J.D. and Nickling, B., 2005. Linking the scales of observation, process, and modelling of dust emissions. Eos, Transactions American Geophysical Union, 86(11), 113-113.

Kok, J.F., 2011a. Does the size distribution of mineral dust aerosols depend on the wind speed at emission?. Atmospheric Chemistry and Physics, 11(19), 10149-10156.

Kok, J.F., 2011b. A scaling theory for the size distribution of emitted dust aerosols suggests climate models underestimate the size of the global dust cycle. Proceedings of the National Academy of Sciences, 108(3), 1016-1021.

Kok, J.F., Parteli, E.J., Michaels, T.I. and Karam, D.B., 2012. The physics of wind-blown sand and dust. Reports on Progress in Physics, 75(10), p.106901.

Koven, C. D., and Fung, I., 2008. Identifying global dust source areas using high-resolution land surface form. Journal of Geophysical Research: Atmospheres, 113(22), 1–19.

Krueger, B.J., Grassian, V.H., Laskin, A. and Cowin, J.P., 2003. The transformation of solid atmospheric particles into liquid droplets through heterogeneous chemistry: Laboratory insights into the processing of calcium containing mineral dust aerosol in the troposphere. Geophysical Research Letters, 30(3).

Lafon, S., Sokolik, I.N., Rajot, J.L., Caquineau, S. and Gaudichet, A., 2006. Characterization of iron oxides in mineral dust aerosols: Implications for light absorption. Journal of Geophysical Research: Atmospheres, 111(D21).

Lancaster, J., Lancaster, N., Seely, M., 1984. Climate of the central Namib Desert. *Madoqua*, 14, 5-61

Laskin, A., Iedema, M.J., Ichkovich, A., Graber, E.R., Taraniuk, I. and Rudich, Y., 2005. Direct observation of completely processed calcium carbonate dust particles. Faraday Discussions, *130*, 453-468.

Lawrence, C.R. and Neff, J.C., 2009. The contemporary physical and chemical flux of aeolian dust: A synthesis of direct measurements of dust deposition. Chemical Geology, 267(1), 46-63.

Lee, J. A., Gill, T. E., Mulligan, K. R., Dominguez Acosta, M., Perez, A. E., 2009. Land use/land cover and point sources of the 15 December 2003 dust storm in southwestern North America. Geomorphology, 105(December 2003), 18–27.

Lee, J. A., Baddock, M. C., Mbuh, M. J., & Gill, T. E., 2012. Geomorphic and land cover characteristics of aeolian dust sources in West Texas and eastern New Mexico, USA. Aeolian Research, 3(4), 459–466.

Little, L. 2016. The development and demonstration of a practical methodology for fine particle shape characterisation in minerals processing, PhD thesis, University of Cape Town, Cape Town, South Africa (August).

Macmillan, R. a, Mcnabb, D. H., Jones, R. K.., 2000. Automated landform classification using DEMs : a conceptual framework for a multi-level , hierarchy of hydrologically and geomorphologicaly oriented physiographic mapping units Background Situation analysis. 4th International Conference on Integrating GIS and Environmental Modelling (GIS/EM4): Problems, Prospects and Research Needs. Banff, Alberta, Canada, September 2 - 8, (October 2016), 1–18.

Maher, B. A., Prospero, J. M., Mackie, D., Gaiero, D., Hesse, P. P., & Balkanski, Y., 2010. Global connections between aeolian dust, climate and ocean biogeochemistry at the present day and at the last glacial maximum. Earth-Science Reviews, 99(1–2), 61–97.

Mahowald, N., Luo, C., Corral, J., Zender, C.S. 2003. Interannual variability in atmospheric mineral aerosols from a 22-year model simulation and observational data. Journal of Geophysical research. 108(D12).

Mahowald, N. M., 2004. Sensitivity of TOMS aerosol index to boundary layer height: Implications for detection of mineral aerosol sources. Geophysical Research Letters, 31(3), 2–5.

Mahowald, N.M., Baker, A.R., Bergametti, G., Brooks, N., Duce, R.A., Jickells, T.D., Kubilay, N., Prospero, J.M. and Tegen, I., 2005. Atmospheric global dust cycle and iron inputs to the ocean. Global biogeochemical cycles, 19(4).

Mahowald, N.M., Engelstaedter, S., Luo, C., Sealy, A., Artaxo, P., Benitez-Nelson, C., Bonnet, S., Chen, Y., Chuang, P.Y., Cohen, D.D. and Dulac, F., 2009. Atmospheric iron deposition: global distribution, variability, and human perturbations. Annual Review of Marine Science, 1, 245-278.

Mahowald, N., 2011. Aerosol indirect effect on biogeochemical cycles and climate. Science, 334(6057), 794-796.

Mahowald, N., Albani, S., Kok, J.F., Engelstaeder, S., Scanza, R., Ward, D.S. and Flanner, M.G., 2014. The size distribution of desert dust aerosols and its impact on the Earth system. Aeolian Research, 15, 53-71.

Marticorena, B. and Bergametti, G., 1995. Modelling the atmospheric dust cycle: 1. Design of a soil-derived dust emission scheme. Journal of Geophysical Research: Atmospheres, 100(D8), 16415-16430.

Martin, J.H., Coale, K.H., Johnson, K.S., Fitzwater, S.E., Gordon, R.M., Tanner, S.J., Hunter, C.N., Elrod, V.A., Nowicki, J.L., Coley, T.L. and Barber, R.T., 1994. Testing the iron hypothesis in ecosystems of the equatorial Pacific Ocean. Nature, 371 (6493), 123-129.

Maurer, T., Herrmann, L. & Stahr, K. 2010. Wind erosion characteristics of Sahelian surface types. Earth Surface Processes and Landforms. 1401(May):1386–1401.

McKenna-Neuman, C. and Nickling, W.G., 1989. A theoretical and wind tunnel investigation of the effect of capillary water on the entrainment of sediment by wind. Canadian Journal of Soil Science, *69*(1), 79-96.

McKenna Neuman, C. and Maxwell, C., 2002. Temporal aspects of the abrasion of microphytic crusts under grain impact. Earth Surface Processes and Landforms, *27*(8), 891-908.

Microsoft Bing, 2017. Huab River -20.90, 13.44, elevation 5 m, Aerial view, viewed October 2017, https://www.bing.com/maps.

Mendez, M.J., Funk, R. and Buschiazzo, D.E., 2011. Field wind erosion measurements with big spring number eight (BSNE) and modified wilson and cook (MWAC) samplers. Geomorphology, 129(1), 43-48.

McTainsh, G., and Strong, C., 2007. The role of aeolian dust in ecosystems. Geomorphology, 89(1–2), 39–54.

Mendelsohn, J., Jarvis, A., Roberts, C., Robertson, T., 2002. Atlas of Namibia. A Portrait of the Land and its People. Cape Town: David Philip Publishers; New Africa Books (Pty) Ltd).

Miller, S. D., 2003. A consolidated technique for enhancing desert dust storms with MODIS. Geophysical Research Letters, 30(20), 2071.

MME (2010). Strategic Environmental Assessment for the central Namib Uranium Rush. Ministry of Mines and Energy, Windhoek, Republic of Namibia.

Morin, E., Grodek, T., Dahan, O., Benito, G., Kulls, C., Jacoby, Y., Van Langenhove, G., Seely, M., Enzel, Y., 2009. Flood routing and alluvial aquifer recharge along the ephemeral arid Kuiseb River, Namibia. Journal of Hydrology, 368(1–4), 262–275.

Munkhtsetseg, E., Shinoda, M., Gillies, J.A., Kimura, R., King, J. & Nikolich, G. 2016. Relationships between soil moisture and dust emissions in a bare sandy soil of Mongolia,. Particuology. 28:131–137.

Namibia Resource Consultants. 1999. Rainfall distribution in Namibia: Data analysis and mapping of spatial, temporal and Southern Oscillation Index aspects. Windhoek: Ministry of Agriculture, Water and Rural Development.

Nield, J.M., King, J., Wiggs, G.F., Leyland, J., Bryant, R.G., Chiverrell, R.C., Darby, S.E., Eckardt, F.D., Thomas, D.S., Vircavs, L.H. and Washington, R., 2013. Estimating aerodynamic roughness over complex surface terrain. Journal of Geophysical Research: Atmospheres, 118 (23).

Nousiainen, T., 2009. Optical modelling of mineral dust particles: A review. Journal of Quantitative Spectroscopy and Radiative Transfer, 110(14), 1261-1279.

Okin, G.S., Baker, A.R., Tegen, I., Mahowald, N.M., Dentener, F.J., Duce, R.A., Galloway, J.N., Hunter, K., Kanakidou, M., Kubilay, N. and Prospero, J.M., 2011. Impacts of atmospheric nutrient deposition on marine productivity: Roles of nitrogen, phosphorus, and iron. Global Biogeochemical Cycles, 25(2).

O'Loingsigh, T., Mitchell, R. M., Campbell, S. K., Drake, N. A., McTainsh, G. H., Tapper, N. J., & Dunkerley, D. L., 2015. Correction of dust event frequency from MODIS Quick-Look imagery using in-situ aerosol measurements over the Lake Eyre Basin, Australia. Remote Sensing of Environment, 169(August 2016), 222–231.

Parajuli, S.P., Yang, Z., Kocurek, G., Yang, Z., Kocurek, G. 2014. Mapping erodibility in dust source regions based on geomorphology, meteorology, and remote sensing. Journal of Geophysical Research: Earth Surface. 119(Clm):1–18.

Parajuli, S.P., Zender, C.S. 2017. Connecting geomorphology to dust emission through high-resolution mapping of global land cover and sediment supply. Aeolian Research. 27:47–65.

Poulton, S.W. and Raiswell, R., 2002. The low-temperature geochemical cycle of iron: from continental fluxes to marine sediment deposition. American Journal of Science, 302(9), 774-805.

Prospero, J. M., 1999. Long-range transport of mineral dust in the global atmosphere: impact of African dust on the environment of the southeastern United States. Proceedings of the National Academy of Sciences of the United States of America, 96(7), 3396–3403.

Prospero, J. M., Ginoux, P., Torres, O., Nicholson, S. E., & Gill, T. E., 2002. Environmental characterization of global sources of atmospheric soil dust identified with the NIMBUS 7 Total Ozone Mapping Spectrometer (TOMS) absorbing aerosol product. Reviews of Geophysics, 40(1), 1002

Pye, K. and Tsoar, H., 1990. Aeolian Sand and Sand Dunes. Unwin Hyman, London. 396p.

QGIS Development Team, 2016. QGIS Geographic Information System. Open Source Geospatial Foundation. URL http://qgis.osgeo.org

Rashki, A., Eriksson, P.G., Rautenbach, C.D.W., Kaskaoutis, D.G., Grote, W. and Dykstra, J., 2013. Assessment of chemical and mineralogical characteristics of airborne dust in the Sistan region, Iran. Chemosphere, 90(2), 227-236.

Ralph, B. and Kurzydłowski, K.J., 1997. Methods for the characterization of grain size. Materials characterization, 38(3), 177-185.

Raupach, M.R., Gillette, D.A. and Leys, J.F., 1993. The effect of roughness elements on wind erosion threshold. Journal of Geophysical Research: Atmospheres, 98(D2), 3023-3029.

Ravi, S., D'odorico, P., Breshears, D.D., Field, J.P., Goudie, A.S., Huxman, T.E., Li, J., Okin, G.S., Swap, R.J., Thomas, A.D. and Van Pelt, S., 2011. Aeolian processes and the biosphere. Reviews of Geophysics, 49(3)

R Core Team (2017). R: A language and environment for statistical computing. R Foundation for Statistical Computing, Vienna, Austria. URL https://www.R-project.org/.

Reid, E.A., Reid, J.S., Meier, M.M., Dunlap, M.R., Cliff, S.S., Broumas, A., Perry, K. and Maring, H., 2003. Characterization of African dust transported to Puerto Rico by individual particle and size segregated bulk analysis. Journal of Geophysical Research: Atmospheres, 108(D19).

Resane, T., Annegarn, H. and Freiman, T., 2004. The day of the white rain: origin of unusual dust deposition in Johannesburg, South Africa. South African journal of science, 100(9-10), 483-487.

Reynolds, R., Goldstein, H. L., Fuller, C. C., Reynolds, R. L., Yount, J. C., Reheis, M., Goldstein, H., Chavez, P., Fulton, R., Whitney, J., Fuller, C., Forester, R. M., 2007. Dust emission from wet and dry playas in the Mojave Desert , USA. Earth Surface Processes and Landforms, 32, 1811–1827.

Reynolds, R.L., Bogle, R., Vogel, J., Goldstein, H. & Yount, J., 2009. Dust emission at Franklin Lake Playa , Mojave Desert (USA): Response to meteorological and hydrologic changes 2005-2008. Natural Resources and Environmental Issues. 15(1):Article 18.

Ryder, C.L., Highwood, E.J., Rosenberg, P.D., Trembath, J., Brooke, J.K., Bart, M., Dean, A., Crosier, J., Dorsey, J., Brindley, H. and Banks, J., 2013. Optical properties of Saharan dust aerosol and contribution from the coarse mode as measured during the Fennec 2011 aircraft campaign. Atmospheric Chemistry and Physics, 13(1), 303-325.

Schepanski, K., Tegen, I., Laurent, B., Heinold, B. and Macke, A., 2007. A new Saharan dust source activation frequency map derived from MSG-SEVIRI IR-channels. Geophysical Research Letters, *34*(18).

Schepanski, K., Tegen, I., Macke, A., 2012. Comparison of satellite based observations of Saharan dust source areas. Remote Sensing of Environment. 123:90–97.

Shao, Y., McTainsh, G.H., Leys, J.F., Raupach, M.R., 1993. Efficiencies of sediment samplers for wind erosion measurement. Soil Research, 31(4), 519-532.

Shao, Y., Wyrwoll, K.H., Chappell, A., Huang, J., Lin, Z., McTainsh, G.H., Mikami, M., Tanaka, T.Y., Wang, X. and Yoon, S., 2011a. Dust cycle: An emerging core theme in Earth system science. Aeolian Research, *2*(4), 181-204.

Shao, Y., Ishizuka, M., Mikami, M. and Leys, J.F., 2011b. Parameterization of size-resolved dust emission and validation with measurements. Journal of Geophysical Research: Atmospheres, 116(D8).

Sharratt, B., Feng, G. and Wendling, L., 2007. Loss of soil and PM10 from agricultural fields associated with high winds on the Columbia Plateau. Earth Surface Processes and Landforms, *32*(4), 621-630.

Shi, Z., Shao, L., Jones, T.P. and Lu, S., 2005. Microscopy and mineralogy of airborne particles collected during severe dust storm episodes in Beijing, China. Journal of Geophysical Research: Atmospheres, 110(D1).

Smith, M., Paron, P., Griffiths, J., 2011. Geomorphological mapping: Methods and applications. Amsterdam: Elsevier.

Soderberg, K., & Compton, J. S., 2007. Dust as a Nutrient Source for Fynbos Ecosystems, South Africa. Ecosystems, 10(4), 550–561

Sokolik, I.N. and Toon, O.B., 1996. Direct radiative forcing by anthropogenic airborne mineral aerosols. Nature, 381(6584), p.681.

Sokolik, I.N. and Toon, O.B., 1999. Incorporation of mineralogical composition into models of the radiative properties of mineral aerosol from UV to IR wavelengths. Journal of Geophysical Research: Atmospheres, 104(D8), 9423-9444.

Sokolik, I.N., Winker, D.M., Bergametti, G., Gillette, D.A., Carmichael, G., Kaufman, Y.J., Gomes, L., Schuetz, L. and Penner, J.E., 2001. Introduction to special section: Outstanding problems in quantifying the radiative impacts of mineral dust. Journal of Geophysical Research: Atmospheres, 106(D16), 18015-18027.

Speirs, J.C., McGowan, H.A. and Neil, D.T., 2008. Polar eolian sand transport: grain characteristics determined by an automated scanning electron microscope (QEMSCAN®). Arctic, Antarctic, and Alpine Research, 40(4), 731-743.

Stout, J. E., 2007. Simultaneous observations of the critical aeolian threshold of two surfaces. Geomorphology, 85(1–2), 3–16.

Sweeney, M., Etyemezian, V., Macpherson, T., Nickling, W., Gillies, J., Nikolich, G., & McDonald, E., 2008. Comparison of PI-SWERL with dust emission measurements

from a straight-line field wind tunnel. Journal of Geophysical Research: Earth Surface, 113(1), 1–12.

Sweeney, M. R., McDonald, E. V., & Etyemezian, V., 2011. Quantifying dust emissions from desert landforms, eastern Mojave Desert, USA. Geomorphology, 135(1–2), 21–34.

Sweeney, M. R., Zlotnik, V. A., Joeckel, R. M., & Stout, J. E., 2016. Geomorphic and hydrologic controls of dust emissions during drought from Yellow Lake playa, West Texas, USA. Journal of Arid Environments, 133, 37–46.

Taramelli, A., Pasqui, M., Barbour, J., Kirschbaum, D., Bottai, L., Busillo, C., Calastrini, F., Guarnieri, F. and Small, C., 2013. Spatial and temporal dust source variability in northern China identified using advanced remote sensing analysis. Earth Surface Processes and Landforms, 38(8), 793-809.

Tegen, I. and Fung, I., 1994. Modelling of mineral dust in the atmosphere: Sources, transport, and optical thickness. Journal of Geophysical Research: Atmospheres, 99(D11), 22897-22914.

Tegen, I., Werner, M., Harrison, S.P. and Kohfeld, K.E., 2004. Relative importance of climate and land use in determining present and future global soil dust emission. Geophysical Research Letters, 31(5).

Thomas, D.S., Durcan, J.A., Dansie, A. and Wiggs, G.F., 2017. Holocene fluvial valley fill sources of atmospheric mineral dust in the Skeleton Coast, Namibia. Earth Surface Processes and Landforms, 42(12), 1884-1894.

Trapp, J.M., Millero, F.J. and Prospero, J.M., 2010. Temporal variability of the elemental composition of African dust measured in trade wind aerosols at Barbados and Miami. Marine Chemistry, 120(1), 71-82.

US EPA, 1995. Compilation of ait pollutant emission factors – Vol. 1. Stationary point and area sources, Report No. AP-42, United States Environmental Protection Agency, Research Triangle Park, NC.

van der Does, M., Korte, L. F., Munday, C. I., Brummer, G. A., & Stuut, J. W. (2016). Particle size traces modern saharan dust transport and deposition across the equatorial north atlantic. Atmospheric Chemistry and Physics, 16(21), 13697-13710.

Vickery, K. 2010. Southern African dust sources as identified by multiple space borne sensors, Master's thesis, University of Cape Town, Cape Town, South Africa (January).

Vickery, K. J., Eckardt, F. D., 2013. Dust emission controls on the lower Kuiseb River valley, Central Namib. Aeolian Research, 10, 125–133.

Vickery, K. J., Eckardt, F. D., & Bryant, R. G., 2013. A sub-basin scale dust plume source frequency inventory for southern Africa, 2005-2008. Geophysical Research Letters, 40(19), 5274–5279

Vickery, K., 2014. The nature of pan sediments: A case study on dust supply from the Makgadikgadi pans, Botswana. PhD Thesis. University of Cape Town.

von Holdt, J.R. and Eckardt, F.D., 2017. Dust activity and surface sediment characteristics of the dustiest river in southern Africa: the Kuiseb River, Central Namib. South African Geographical Journal, 1-18.

von Holdt, J.R., Eckardt, F.D., Wiggs, G.F.S. 2017. Landsat identifies aeolian dust emission dynamics at the landform scale. Remote Sensing of Environment. 198:229–243.

Wang, X., Dong, Z., Yan, P., Yang, Z. and Hu, Z., 2005. Surface sample collection and dust source analysis in northwestern China. Catena, 59(1), 35-53.

Wang, X., Lang, L., Hua, T., Wang, H., Zhang, C., & Wang, Z., 2012. Characteristics of the Gobi desert and their significance for dust emissions in the Ala Shan Plateau (Central Asia): An experimental study. Journal of Arid Environments, 81, 35–46.

Wang, X., Chow, J.C., Kohl, S.D., Yatavelli, L.N.R., Percy, K.E., Legge, A.H. and Watson, J.G., 2015. Wind erosion potential for fugitive dust sources in the Athabasca Oil Sands Region. Aeolian Research, 18, 121-134.

Wang, X., Lang, L., Hua, T., Zhang, C. and Li, H., 2017. The effects of sorting by aeolian processes on the geochemical characteristics of surface materials: a wind tunnel experiment. Frontiers of Earth Science, 1-9.

Warren, A., Chappell, A., Todd, M.C., Bristow, C., Drake, N., Engelstaedter, S., Martins, V., M'bainayel, S. and Washington, R., 2007. Dust-raising in the dustiest place on earth. Geomorphology, 92(1), 25-37.

Washington, R., Todd, M., Middleton, N. J., & Goudie, A. S., 2003. Dust-storm source areas determined by the total ozone monitoring spectrometer and surface observations. Annals of the Association of American Geographers, 93(2), 297–313.

Wassenaar, T.D., Henschel, J.R., Pfaffenthaler, M.M., Mutota, E.N., Seely, M.K.., Pallett, J., 2013, Ensuring the future of the Namib's biodiversity: Ecological restoration as a key management response to a mining boom. Journal of Arid Environments, 93, 126–135.

Webb, N. P., Strong, C. L., 2011. Soil erodibility dynamics and its representation for wind erosion and dust emission models. Aeolian Research, 3(2), 165–179.

Wiggs, G., Holmes, P., 2011. Dynamic controls on wind erosion and dust generation on west-central Free State agricultural land, South Africa. Earth Surface Processes and Landforms, 36(6), 827–838.

World Bank Group., 2013. Industrial Groundwater recharge. https://www.waterscarcitysolutions.org/wp-content/uploads/2015/07/Groundwater-recharge-Omdel-Dam-Namibia.pdf

Xuan, J., & Sokolik, I. N., 2002. Characterization of sources and emission rates of mineral dust in Northern China. Atmospheric Environment, 36(31), 4863–4876.

Yang, X., Liu, Y., Li, C., Song, Y., Zhu, H. and Jin, X., 2007. Rare earth elements of aeolian deposits in Northern China and their implications for determining the provenance of dust storms in Beijing. Geomorphology, 87(4), 365-377.

Zender, C.S., Bian, H. and Newman, D., 2003. Mineral Dust Entrainment and Deposition (DEAD) model: Description and 1990s dust climatology. Journal of Geophysical Research: Atmospheres, 108(D14).

Zhang, J., Wu, Y., Liu, C.L., Shen, Z.B., Yu, Z.G. and Zhang, Y., 2001. Aerosol characters from the desert region of Northwest China and the Yellow Sea in spring and summer: observations at Minqin, Qingdao, and Qianliyan in 1995–1996. Atmospheric Environment, 35(29), 5007-5018.

Zhuang, G., Guo, J., Yuan, H. and Zhao, C., 2001. The compositions, sources, and size distribution of the dust storm from China in spring of 2000 and its impact on the global environment. Chinese Science Bulletin, 46(11), 895-900.

Zobeck, T.M., Sterk, G., Funk, R., Rajot, J.L., Stout, J.E.., Van Pelt, R.S. 2003. Measurement and data analysis methods for field-scale wind erosion studies and model validation. Earth Surface Processes and Landforms. 28(11):1163–1188.

Zobeck, T.M., Baddock, M., Van Pelt, R.S., Tatarko, J. and Acosta-Martinez, V., 2013. Soil property effects on wind erosion of organic soils. Aeolian Research, 10, 43-51.

Appendices

7.1 Landsat dust images from 1989 to 2016

Landsat dust images		
Number	Julian day	Image number
1	1989202	LT51790761989202JSA00
		LT51790771989202JSA00
2	1989250	LT51790761989250JSA00
		LT51790771989250JSA00
3	1990148	LT51800751990148JSA01
4	1990205	LT51790761990205JSA00
		LT51790771990205JSA00
5	1991126	LT51810731991126JSA01
		LT51810741991126JSA01
6	1991135	LT51800751991135JSA01
7	1992218	LT51800751992218JSA00
8	1993172	LT51800751993172JSA00
		LT51800761993172JSA00
9	1993181	LT51790761993181JSA00
		LT51790771993181JSA00
10	1995130	LT51800761995130JSA00
11	1995137	LT51810741995137JSA00
12	1996174	LT51790761996174JSA00
		LT51790771996174JSA00
13	1996181	LT51800751996181JSA00
		LT51800761996181JSA00
14	1997151	LT51800751997151JSA00
		LT51800761997151JSA00
15	1999188	LE71810741999188EDC00
16	2000159	LE71810742000159EDC00
17	2000184	LE71800752000184EDC00
		LE71800762000184EDC00
18	2000225	LE71790762000225EDC00
		LE71790772000225EDC00
19	2001138	LE71800752001138EDC00
		LE71800762001138EDC00
20	2002221	LE71800752002221JSA00
		LE71800762002221EDC00

Landsat dust images		
Number	Julian day	Image number
21	2002173	LE71800752002173JSA00
22	2004146	LT51810732004146JSA00
		LT51810742004146JSA00
23	2004162	LT51810732004162JSA00
		LT51810742004162JSA00
24	2004163	LE71800752004163ASN01
		LE71800762004163ASN01
25	2004196	LT51790762004196JSA00
		LT51790772004196JSA00
26	2005189	LT51800752005189JSA00
27	2007131	LT51800752007131JSA00
		LT51800762007131JSA00
28	2007132	LE71790772007132ASN00
29	2007195	LT51800752007195JSA00
		LT51800762007195JSA00
30	2007212	LE71790772007212ASN00
31	2007220	LT51790762007220JSA00
		LT51790772007220JSA00
32	2011189	LE71810742011189ASN00
33	2013122	LC81810732013122LGN01
		LC81810742013122LGN01
34	2013124	LC81790762013124LGN01
		LC81790772013124LGN01
35	2013202	LC81810732013202LGN00
		LC81810742013202LGN00
36	2013211	LC81800752013211LGN00
		LC81800762013211LGN00
37	2014101	LE71810732014101ASN00
		LE71810742014101ASN00
38	2014102	LC81800752014102LGN00
		LC81800762014102LGN00
39	2014109	LC81810742014109LGN00
40	2014159	LC81790762014159LGN00
		LC81790772014159LGN00
41	2016149	LC81790762016149LGN00

7.2 Preliminary predictive BRT dust emission scheme

A preliminary predictive BRT for the Namib study area is included here to give an indication of the potential of such a model (Figure 7-1 BRT DES). The PDS map reflecting the geomorphic units of the Namib study area was included as a categorical variable and was the number one predictor variable accounting for 53% of the variance in the model (Figure 7-2). The top ranking of PDS attests to the success of this scheme to reflect dust emission potential within the landscape. The soils layers did not make a significant contribution to the predictive model potentially because the influence of the soil characteristics is already captured in the PDS layer. This method of modelling significant factors and the interactions between them to predict dust emission hot spots has great potential for mapping erodibility at a global scale. The inclusion of areas in the BRT model other than the Namib study area would undoubtedly improve the model and potentially overcome the limitations of the LSM and SSM, both of which are based on a specific region or a single geomorphic unit such as large inland draining basins with the Bodélé Depression. Ground-based testing with instruments like the PI-SWERL from different source regions can be used to quantify the dust emission potential modelled by the BRT. This goal will be possible with a high-resolution source point identification as carried out in this study and emission measurements consistently targeting the geomorphic units as specified by a scheme such as the PDS.

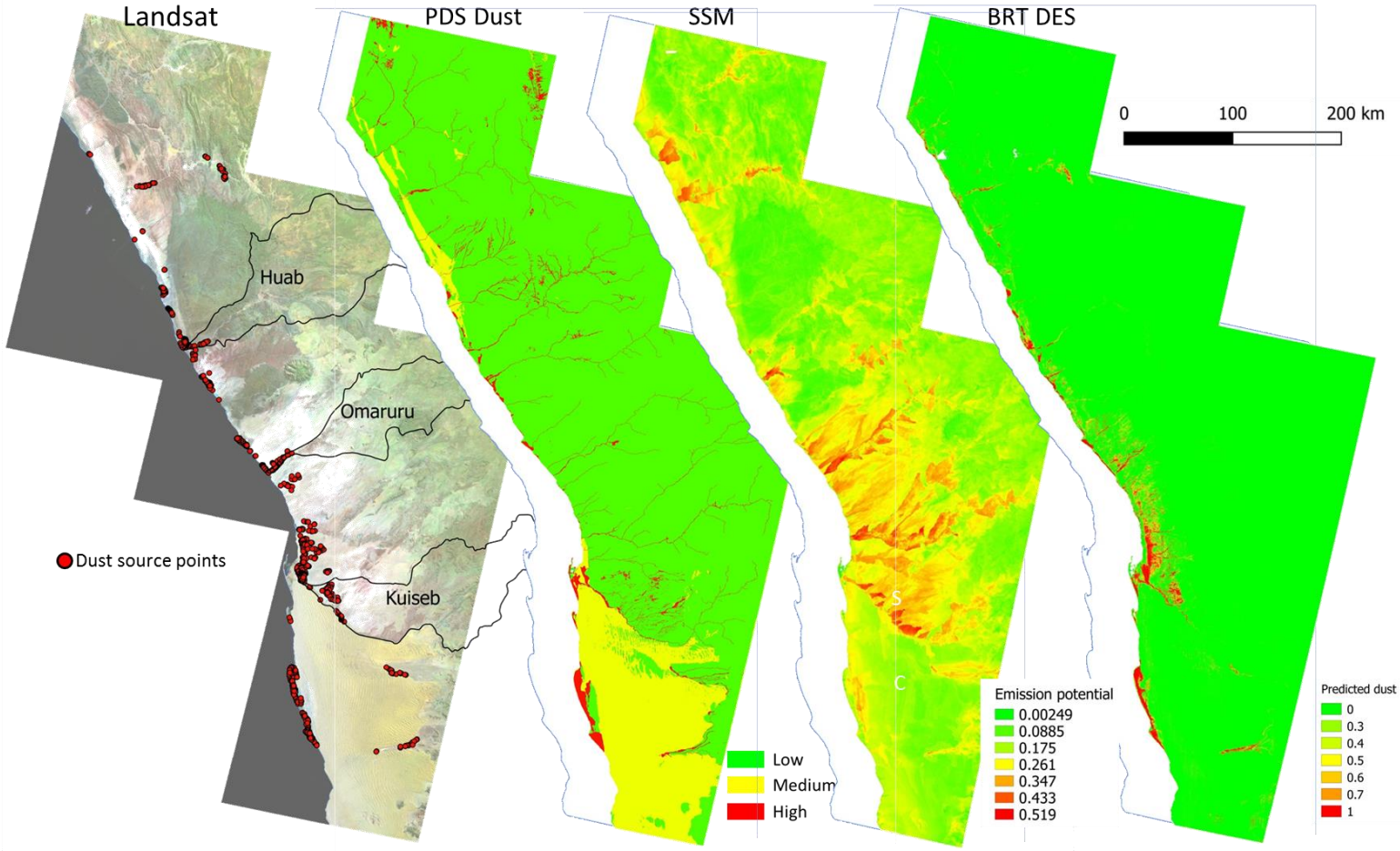
Landsat
PDS Dust
SSM
BRT DES
0
100
200 km
Huab
Omaruru
Kuiseb
Dust source points
Low
Medium
High
Emission potential
0.00249
0.0885
0.175
0.261
0.347
0.433
0.519
Predicted dust
0
0.3
0.4
0.5
0.6
0.7
1

Figure 7-1 Comparison of dust emission schemes for the Namib study area: Landsat false colour with dust source points identified with Landsat, PDS Dust, SSM and preliminary BRT DES. All emission schemes are in raster format with PDS and BRT DES at 250 m and SSM at 500m resolution.

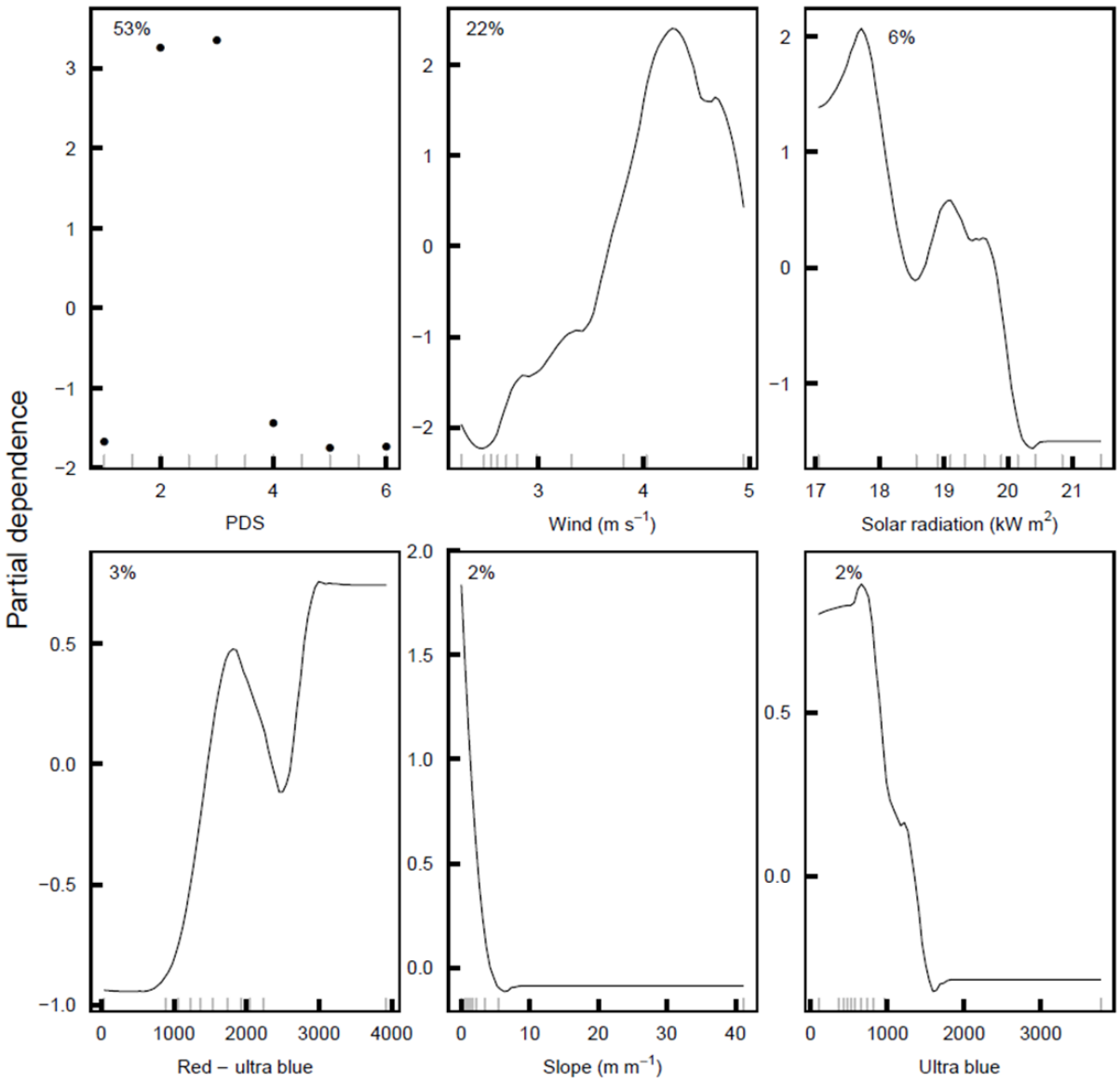

Figure 7-2 Partial dependencies of the top six predictors for the preliminary BRT Dust Emission Scheme model.

7.2.1 BRT Dust Emission Scheme Methodology

The BRT model (Elith et al., 2009) was performed in R using the gbm.step function within the *dismo* package version 1.1-4 (Hijmans et al., 2016). The variables included in the model as potential predictors are listed in Table 1-1 with the source points identified with Landsat in Chapter 2 as dust sources points. A Bernoulli BRT predicted dust emission potential after optimisation of tree complexity (1 to 5) and learning rate (0.01, 0.005, 0.001, 0.0005, 0.0001), with tree complexity set at 6 and learning rate at 0.01 and bagging fraction of 0.7 and cross-fold validation of 5. The most important predictors were ranked after model simplification and used to generate partial dependence plots. The model was used to predict the dust emission potential of the study area using the *predict* function in the library 'dismo'. The dust emission potential BRT model had a cross-validation AUC score of 0.996 ± 0.0004 and explained 86% of the deviance.

Table 7-1 Independent variables included in the regression model.

Category	Details
Geomorphic mapping	PDS geomorphic units (Bullard et al., 2011) mapped as in Chapter 3 and rasterised in R. Iwahashi and Pike classification of topography from DEM (Iwahashi and Pike, 2007)
DEM	Slope and aspect calculated from SRTM-1 data obtained from https://earthexplorer.usgs.gov/
Worldclim	Wind, solar radiation and precipitation annual averages obtained from http://worldclim.org/version2.
Soils	Clay %, silt %, sand %, gravel %, pH, Cation exchange capacity data were obtained from Soilsgrid (Hengl et al., 2017) at 250 m resolution. http://www.isric.org/explore/isric-soil-data-hub
Landsat bands	A Landsat composite was created in the Google Earth Engine (Google Earth Engine Team, 2015) cloud computing platform for geospatial analysis from cloud-free images obtained between May and September 2016 and included the following bands: 1 (Ultrablue), 2 (Blue), 3 (Green), 4 (Red), 5 (Near infrared, NIR), 6 (Shortwave infrared 1, SWIR1), 7 (Shortwave infrared 2, SWIR2). NDVI was calculated from these data layers.
Red – ultra blue	Contrast of absorption between red (640-670 nm) and ultra-blue (430-450 nm) following Ginoux et al. (2012), but for only one image set. This should be extended to specifically target dust emission events.

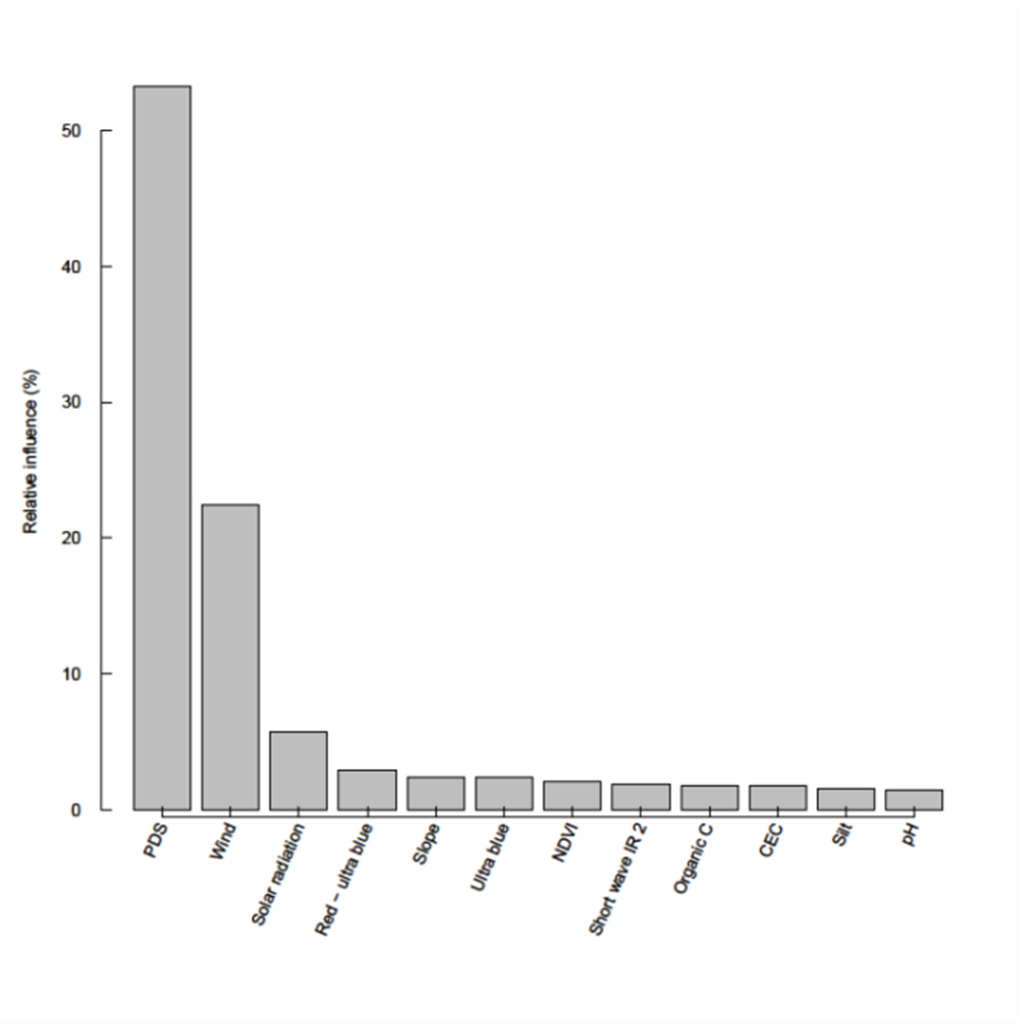

Figure 7-3 Relative influence of the top predicted variables contributing to the BRT Dust Emission Scheme. See Table 7-1 for description of variables.